Synthesis and Evaluation of the Service Limit State of Engineered Fills for Bridge Support

PUBLICATION NO. FHWA-HRT-15-080

FEBRUARY 2016

U.S. Department of Transportation
Federal Highway Administration

Research, Development, and Technology
Turner-Fairbank Highway Research Center
6300 Georgetown Pike
McLean, VA 22101-2296

FOREWORD

Engineered fills, including compacted granular fill and reinforced soil, are a cost-effective alternative to conventional bridge foundation systems; however, limited guidance exists on estimating the settlement and lateral deformation of these features under service conditions. Additionally, the stress distribution within these features is not well understood, leading to uncertainty in performance. To address these gaps, the Federal Highway Administration initiated a study to evaluate the service limit state (SLS) design and analysis of engineered fills for bridge support. This synthesis report is the product of an extensive literature search on current practices, available load tests, and numerical modeling results. It presents factors impacting the service limit of engineered fills and also provides a preliminary analysis on the reliability of existing prediction methods. The summarization of this work will assist in the continued development of research efforts to establish SLS design guidance for the use of engineered fills. This report will be of interest to engineers involved with bridge foundation research and design.

Jorge E. Pagán-Ortiz
Director, Office of Infrastructure
Research and Development

TECHNICAL REPORT DOCUMENTATION PAGE

1. Report No. FHWA-HRT-15-080	2. Government Accession No.	3. Recipient's Catalog No.
4. Title and Subtitle Synthesis and Evaluation of the Service Limit State of Engineered Fills for Bridge Support		5. Report Date February 2016 6. Performing Organization Code
7. Author(s) Xiao, M., Qiu, T., Khosrojerdi, M., Basu, P., and Withiam, J.L.		8. Performing Organization Report No.
9. Performing Organization Name and Address The Larson Transportation Institute The Pennsylvania State University 201 Transportation Research Building University Park, PA 16802 D'Appolonia Engineering Division of Ground Technology, Inc. 275 Center Road #2 Monroeville, PA 15146		10. Work Unit No. 11. Contract or Grant No. DTFH61-14-C-00012
12. Sponsoring Agency Name and Address Office of Infrastructure Research and Development Federal Highway Administration 6300 Georgetown Pike McLean, VA 22101-2296		13. Type of Report and Period Covered Technical 14. Sponsoring Agency Code
15. Supplementary Notes The Contracting Officer's Representative (COR) was Jennifer Nicks, HRDI-40. Additional Federal Highway Administration technical consultants included Naser Abu-Hejleh, Michael Adams, and Khalid Mohamed.		
16. Abstract This report synthesizes the current service limit state (SLS) design and analyses of engineered fills for bridge support used as shallow foundations. The SLS for settlement and deformations of bridge supports are summarized. Extensive literature reviews were conducted to synthesize the effects of various parameters on the SLS of engineered fills. The reliability of current prediction methods for deformations of bridge supports on granular soils are presented and evaluated using measured deformation data in the literature. Based on the literature review and synthesis, knowledge gaps and data needs for bridge supports with engineered fills were identified.		
17. Key Words Engineered fills, Settlement, Deformations, Service limit state, Bridge abutment, Shallow foundation, Geosynthetic reinforced soil, Mechanically stabilized earth, Reinforced soil foundation		18. Distribution Statement No restrictions. The report will be available to the public at FHWA: www.fhwa.dot.gov/research or NTIS: www.ntis.gov.

19. Security Classif. (of this report)	20. Security Classif. (of this page)	21. No. of Pages	22. Price
Unclassified	Unclassified	151	N/A

Form DOT F 1700.7 (8-72) Reproduction of completed page authorized

SI* (MODERN METRIC) CONVERSION FACTORS

APPROXIMATE CONVERSIONS TO SI UNITS

Symbol	When You Know	Multiply By	To Find	Symbol
		LENGTH		
in	inches	25.4	millimeters	mm
ft	feet	0.305	meters	m
yd	yards	0.914	meters	m
mi	miles	1.61	kilometers	km
		AREA		
in^2	square inches	645.2	square millimeters	mm^2
ft^2	square feet	0.093	square meters	m^2
yd^2	square yard	0.836	square meters	m^2
ac	acres	0.405	hectares	ha
mi^2	square miles	2.59	square kilometers	km^2
		VOLUME		
fl oz	fluid ounces	29.57	milliliters	mL
gal	gallons	3.785	liters	L
ft^3	cubic feet	0.028	cubic meters	m^3
yd^3	cubic yards	0.765	cubic meters	m^3
		NOTE: volumes greater than 1000 L shall be shown in m^3		
		MASS		
oz	ounces	28.35	grams	g
lb	pounds	0.454	kilograms	kg
T	short tons (2000 lb)	0.907	megagrams (or "metric ton")	Mg (or "t")
		TEMPERATURE (exact degrees)		
^oF	Fahrenheit	5 (F-32)/9 or (F-32)/1.8	Celsius	^oC
		ILLUMINATION		
fc	foot-candles	10.76	lux	lx
fl	foot-Lamberts	3.426	$candela/m^2$	cd/m^2
		FORCE and PRESSURE or STRESS		
lbf	poundforce	4.45	newtons	N
lbf/in^2	poundforce per square inch	6.89	kilopascals	kPa

APPROXIMATE CONVERSIONS FROM SI UNITS

Symbol	When You Know	Multiply By	To Find	Symbol
		LENGTH		
mm	millimeters	0.039	inches	in
m	meters	3.28	feet	ft
m	meters	1.09	yards	yd
km	kilometers	0.621	miles	mi
		AREA		
mm^2	square millimeters	0.0016	square inches	in^2
m^2	square meters	10.764	square feet	ft^2
m^2	square meters	1.195	square yards	yd^2
ha	hectares	2.47	acres	ac
km^2	square kilometers	0.386	square miles	mi^2
		VOLUME		
mL	milliliters	0.034	fluid ounces	fl oz
L	liters	0.264	gallons	gal
m^3	cubic meters	35.314	cubic feet	ft^3
m^3	cubic meters	1.307	cubic yards	yd^3
		MASS		
g	grams	0.035	ounces	oz
kg	kilograms	2.202	pounds	lb
Mg (or "t")	megagrams (or "metric ton")	1.103	short tons (2000 lb)	T
		TEMPERATURE (exact degrees)		
^oC	Celsius	1.8C+32	Fahrenheit	^oF
		ILLUMINATION		
lx	lux	0.0929	foot-candles	fc
cd/m^2	$candela/m^2$	0.2919	foot-Lamberts	fl
		FORCE and PRESSURE or STRESS		
N	newtons	0.225	poundforce	lbf
kPa	kilopascals	0.145	poundforce per square inch	lbf/in^2

*SI is the symbol for the International System of Units. Appropriate rounding should be made to comply with Section 4 of ASTM E380.
(Revised March 2003)

TABLE OF CONTENTS

CHAPTER 1. OVERVIEW OF BRIDGE SUPPORTS USING ENGINEERED FILLS 1
1.1 INTRODUCTION AND SCOPE OF WORK 1
1.2 SUMMARY OF ENGINEERED FILLS 1
1.3 BRIDGE SUPPORTS USING UNREINFORCED ENGINEERED FILLS 5
1.4 BRIDGE SUPPORTS USING MSE 6
1.5 BRIDGE SUPPORTS USING GRS 7

CHAPTER 2. CURRENT SLS DESIGN PROCEDURES AND CRITERIA 11
2.1 *AASHTO LOAD AND RESISTANCE FACTOR DESIGN (LRFD) BRIDGE DESIGN SPECIFICATIONS* 11
2.2 BRIDGE SUPPORTS USING MSE 11
2.3 BRIDGE SUPPORTS USING GRS 12
2.4 CURRENT SLS CRITERIA FOR BRIDGE SUPPORTS 13
Criteria for Settlement of Shallow Foundations of Bridges 13
Tolerable Horizontal Deformation Criteria for Bridge Supports 14
Tolerable Deformation Criteria for Reinforced Bridge Supports 15

CHAPTER 3. LITERATURE REVIEW OF PREVIOUS WORK IN ENGINEERED FILLS FOR BRIDGE SUPPORTS 17
3.1 OVERVIEW OF LOAD DEFORMATION DATA CATALOG OF ENGINEERED FILLS FOR BRIDGE SUPPORTS 17
3.2 SYNTHESIS OF FACTORS AFFECTING SETTLEMENT OF SHALLOW FOUNDATIONS 18
Effect of Relative Density of Soil on Settlement of Shallow Foundations 18
Effect of N on Settlement of Shallow Foundations 19
Effect of L and T_f of Reinforcement on Settlement of Shallow Foundations 25
Effect of B on Settlement of Shallow Foundations 29
Effect of Embedment Depth of Top Reinforcement Layer on Settlement of Shallow Foundations 30
Effect of Vertical Spacing of Reinforcement (S_v) Layers on Settlement of Shallow Foundations 32
Effect of Covering Ratio (CR) of Metallic Strip Reinforcement on Settlement of Shallow Foundations 33
3.3 SYNTHESIS OF LOAD DEFORMATION RELATIONSHIPS OF BRIDGE ABUTMENTS AND PIERS 34
Effect of Soil Parameters on Load Deformation Relationships 34
Effect of Reinforcement Characteristics on Load Deformation Relationships 46
Effect of Facing Blocks on Load Deformation Relationships 58
Effect of Prestraining on Load Deformation Relationships 59
3.4 EFFECTS OF TRANSIENT LOADS ON DEFORMATIONS OF BRIDGE SUPPORTS ON GRANULAR SOILS 62
3.5 DETERMINATION OF STRESS DISTRIBUTIONS IN GRANULAR SOILS UNDER SHALLOW FOUNDATIONS 63

CHAPTER 4. EVALUATION OF PREDICTION METHODS FOR DEFORMATIONS OF BRIDGE SUPPORTS ON GRANULAR SOILS 65
4.1 METHODS FOR IMMEDIATE SETTLEMENT OF SHALLOW FOUNDATIONS OF BRIDGES ON GRANULAR SOILS 65
Modified Schmertmann Method 65
Hough Method 66
Peck and Bazaraa method 67
Burland and Burbidge Method 68
D'Appolonia Method 68
4.2 LONG-TERM SETTLEMENT OF SHALLOW FOUNDATIONS ON GRANULAR SOILS 68
4.3 VERTICAL DEFORMATION OF GRS ABUTMENTS 70
4.4 LATERAL DISPLACEMENT OF GRS WALLS AND ABUTMENTS 70
FHWA Method 71
Geoservices Method 72
Colorado Transportation Institute (CTI) Method 72
Jewell-Milligan Method 72
Wu Method 73
Adams Method 74
4.5 EVALUATION OF THE DEFORMATION PREDICTION METHODS 74
Immediate Settlement 75
Vertical Deformations of GRS Walls and Abutments 88
Lateral Displacements of GRS Walls and Abutments 91

CHAPTER 5. NUMERICAL AND CONSTITUTIVE MODELS FOR COMPACTED FILL AND REINFORCED SOIL FOR BRIDGE SUPPORTS 109
5.1 MODELING OF COMPACTED SOILS 109
5.2 MODELING REINFORCED SOIL AS A SINGLE COMPOSITE MATERIAL 110
5.3 MODELING OF REINFORCEMENTS 111
5.4 MODELING OF SOIL-REINFORCEMENT INTERACTIONS 112
5.5 NUMERICAL MODELING OF STRUCTURES SUPPORTED BY ENGINEERED SOILS 113
5.6 NUMERICAL MODELING OF LONG-TERM BEHAVIOR OF GRS STRUCTURES 116
5.7 SIMILARITIES AND DIFFERENCES BETWEEN PIER AND ABUTMENT FOUNDATION DEFORMATION MODELS 117

CHAPTER 6. CONCLUSIONS 119
6.1 CONCLUSIONS 119
6.2 KNOWLEDGE GAPS AND DATA NEEDS FOR BRIDGE SUPPORTS USING ENGINEERED FILLS 119

REFERENCES 121

LIST OF FIGURES

Figure 1. Illustration. Engineered fill details of structural approach road and bridge foundation 6
Figure 2. Illustration. True MSE abutment types 7
Figure 3. Illustration. Typical cross-section of GRS bridge abutment 8
Figure 4. Illustration. Annotations of parameters of a shallow foundation on reinforced soil 9
Figure 5. Graph. Load-settlement results on unreinforced and reinforced sand 18
Figure 6. Graph. Load-settlement results for different relative densities 19
Figure 7. Graph. Load-settlement results for strip footing for $u/B = h/B = 0.333$, $b/B = 10$ 20
Figure 8. Graph. Load-settlement results for square footing for $u/B = h/B = 0.333$, $b/B = 6$ 20
Figure 9. Graph. Load-settlement results for square footing on unreinforced and reinforced soil with polypropylene (PP) geogrid layers 21
Figure 10. Graph. Load-settlement results for sandy soil for $u/B = 0.4$, $h/B = 0.33$, and $b/B = 4$ 22
Figure 11. Graph. Load-settlement results for 1.18-inch (30-mm)-diameter circular footing 23
Figure 12. Graph. Effect of number of geogrids on the load required for a settlement of 0.02 inch (0.5 mm) 24
Figure 13. Graph. Load-settlement results for different numbers of metallic reinforcement 24
Figure 14. Graph. Load-settlement results for different widths of geonet ($N = 4$, $d = 2B$) 25
Figure 15. Graph. Stress-strain relationship of reinforced soil 26
Figure 16. Graph. Stress-strain relationship of the mini-pier experiments 27
Figure 17. Graph. Load-settlement results for different reinforcement lengths ($N = 3$) 29
Figure 18. Graph. Load-settlement results in reinforced sand ($D_R = 75$ percent) 30
Figure 19. Graph. Load-settlement results of model footings on clay subgrade reinforced with geogrid 31
Figure 20. Graph. Load-settlement results for different depth of top layer of metallic reinforcement ($N = 3$) 32
Figure 21. Graph. Load-settlement results for square footing tests with three layers of geogrids placed at different vertical spacing 33
Figure 22. Graph. Load-settlement results for different CRs of reinforcement ($L = 2B$, $N = 3$) 34
Figure 23. Graph. Load-deformation behavior from PTs on GRS piers using five types of DC backfills 36
Figure 24. Graph. Effects of backfill internal f on vertical displacement at abutment seat (reinforcement spacing = 7.87 inches (20 cm)) 37
Figure 25. Graph. Effects of backfill internal f (reinforcement spacing = 7.87 inches (20 cm)) on horizontal displacement at abutment seat 38
Figure 26. Graph. Effects of backfill internal f (reinforcement spacing = 7.87 inches (20 cm)) on the maximum lateral displacement of the facing 38
Figure 27. Graph. Influence of apparent c and f on lateral displacement of the wall 39
Figure 28. Graph. Influence of backfill apparent c and f values on maximum reinforcement loads in wall models at EOC 40
Figure 29. Graph. Horizontal displacements at wall face 41
Figure 30. Graph. Maximum lateral displacement versus geosynthetic stiffness for soils 1–4 43
Figure 31. Graph. Maximum lateral displacement versus geosynthetic stiffness for soils 5–8 44

Figure 32. Graph. Maximum lateral displacement versus geosynthetic stiffness for soils 9–12.. 45
Figure 33. Graph. Maximum lateral displacement versus geosynthetic stiffness for soils 13–16 46
Figure 34. Graph. Effect of bearing bed reinforcement for TF-7 and TF-8 47
Figure 35. Graph. Measured lateral deformation at 3,600 psf (172.5 kPa) applied pressure for TF-7 (no bearing bed reinforcement) and TF-8 (two courses of bearing bed reinforcement)..... 47
Figure 36. Graph. Load-deformation behaviors for GSGC tests 49
Figure 37. Graph. Lateral deformation of test specimens at 12,531 psf (600 kPa) and the ultimate applied pressure 49
Figure 38. Graph. Effect of geosynthetic stiffness (reinforcement spacing = 7.87 inches (20 cm)) on vertical displacement at abutment seat..... 50
Figure 39. Graph. Effect of geosynthetic spacing on vertical displacement at abutment seat 51
Figure 40. Graph. Effect of geosynthetic stiffness (reinforcement spacing = 7.87 inches (20 cm)) on horizontal displacement at abutment seat 51
Figure 41. Graph. Effect of geosynthetic stiffness (reinforcement spacing = 7.87 inches (20 cm)) on the maximum lateral displacement of the facing 52
Figure 42. Graph. Effect of geosynthetic spacing on horizontal displacement at abutment seat 53
Figure 43. Graph. Effect of geosynthetic spacing on the maximum lateral displacement of the facing 53
Figure 44. Graph. Central settlement of the foundation versus applied load 54
Figure 45. Graph. Wall face displacement at applied pressure of 3,969.1 lb/ft^2 (190 kN/m^2) for non-woven and woven reinforcement..... 54
Figure 46. Graph. Relative horizontal displacement of wall facing recorded at EOC 55
Figure 47. Graph. Influence of soil-reinforcement interface stiffness value on lateral displacement of the wall 56
Figure 48. Graph. Effect of E_R on the maximum vertical displacement of MSE abutments with metal strips..... 57
Figure 49. Graph. Load-settlement results for the foundation on top of MSE abutment 58
Figure 50. Graph. Stress-strain response for different piers 59
Figure 51. Graph. Load-settlement curves for the pier..... 60
Figure 52. Graph. Lateral displacement measured by LVDT..... 60
Figure 53. Graph. Lateral deformation profiles of the west abutment..... 61
Figure 54. Graph. Lateral deformation profiles of the east abutment..... 62
Figure 55. Equation. Immediate settlement of spread footing based on modified Schmertmann method 66
Figure 56. Equation. Correction factor to consider foundation embedment depth..... 66
Figure 57. Equation. Correction factor to consider creep..... 66
Figure 58. Equation. Immediate settlement of each soil layer based on the Hough method..... 67
Figure 59. Equation. Immediate settlement of footing based on Peck and Bazaraa method..... 67
Figure 60. Equation. SPT blow count corrected for overburden pressure less than or equal to 1,566 lb/ft^2 (75 kPa)..... 67
Figure 61. Equation. SPT blow count corrected for overburden pressure greater than 1,566 lb/ft^2 (75 kPa)..... 68
Figure 62. Equation. Immediate settlement of a footing based on Burland and Burbidge method..... 68

Figure 63. Equation. Immediate settlement of a footing based on D'Appolonia method 68
Figure 64. Equation. Settlement due to creep 69
Figure 65. Equation. Creep rate of shallow foundations 69
Figure 66. Equation. Time-dependent settlement of footings in sand 70
Figure 67. Equation. Vertical displacement of a GRS abutment with a strip footing 70
Figure 68. Equation. Displacement coefficient of a reinforced soil wall 71
Figure 69. Equation. Maximum lateral deformation of a GRS wall with inextensible reinforcement (i.e., metallic reinforcement) 71
Figure 70. Equation. Maximum lateral deformation of a GRS wall with extensible reinforcement (i.e., geosynthetic reinforcement) 71
Figure 71. Equation. Maximum horizontal displacement of a GRS wall or abutment based on Geoservices method 72
Figure 72. Equation. Maximum lateral displacement of a GRS wall or abutment based on CTI method 72
Figure 73. Equation. Lateral displacement of a GRS wall or abutment with flexible facing 73
Figure 74. Equation. Lateral movement of a GRS wall with modular block facing 73
Figure 75. Equation. Lateral movement of a GRS wall with modular block facing (no friction between wall and soil) 74
Figure 76. Equation. Lateral displacement of GRS abutments in response to a vertical load 74
Figure 77. Equation. Lateral strain of GRS abutments in response to a vertical load 74
Figure 78. Equation. Arithmetic mean value 75
Figure 79. Equation. Standard deviation 75
Figure 80. Equation. COV 75
Figure 81. Graph. Frequency of occurrence histogram of λ for immediate settlements of shallow foundations using the modified Schmertmann method 78
Figure 82. Graph. Probability plot for measured and predicted settlements using the modified Schmertmann method 78
Figure 83. Graph. Frequency of occurrence histogram of λ for immediate settlements of shallow foundations using the Hough method 80
Figure 84. Graph. Probability plot for measured and predicted settlement using the Hough method 80
Figure 85. Graph. Frequency of occurrence histogram of λ for immediate settlements of shallow foundations using the Peck and Bazaraa method 82
Figure 86. Graph. Probability plot for measured and predicted settlement using the Peck and Bazaraa method 82
Figure 87. Graph. Frequency of occurrence histogram of λ for immediate settlements of shallow foundations using the Burland and Burbidge method 84
Figure 88. Graph. Probability plot for measured and predicted settlement using the Burland and Burbidge method 84
Figure 89. Graph. Frequency of occurrence histogram of λ for immediate settlements of shallow foundations using the D'Appolonia method 86
Figure 90. Graph. Probability plot for measured and predicted settlement using the D'Appolonia method 86
Figure 91. Equation. Elastic modulus of GRS composite 88
Figure 92. Equation. Elastic modulus of GRS composite (modified equation) 88

Figure 93. Graph. Frequency of occurrence histogram of λ of vertical displacement of abutments and GRS walls 90
Figure 94. Graph. Probability plot for measured and predicted vertical displacement of abutments and GRS walls 90
Figure 95. Graph. Frequency of occurrence histogram of λ for the lateral displacement of GRS walls and abutments using the FHWA method 92
Figure 96. Graph. Probability plot for measured and predicted lateral displacement of GRS walls using the FHWA method 93
Figure 97. Graph. Frequency of occurrence histogram of λ for the lateral displacement of GRS walls and abutments using the Geoservices method 95
Figure 98. Graph. Probability plot for measured and predicted lateral displacement of GRS walls using the Geoservices method 96
Figure 99. Graph. Frequency of occurrence histogram of λ for the lateral displacement of GRS walls and abutments using the CTI method 98
Figure 100. Graph. Probability plot for measured and predicted lateral displacement of GRS walls using the CTI method 99
Figure 101. Graph. Frequency of occurrence histogram of λ for the lateral displacement of GRS walls and abutments using the Jewell-Milligan method 101
Figure 102. Graph. Probability plot for measured and predicted lateral displacement of GRS walls using the Jewell-Milligan method 101
Figure 103. Graph. Frequency of occurrence histogram of λ for the lateral displacement of GRS walls and abutments using the Wu method 104
Figure 104. Graph. Probability plot for measured and predicted lateral displacement of GRS walls using the Wu method 104
Figure 105. Graph. Frequency of occurrence histogram of λ for the lateral displacement of GRS walls and abutments using the Adams method 106
Figure 106. Graph. Probability plot for measured and predicted lateral displacement of GRS walls using the Adams method 106

LIST OF TABLES

Table 1. FHWA materials and construction requirements for engineered granular fills 2
Table 2. General considerations for select structural backfill 3
Table 3. Criteria for settlement of shallow foundations of bridges 13
Table 4. WSDOT settlement criteria for bridge piers and abutments 14
Table 5. Properties of test sands 23
Table 6. Geotextile properties 25
Table 7. Placed geogrid strength 27
Table 8. Summary of the maximum displacements of the front wall facing and of the settlements of the bridge abutment footing 28
Table 9. GRS pier materials and results recorded from vertical deformation survey 35
Table 10. Parametric study on aggregate size 36
Table 11. GRS retaining wall dimensions 41
Table 12. Representative soil parameters 42
Table 13. Test conditions and results summary of GSGC tests 48
Table 14. Soil and foundation parameters for the case histories 76
Table 15. Predicted and measured immediate settlements of shallow foundations using the modified Schmertmann method 77
Table 16. Predicted and measured immediate settlements of shallow foundations using the Hough method 79
Table 17. Predicted and measured immediate settlements of shallow foundations using the Peck and Bazaraa method 81
Table 18. Predicted and measured immediate settlements of shallow foundations using the Burland and Burbidge method 83
Table 19. Predicted and measured immediate settlements of shallow foundations using the D'Appolonia method 85
Table 20. Summary of the statistical analyses of the five prediction methods for immediate settlement of shallow foundations on granular soil, results from this study 87
Table 21. Summary of the statistical analyses of the five prediction methods for immediate settlement of shallow foundations on granular soil, results from Gifford 87
Table 22. Abutment and GRS wall parameters in case histories 88
Table 23. Predicted and measured vertical displacements of abutments and GRS walls 89
Table 24. Abutment and GRS wall parameters in case histories 91
Table 25. Predicted and measured maximum lateral displacements of GRS walls at EOC using the FHWA method 92
Table 26. Predicted and measured lateral displacements of GRS walls and abutments using the Geoservices method 94
Table 27. Predicted and measured maximum lateral displacements of GRS walls using the CTI method 97
Table 28. Predicted and measured lateral displacements of GRS walls and abutments using the Jewell-Milligan method 100
Table 29. Predicted and measured lateral displacements of GRS walls and abutments with modular block facing using the Wu method 102
Table 30. Predicted and measured lateral displacements of GRS walls and abutments using the Adams method 105

Table 31. Summary of the statistical analyses of the six prediction methods for lateral displacements of GRS abutments and walls 107

LIST OF ABBREVIATIONS AND SYMBOLS

Abbreviations

3D	three-dimensional
AASHTO	American Association of State Highway and Transportation Officials
ADOT	Arizona Department of Transportation
CR	covering ratio
CMU	Concrete Masonry Unit
COV	coefficient of variation
CTI	Colorado Transportation Institute
DC	Defiance County, OH
EOC	end of construction
FE	finite element
FEA	finite element analysis
FEM	finite element method
FHWA	Federal Highway Administration
GRS	geosynthetic reinforced soil
GSGC	generic soil geosynthetic composite
IBS	integrated bridge system
LRFD	load and resistance factor design
LTDS	long-term design strength
LVDT	linear voltage displacement transducer
MSE	mechanically stabilized earth
NHI	National Highway Institute
PET	polyester
POT	potentiometer
PI	Plasticity Index
PP	polypropylene
PT	performance test
RC	relative compaction
RSF	reinforced soil foundation
SHRP	Strategic Highway Research Program

SLS	service limit state
SPT	standard penetration test
SRW	segmental retaining wall
TF	Turner-Fairbank
TFHRC	Turner-Fairbank Highway Research Center
ULS	ultimate limit state
UX	uniaxial
WSDOT	Washington State Department of Transportation
WWM	welded wire mesh

Symbols

a	footing offset from the edge of the wall face (i.e., setback distance)
B	width of foundation
b	length of reinforcement layers below foundation
$b¢$	width of facing block
$b_{q,vol}$	width of the load along the top of the wall (including the setback)
c	cohesion
C_1	correction factor for strain relief due to soil excavation for foundation embedment used in Schmertmann method
C_2	correction factor to consider creep as the time-dependent increase in settlement for t number of years after construction used in Schmertmann method
d	depth of bearing bed reinforcement
d_{max}	maximum aggregate size
D_f	depth of embedment of foundation
D_L	lateral displacement of GRS abutments in response to a vertical load
D_R	soil relative density
D_v	vertical settlement in the GRS abutment
D_{10}	particle diameter at which 10 percent of the sample is finer, by mass
E_{GRS}	Young's elastic modulus of GRS composition
E_R	elastic modulus of reinforcement
E_s	elastic modulus of soil
h	spacing of reinforcement layers
H	height of abutment/pier

H_i	thickness of each soil layer
k_b	interface stiffness between backfill soil and reinforcement layers
K_h	horizontal earth pressure coefficient
K_{reinf}	stiffness of reinforcement
L	length of foundation/reinforcement layers within pier or abutment
L_{as}	distance between adjacent supports
L_{total}	total length of foundation
n	time dependency exponent in time-dependent settlement equation
N	number of reinforcement layers
N_0	total number (population) of values
N_{60}	standard penetration number that is corrected based on the field conditions
$(N_1)_{60}$	corrected SPT blow count
N-value	blow count for an SPT sampler to penetrate the second and third 6 inches into the subsoil
p	footing bearing pressure
q	applied pressure
q_c	static cone resistance of cone penetration test
R^2	coefficient of determination
S_v	vertical spacing between reinforcement
s/B	ratio of settlement of foundation to its width
T_f	tensile strength
t	time
t_R	thickness of reinforcement
u	embedment depth of top geogrid layer
z	standard normal variable
Z	depth from the crest of wall
z_i	depth of influence zone
d_h	lateral displacement of a GRS wall or abutment with flexible facing
ΔH_{100}	differential settlement 100 ft (30.5 m) within pier or abutment and between piers
Δ_i	lateral movement of a GRS wall with modular block facing
Δp	net uniform pressure applied at the foundation depth used in Schmertmann method

γ_b	bulk unit weight of facing (such as modular block)
γ_s	unit weight of soil
ε_d	strain limit
η	arithmetic mean of λ
λ_i	sampled λ value
ϕ	friction angle
ϕ_{ds}	friction angle of soil based on direct shear test
ψ	dilation angle of soil
δ	friction angle between modular block facing elements
δ_h	lateral deformation of a GRS wall or abutment
δ_{max}	maximum lateral deformation of a GRS wall or abutment
δ_R	relative displacement coefficient
$\sigma_0^{'}$	initial average effective stress of the subdivided soil layer
σ	standard deviation
η	arithmetic mean of bias value
λ	bias value (ratio of the measured value to the predicted value)

CHAPTER 1. OVERVIEW OF BRIDGE SUPPORTS USING ENGINEERED FILLS

1.1 INTRODUCTION AND SCOPE OF WORK

This report focuses on the service limit states (SLSs) of deformations and stresses of engineered fills used as bridge supports for abutments and piers. The engineered fills focus on compacted granular engineered fills of mineral origin and reinforced soil systems. The SLSs ensure the durability and serviceability of a bridge and its components under typical everyday loads, traditionally termed "service loads."[1] In this report, "service limit" refers to the vertical and lateral deformations of bridge supports.

The use of engineered fills with and without layered reinforced soil systems is an economical solution to reduce deformations and improve bearing resistance of shallow foundations for bridge supports. Notable studies of spread footings on engineered fills published by the Federal Highway Administration (FHWA) concluded that this technique was a suitable alternative to deep foundations.[2,3] Engineered fills can be used to support bridge abutments and piers with various configurations. In bridge abutments, the engineered fills can be compacted granular fills or compacted granular fills with metallic or geosynthetic reinforcement, while in bridge piers, the engineered fills can be compacted granular fills or compacted granular fills with geosynthetic reinforcement. Bridge supports using reinforced engineered fills contribute to better compatibility of deformation between the components of bridge systems, thus minimizing the effects of differential settlements and the occurrence of undesirable "bumps" between the bridge deck and the approach embankment transitions.[4] Recent FHWA national surveys revealed that State transportation departments have safely and economically constructed highway bridges supported on spread footings bearing on competent and improved natural soils as well as engineered granular and mechanically stabilized earth (MSE) fills.[5]

Despite these advantages, many transportation agencies do not consider shallow foundation alternatives, even when appropriate, for a variety of reasons, including concerns related to meeting serviceability requirements (e.g., vertical and lateral deformations). Due to the large size of spread footings for highway bridges, soil bearing failure is not likely.[6] Therefore, the performance of spread footings in highway bridge design is evaluated primarily on the basis of vertical displacement (i.e., settlement and how differential settlements affect angular distortion).[7] SLS for shallow foundations often controls the design of bridge foundations; however, little guidance on SLS has been provided for engineered fills.[8] According to the American Association of State Highway and Transportation Officials (AASHTO) *Manual for Bridge Evaluation*, SLS relates to stress, deformation, and cracking.[9] The Strategic Highway Research Program 2 (SHRP2) report, *Bridges for Service Life Beyond 100 Years: Service Limit State Design* presents the existing limit states and tolerances of bridge components set forth by various agencies in the United States and internationally.[10]

1.2 SUMMARY OF ENGINEERED FILLS

FHWA defines *engineered granular fill* as high-quality granular soil selected and constructed to meet certain material and construction specifications (also called "compacted structural fill" and "compacted granular soil").[5] Engineered fill may be reinforced with geosynthetics or metal

strips. The high quality refers to gradation, soundness, compaction level, durability, and compatibility. Such specifications are further described in table 1 and table 2.

A number of State transportation departments, including the Washington State Department of Transportation (WSDOT), the New Mexico Department of Transportation, and the Minnesota Department of Transportation, have successfully utilized compacted engineered granular fills.[5] For example, based on a survey of 148 bridges in Washington, FHWA concluded that spread footings on engineered fill can provide a satisfactory alternative to deep foundations, especially if high-quality fill materials are constructed over competent foundation soil.[2] National Cooperative Highway Research Program Report No. 651 reported higher resistance factors for the compacted granular fill than natural granular soil because of better control for compacted fill.[11] Nevertheless, concerns exist regarding the use of spread footing bearing on engineered granular and MSE fills. A number of State transportation departments have allowed and constructed spread footings on natural soils but not on engineered granular and MSE fills due to the concerns related to the quality and uniformity of compacted fill materials as well as costly design and construction of bridge footings on MSE walls.[5] Table 1 lists the FHWA material and construction requirements for engineered granular fills.[12]

Table 1. FHWA materials and construction requirements for engineered granular fills.[12]

Soil Properties	Requirements	
	U.S. Sieve Size	**Percentage Passing (percent)**
Gradation (AASHTO T27)[13]	4 inches	100
	#40 (0.0165 inch)	0–70
	#200 (0.0029 inch)	0–15

1 inch = 25.4 mm

Additional general considerations in selecting structural backfills are as follows:[6]

- **Plasticity Index (PI) (AASHTO T90)**: PI < 6 percent.[14]
- **Soundness**: Based on AASHTO T104.[15]
- **Compaction level**: Compaction level is 100 percent of maximum dry density based on standard Proctor test per AASHTO T99; moisture content should be ±2 percent of optimum moisture content.[16]

Table 2 provides general considerations in selecting structural backfills, as highlighted in FHWA's *Soils and Foundations Reference Manual: Volume I*.[6]

Table 2. General considerations for select structural backfill.[6]

Consideration	Comments
Lift thickness	Limit to 6 to 8 inches so compaction is possible with small equipment.
Topsize (largest particle size)	Limit to less than three-fourths of lift thickness.
Gradation/percent fines	Use well-graded soil for ease of compaction. Typical gradation is as follows: · 4-inch sieve = 100 percent passing by weight. · #40 sieve (0.0165 inch) = 0 to 70 percent passing by weight. · #200 sieve (0.0029 inch) = 0 to 15 percent passing by weight. The limitation on percent fines (particles smaller than #200 sieve) is to prevent piping and allow gravity drainage. For rapid drainage, consideration may be given to limiting the percent fines to 5 percent.
PI	PI should not exceed 10 to control long-term deformation.
Durability	This consideration attempts to address breakdown of particles and resultant settlement. The material should be substantially free of shale or other soft, poor-durability particles. Where the agency elects to test for this requirement, a material with a magnesium sulfate soundness loss exceeding 30 should be rejected.
AASHTO T99 density control[16]	Small equipment cannot achieve AASHTO T180 densities. Minimum of 100 percent of standard Proctor maximum density is required.[17]
Compatibility	Particles should not move into voids of adjacent fill or drain material.

1 inch = 25.4 mm

The FHWA report, *Soils and Foundations Reference Manual: Volume II*, recommends that compacted structural fills used for supporting spread footings should be a select and specified material that includes sand- and gravel-sized particles.[18] Furthermore, the fill should be compacted to a minimum relative compaction (RC) of 95 percent based on the modified Proctor compaction energy, and structural fill should extend for the entire embankment below the footing.

In the United States, the concept and principles of MSE technology were introduced in 1969.[19] There are two basic types of soil reinforcements in MSE structures: inextensible (metallic) and extensible (polymeric). Metallic reinforcement has been primarily used as the reinforcement of soils. The first reported MSE abutment in the United States was constructed in 1974 in Lovelock, NV, to support a precast bridge span of 70 ft (21 m).[20] MSE structures built with inextensible reinforcement, such as discrete metallic strips or welded wire mats, have a unique combination of precast panels, reinforcement, and connection details.[21] For bridge supports using extensible geosynthetics, Adams is among the first to report on the performance of a pre-strained geosynthetic reinforced soil (GRS) bridge pier, which demonstrated the feasibility of such a technique in bridge supports. [22] Since then, many full-scale studies on GRS as bridge supports and many bridge abutments built using such technologies continued to recognize its advantage over conventional bridge supports. (See references 5 and 23–29.) Moreover,

engineered fills have been used for bearing of bridge abutments in other countries and have also proven to be effective.[30,31] These previous studies have shown that engineered fills offer advantages of improved performance and savings in labor costs, equipment, and time. Cost savings could total up to 65 percent compared to conventional deep foundations for bridge systems.[18]

For GRS abutments, backfill selection is important because it is a major structural component for the abutment. FHWA's *Geosynthetic Reinforced Soil Integrated Bridge System Interim Implementation Guide* provides recommendations for the gradations for well-graded and open-graded backfills used for GRS abutments.[32] "Open-graded material" refers to a gradation where skips between the sieve gradations have been deliberately achieved so that the voids are not filled with intermediate-size particles. The main criteria are: (1) there is a minimum friction angle (f) of 38 degrees, (2) the maximum grain size is between 0.5 and 2 inches (13 and 51 mm), (3) PI should be less than or equal to 6, (4) the mass percentage of soils finer than #200 sieve should be less than 12 percent, and (5) the backfill shall be substantially free of shale or other poor durability particles, and the material shall have a magnesium sulfate loss of less than 30 percent after four cycles (or a sodium value less than 15 percent after five cycles).

In addition to the gradation requirement, backfill selection depends on the following factors:[32]

- Ability to ensure compaction.
- Open-graded backfill is recommended for an abutment located in a flood zone to facilitate the flow of water out of the abutment.
- Open-graded fine aggregates (i.e., about 0.5 inch (12.7 mm)) are easier to spread, level, and compact than well-graded fill.
- Angular particles are recommended to maximize the shear strength and minimize the compressibility of the GRS mass.

FHWA indicated that for GRS abutments, reinforced soil foundation (RSF), and approach-way backfills for GRS integrated bridge systems (GRS-IBSs), the backfill of well-graded aggregates must be properly compacted to a minimum of 95 percent of maximum dry density according to AASHTO T99.[32,16]

As of 2012, all GRS-IBS projects had selected open-graded gravel due to its relative ease of construction and drainage characteristics. The various counties and agencies that are building GRS-IBS have selected locally available structural backfills for their projects.[21] Adams et al. provided the fill gradations of five GRS-IBS projects; the majority of the grains were in the range of 0.375 to 1 inch (9.5 to 25.4 mm), but their size distributions varied.[21] It is noted that how the different grain sizes affect the load-deformation behavior remains to be studied.

Using different types of engineered fills for bridge support has its benefits and limitations. One benefit is that contractors and bridge owners have wider choice and availability of backfill materials; this will result in savings in cost and labor.

The limitations include the following:

- Currently, granular soils and aggregates are mainly used as engineered fills for bridge support, while the performance of other types of engineered fills, such as those with higher fine content, remain uncertain.

- When higher fines content exists in fills supporting bridge substructures, segregation can occur, and drainage of backfill can be compromised. This directly affects the stability and compressibility of the foundation and bridge structure.

- Strength, compressibility, and index properties of other types of engineered fills may not meet the requirements for bridge supports, thus making them less desirable than other fill types.

1.3 BRIDGE SUPPORTS USING UNREINFORCED ENGINEERED FILLS

Special details and specifications are necessary when constructing a compacted structural fill to support a bridge foundation such as an abutment. Figure 1 shows the recommended details for construction of a structural approach embankment and bridge foundation. The material specifications are chosen so that the engineered fill material is capable of being compacted to a firm, non-yielding condition to support a bridge abutment spread footing. FHWA's *Geotechnical Engineering Circular No. 6: Shallow Foundations* recommends that structural fill for highway embankment material should not include unsuitable or deleterious material such as peat, muck, wood, organic waste, coal, charcoal, or any other material that would perform poorly in an embankment.[12]

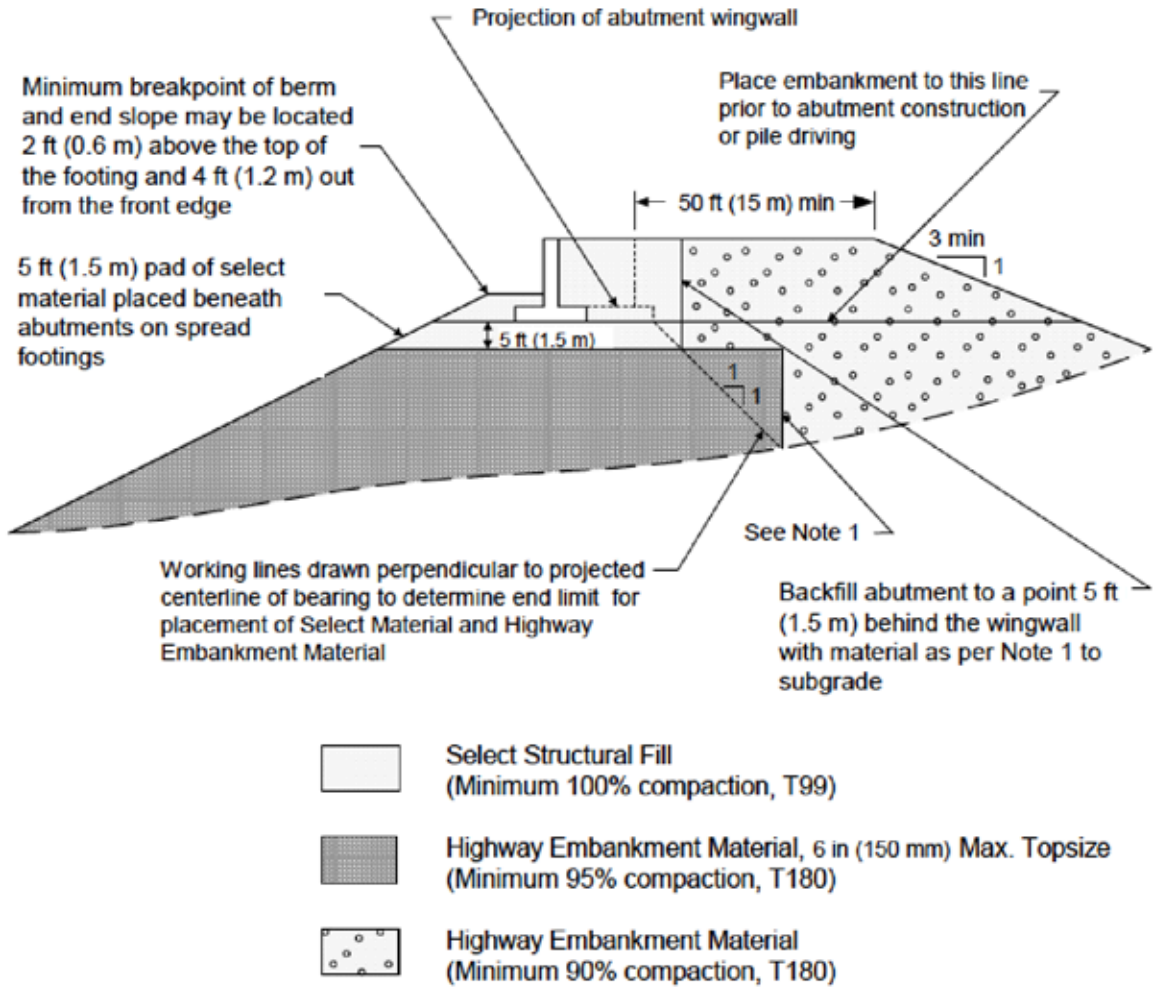

Note 1: Highway embankment material and select material shall be placed simultaneously of the vertical payment line

1 ft = 0.305 m

Figure 1. Illustration. Engineered fill details of structural approach road and bridge foundation.[33]

1.4 BRIDGE SUPPORTS USING MSE

Since the first MSE abutment was constructed in the United States in 1974, MSE technology has been used in bridge-supporting structures such as bridge abutments, and both metallic and geosynthetic reinforcements have been used.[34] MSE abutments are MSE retaining walls subjected to much higher area loads that are located close to the wall face. Using MSE structures as direct support for bridge abutments can be a significant simplification in the design and construction of current bridge abutment systems and may lead to faster construction of highway bridge infrastructure. When a bridge beam is supported on a spread footing that bears directly on top of an MSE structure, this configuration is known as true MSE abutment, as shown in figure 2. To prevent overstressing the soil from the excess load exerted on a true MSE abutment, the beam seat is sized so that the centerline of bearing is at least 3.05 ft (1 m) behind the MSE

wall face, and the service bearing pressure on the reinforced soil is no more than 4 kip/ft^2 (192 kPa).[34] Anderson and Brabant reported that there are approximately 600 MSE abutments (300 bridges) built annually in the United States, of which 25 percent are true MSE abutments.[34]

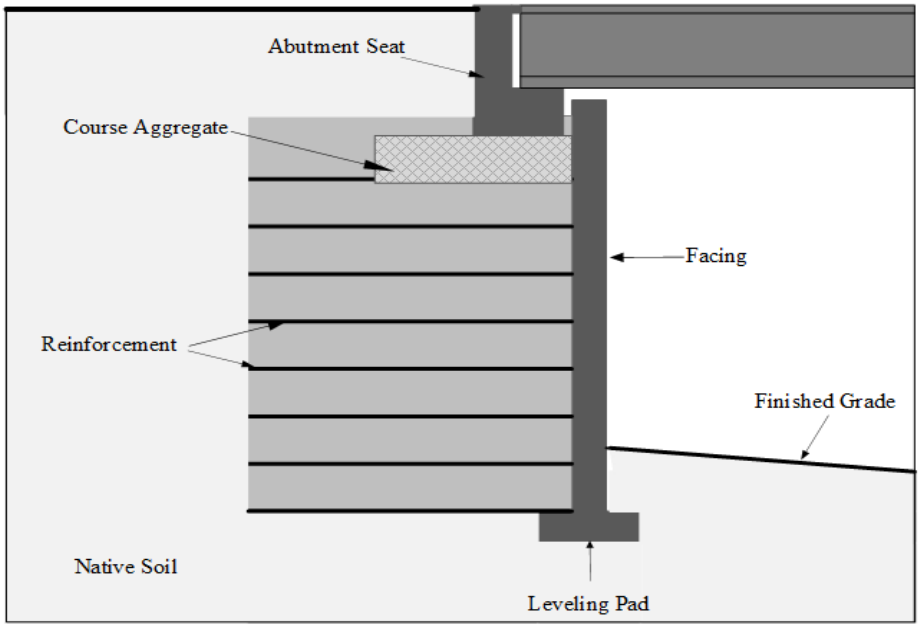

Note: This figure was created by FHWA after Anderson and Brabant.[34]

Figure 2. Illustration. True MSE abutment types.

MSE abutments may result in construction cost savings where deep foundations are not needed. Additionally, the use of true bridge abutments can result in significant cost savings.[34] True bridge abutments also have significant advantages over conventional abutments. The proverbial bump at the end of the bridge is alleviated because the footing settles along with the MSE wall in contrast to a deep foundation that does not settle at the same rate. Additionally, approach slabs are not necessary because of the elimination of conditions that would lead to the bump at the end of the bridge, and the elimination of approach slabs results in significant cost savings.[7] While there are proven advantages of MSE abutments, there are some limits for their applicability, as with any technology. A study by Purdue University and the Indiana Department of Transportation revealed that MSE structures on shallow foundations should not be used as direct bridge abutments when soft soil layers, such as normally consolidated clays, are present near the surface where significant deformation and differential settlement are expected.[4] In such conditions, a design configuration including piles should be used. In more competent foundation profiles, MSE walls can be used for direct support of bridge abutments.

1.5 BRIDGE SUPPORTS USING GRS

GRS technology consists of closely spaced layers of geosynthetic reinforcement and compacted granular fill material. GRS has been used for a variety of earthwork applications since the U.S. Forest Service first used it to build walls for roads in steep mountain terrain in the 1970s.[21] The spacing of GRS reinforcement should not exceed 12 inches (304.8 mm) and is typically 8 inches (203.2 mm).[21] As shown in figure 3, GRS-IBS typically includes an RSF, a GRS abutment, and

a GRS integrated approach to transition to the superstructure. The RSF is composed of granular fill material that is compacted and encapsulated with a geotextile fabric. The application of GRS has several advantages: the system is easy to design and economically construct; it can be built in variable weather conditions with readily available labor, materials, and equipment; and it can easily be modified in the field.[21] Figure 4 shows an illustration of RSF and the common parameters used in RSF in this report.

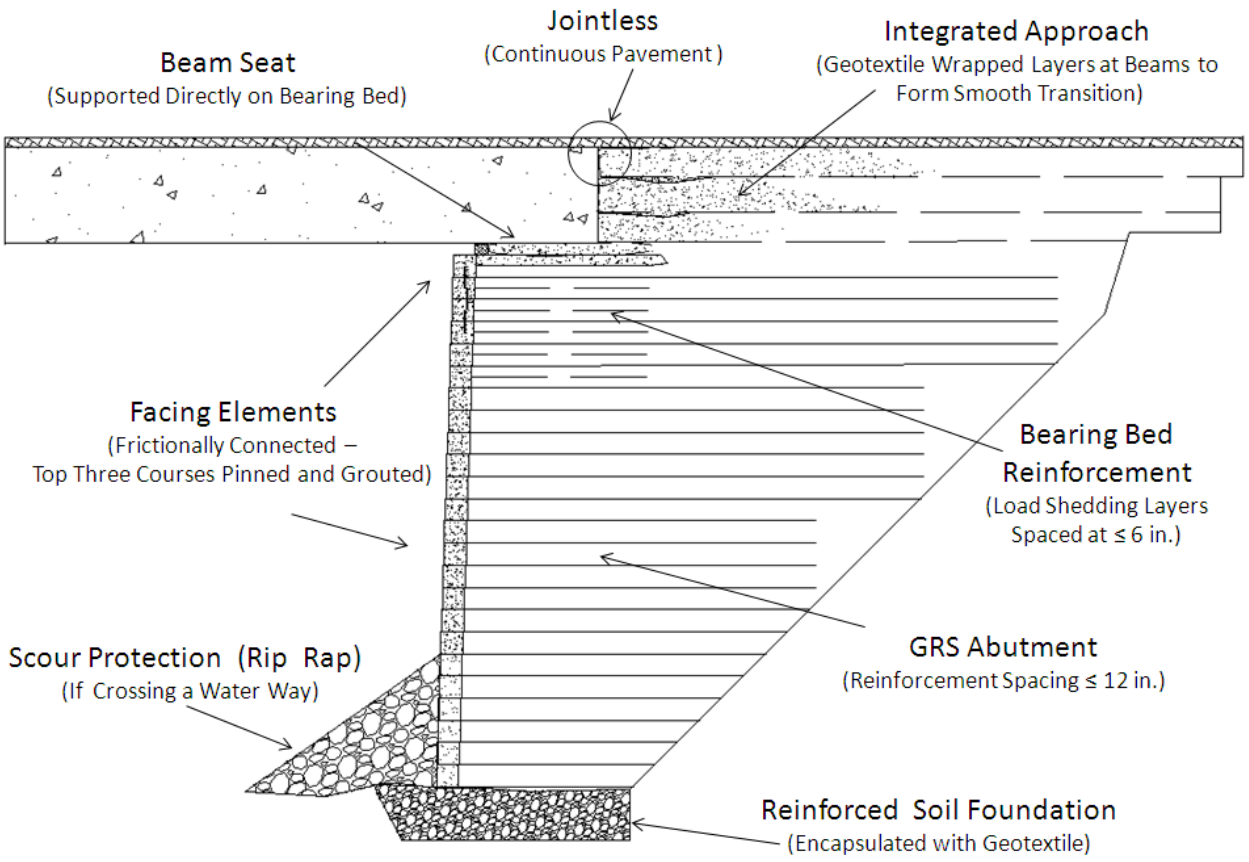

1 inch = 25.4 mm

Figure 3. Illustration. Typical cross-section of GRS bridge abutment.[21]

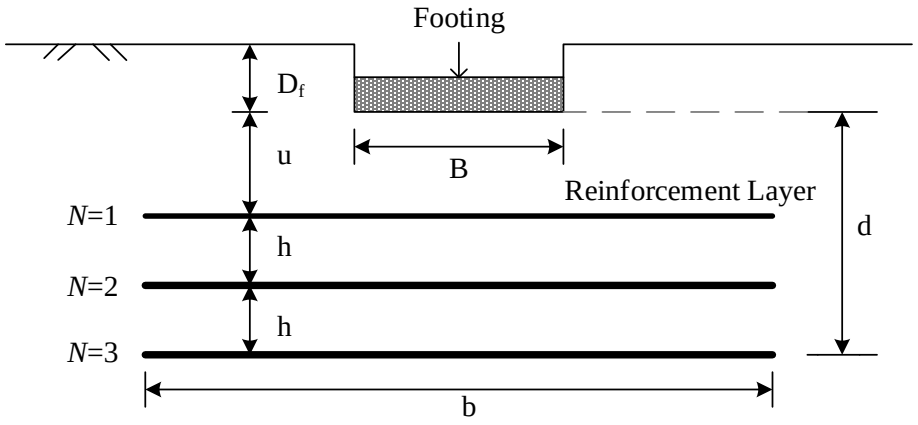

Figure 4. Illustration. Annotations of parameters of a shallow foundation on reinforced soil.

Where:

B = Width of foundation.
b = Length of reinforcement layers below foundation.
N = Number of reinforcement layers.
u = Embedment depth of top geogrid layer.
h = Spacing of reinforcing layers.
d = Depth of bearing bed reinforcement.
D_f = Depth of embedment of foundation.

CHAPTER 2. CURRENT SLS DESIGN PROCEDURES AND CRITERIA

2.1 *AASHTO LOAD AND RESISTANCE FACTOR DESIGN (LRFD) BRIDGE DESIGN SPECIFICATIONS*[8]

The *AASHTO LRFD Bridge Design Specifications* incorporates limit state design in LRFD.[8] A "limit state" is a condition beyond which a bridge component ceases to satisfy the criteria for which it was designed. All possible structural and geotechnical failure modes for foundations that can lead to bridge failure are grouped into three distinct structural and geotechnical limit states: SLS, strength limit state, and extreme event limit state.[8] The SLSs are defined as the limit states related to stress, deformation, and cracking under regular operating conditions. In SLSs, *failure* may be defined as exceeding the tolerable displacement. For example, the foundations must have adequate structural and geotechnical stiffness to keep the bridge displacements less than the bridge tolerable displacements. The failure modes in strength limit states are related to the strength and stability of the foundations under loads and conditions applied continuously or frequently during the bridge design life. The failure modes in extreme event limit states are related to the strength and stability of the foundations under loads and conditions applied during certain events that have a return period greater than the bridge design life. LRFD of spread footings at all limit states is prescribed in the *AASHTO LRFD Bridge Design Specifications*.[8] SLS design (Article 10.6.2) covers the settlement and overall stability of spread footings, and Article 10.6.2.4 describes the methods that should be used to estimate settlement of spread footings of bridges on cohesionless and cohesive soils.[8]

Although not explicitly prescribed in the current *AASHTO LRFD Bridge Design Specifications*, the SLS design of engineered fills follows the same acceptance criterion used for bridge foundations.[8] Namely, the estimated movement must not exceed the tolerable movement. Thus, current practice uses a variety of empirical, semi-empirical, and numerical modeling approaches to estimate fill deformation, and tolerable movement criteria are based on the permissible deformation of a bridge abutment, approach slab, pavement, or other structural feature in or on the fill.

2.2 BRIDGE SUPPORTS USING MSE

Guidelines for the static design of MSE walls have been published by AASHTO and FHWA. (See references 8 and 35–37.) A study by Koerner and Soong compared three static MSE design methods: the modified Rankine method, the FHWA method, and the National Concrete Masonry Association method.[38,39] They found that the FHWA method provided a factor of safety value between those by the other two methods. Guidelines for the design of MSE as true bridge abutments are also available that limit MSE settlement to 0.5 inch (13 mm) if service loads are kept below 27.84 psi (192 kPa), but details on the parameters impacting the deformation response are still lacking.[21,32,37] In addition, the parameters used (e.g., f, cohesion (c), etc.) may vary depending on the measurement technique and the design method selected, which may have an impact on the SLS analysis.

The FHWA National Highway Institute (NHI) reference manual, *Mechanically Stabilized Earth Walls and Reinforced Soil Slopes Design and Construction Guidelines*, provides a design method

for MSE bridge abutments.[36] In addition, the FHWA NHI manual, *Design of Mechanically Stabilized Earth Walls and Reinforced Soil Slopes—Volume I*, suggests that the following conditions be implemented in the design of MSE abutments:[37]

- The tolerable angular distortions (i.e., limiting differential settlement) between abutments or between piers and abutments should be limited to $0.005L_{as}$ for simple-span bridges and $0.004L_{as}$ for continuous-span bridges, where L_{as} is the distance between adjacent supports.

- A minimum offset of 3.05 ft (1 m) from the front of the facing to the centerline of the bridge bearing is required.

- A clear distance of 6 inches (150 mm) between the back face of the facing units and front edge of footing is required.

- The abutment should be placed on a 3.05-ft (1-m)-thick bed of compacted coarse aggregate where significant frost penetration is anticipated.

- The bearing capacity on the reinforced volume should be limited to 4,000 lb/ft^2 (192 kPa).

- The maximum horizontal force at each reinforcement level should be used for the design of connections to the facing units.

- The density, length, and cross-section of reinforcements of the abutment should be extended to wing walls for a horizontal distance of $0.5H$, where H is the height of the abutment wall.

- The seismic design forces should also include seismic forces transferred from the bridge through bearing supports that do not slide freely (e.g., elastomeric bearings).

2.3 BRIDGE SUPPORTS USING GRS

FHWA's *Geosynthetic Reinforced Soil Integrated Bridge System Interim Implementation Guide* provides the current design procedure for GRS abutments.[32] The guide notes that the design methods are appropriate for GRS structures (an abutment and wing walls) with a vertical or near vertical face and at a height that does not exceed 30 ft (9.15 m). The bearing stress on the GRS abutment is limited to a service load of 4,000 lb/ft^2 (192 kPa). The guide recommends that engineers should limit bridge spans to approximately 140 ft (42.7 m) since the SLS performances (such as thermal-induced movements) of longer spans on GRS-IBS were not as well understood.[32] GRS abutment capacities are dependent on a combination of the strength of the fill material and the strength of the reinforcement when built in accordance with the two rules of GRS construction: (1) good compaction (95 percent of maximum dry unit weight, according to AASHTO T99 for well-graded aggregate backfill) of high-quality granular fill and (2) closely spaced layers of reinforcement (less than or equal to 12 inches (304.8 mm)).[16]

Basic design guidelines for GRS foundations are available that outline recommended spacing along with length and depth of reinforcement layers for pier foundations and abutment supports.[32,40] The work is largely based on load tests on reinforced soil shallow foundations and performance tests (PTs) on abutment supports.[41,22,42] However, the design guidelines are limited to the conditions and parameters under which testing has occurred. While recent FHWA research has added to the database and provided recommendations on methods to limit deformations to a target value, quantifying the vertical and lateral deformations is still empirically based.[42]

2.4 CURRENT SLS CRITERIA FOR BRIDGE SUPPORTS

In general, foundation movement criteria should be consistent with the function and type of structure, anticipated service life, and consequences of unacceptable movements on structure performance. Specifications and reports published by FHWA, AASHTO, and some State transportation departments provide criteria for the settlement of shallow foundations of bridges and vertical and horizontal deformations of bridge abutments and piers. The following section summarizes the current SLS criteria for bridge supports using shallow foundations.

Criteria for Settlement of Shallow Foundations of Bridges

According to section 11 in *AASHTO LRFD Bridge Design Specifications*, "Abutments, piers, and walls shall be investigated for excessive vertical and lateral displacement, and overall stability, at the service limit state."[8] The vertical settlements of bridge foundations can be expressed in terms of *angular distortion*, which is defined as the differential settlement divided by span length. Uneven displacements of bridge abutments and pier foundations can affect the ride quality, functioning of deck drainage, and the safety of the traveling public as well as the structural integrity and aesthetics of the bridge. Such movements often lead to costly maintenance and repair measures.[10] Table 3 shows the criteria from various reports. Three different reports show the same criteria for the angular distortion for continuous span bridges, while the criteria for the angular distortion for simple span bridges vary.

Table 3. Criteria for settlement of shallow foundations of bridges.

Aspects Used for Settlement Evaluation	Source		
	Moulton et al. and Elias et al.[43,36]	**Moulton et al.[44]**	***AASHTO LRFD Bridge Design Specifications*[8] (based on Moulton et al., DiMillio, and Barker et al.[44,2,45])**
Maximum angular distortion for continuous span bridges	0.004	0.004	0.004
Maximum angular distortion for simple span bridges	0.005	0.007	0.008

WSDOT provided the differential settlement criteria and the associated action based on the total settlement. Table 4 lists the settlement criteria for pier and abutment.[46]

Table 4. WSDOT settlement criteria for bridge piers and abutments.[46]

Total Settlement at Pier or Abutment (ΔH)	Differential Settlement 100 ft within Pier or Abutment and between Piers (ΔH_{100})	Action
$\Delta H \leq 1$ inch	$\Delta H_{100} \leq 10.75$ inches	Design and construct the bridge foundation, since criteria are met.
1 inch < $\Delta H \leq 4$ inches	0.75 inches < $\Delta H_{100} \leq 3$ inches	Ensure structure can tolerate settlement.
$\Delta H > 4$ inches	$\Delta H_{100} > 3$ inches	Obtain approval* prior to proceeding with design and construction.

1 ft = 0.305 m
1 inch = 25.4 mm
*Approval of WSDOT State Geotechnical Engineer and WSDOT Bridge Design Engineer required.

Chapter 10 of Arizona Department of Transportation's (ADOT) *Bridge Design Guidelines* states the following:

> "The bridge designer should limit the total settlement of a foundation per 30 m (100 ft) span to 13 mm (0.5 in). Linear interpolation should be used for other span lengths. Higher total settlement limits may be used when the superstructure is adequately designed for such settlements. The designer shall also check other factors such as rideability and aesthetics. Any total settlement that is higher than 2.5 in, per 30 m (100 ft) span, must be approved by the ADOT Bridge Group."[47]

Through tolerable movement analysis of 148 highway bridges supported by spread footings on compacted fill throughout Washington, an FHWA report concluded that these bridges have easily tolerated differential settlement of 1 to 3 inches (25.4 to 76.2 mm) without serious distress.[2] Based on field studies of 314 bridges and theoretical analyses, Moulton et al. found that the bridges that performed acceptably had average settlement of 2 inches (50.8 mm).[43]

Tolerable Horizontal Deformation Criteria for Bridge Supports

Horizontal deformations cause more severe and widespread problems for highway bridge structures than do equal magnitudes of vertical movement.[10] The data presented by Moulton et al. also show that horizontal movements resulted in more damage when accompanied by settlement than when occurring alone.[44] Tolerance of the superstructure to horizontal (lateral) movement depends on bridge seat or joint widths, bearing type(s), structure type, and load distribution effects. Moulton et al. found that horizontal movements less than 1 inch (25.4 mm) were almost always tolerable, while horizontal movements greater than 2 inches (50.8 mm) were typically considered to be intolerable.[44] Wahls states, "Horizontal movements in excess of 2 inches (50 mm) appear likely to cause structural distress."[48] Moulton et al. recommends that horizontal movements be limited to 1.5 inches (38.1 mm).[40] Similarly, surveys of the performance of bridges by Bozozuk, Walkinshaw, and Wahls also indicate that horizontal abutment movements less than 1.5 inches (38.1 mm) can usually be tolerated by bridge superstructures without significant damage.[49–51]

On the other hand, abutments are often designed for active lateral earth pressure conditions, which require a certain amount of movement. Depending on the configuration of the bridge end spans and expansion joints, horizontal movements of an abutment can be restrained. However, such restraint can lead to an increase in the lateral earth pressures above the active earth pressures normally used in design. Samtani and Nowatzki recommends that, "Design of expansion joints should allow for sufficient movement to keep earth pressures at or close to their design values and still allow the joints to perform properly under all temperature conditions."(Chapter 8, pp. 69)[18]

Tolerable Deformation Criteria for Reinforced Bridge Supports

MSE walls can tolerate larger total and differential vertical deflections than rigid walls. The amount of total and differential vertical deflections that can be tolerated depends on the wall facing material, configuration, and timing of facing construction.[8] AASHTO states that abutments should not be constructed on MSE walls if the anticipated angular distortion is greater than 50 percent of the values recommended by Moulton et al. as shown in table 3.[52,44] For GRS abutment, the vertical strain should be limited to 0.5 percent unless the engineer decides to permit additional deformation, and the lateral strain should be limited to 1 percent.[32]

CHAPTER 3. LITERATURE REVIEW OF PREVIOUS WORK IN ENGINEERED FILLS FOR BRIDGE SUPPORTS

3.1 OVERVIEW OF LOAD DEFORMATION DATA CATALOG OF ENGINEERED FILLS FOR BRIDGE SUPPORTS

Various factors may affect the behavior of bridge supports using engineered fills. They include the following:

- Backfill soil types, unit weight, and strength parameters.
- Geosynthetic type and ultimate tensile strength (T_f).
- Reinforcement spacing, total depth of reinforcement placement (N), and horizontal length (extent) of reinforcement.
- Bridge support geometry.
- Foundation shape and size.
- GRS foundation soil type, density, strength parameters, and reinforcement.
- Natural soil type, unit weight, and strength parameters beneath the GRS foundation.
- Loading condition.
- Ambient temperature range.
- Effect of transient load versus static load on SLS of bridge supports.

The performance of bridge supports using engineering fills can be characterized by the following:

- Load bearing resistance (a check corresponding to ultimate limit state (ULS)).
- Immediate and long-term vertical and horizontal deformations of the reinforced and foundation soils (components of SLS design).

In this chapter, the factors that affect the behaviors of shallow foundations are synthesized based on the published results in the literature. They include factors affecting the settlement of shallow foundations with and without reinforcement and factors affecting vertical and lateral deformations of bridge piers and abutments using engineered fills. Further, the effects of transient loads on deformations of bridges supports on granular soils and the determination of stress distributions in granular soils under shallow foundations are reviewed. Based on the literature review, a load-deformation data catalog was compiled into an unpublished Microsoft® Excel spreadsheet.

3.2 SYNTHESIS OF FACTORS AFFECTING SETTLEMENT OF SHALLOW FOUNDATIONS

Effect of Relative Density of Soil on Settlement of Shallow Foundations

Fragaszy and Lawton performed a series of laboratory model tests designed to determine the influence of soil relative density (D_R) on the load-settlement behavior of reinforced sand.[53] The uniformly graded native sand was reinforced with three layers of aluminum foils in all tests. As figure 5 shows, in all cases, the ultimate bearing capacity increased with increasing D_R. Additionally, the load-settlement behavior of the strip footings on reinforced soil was stiffer than those bearing on unreinforced soil at the same relative density. The results show that with a 10 percent increase in D_R, at 14.5 psi (100 kPa) pressure, the settlement of the foundation decreased by about 20 percent. By reinforcing the soil, the ultimate bearing capacity of the foundation increased at least 60 percent at a ratio of settlement of foundation to its width (s/B) of 10 percent. Note that the increase in confinement with the addition of reinforcement layers suppressed the dilative behavior, as observed through the suppressed peak in load-settlement response. Basudhar et al. conducted an experimental study on circular footings resting on sand reinforced with geotextiles.[54] They concluded that the immediate settlement of the foundation decreased with an increase in D_R (see figure 6).

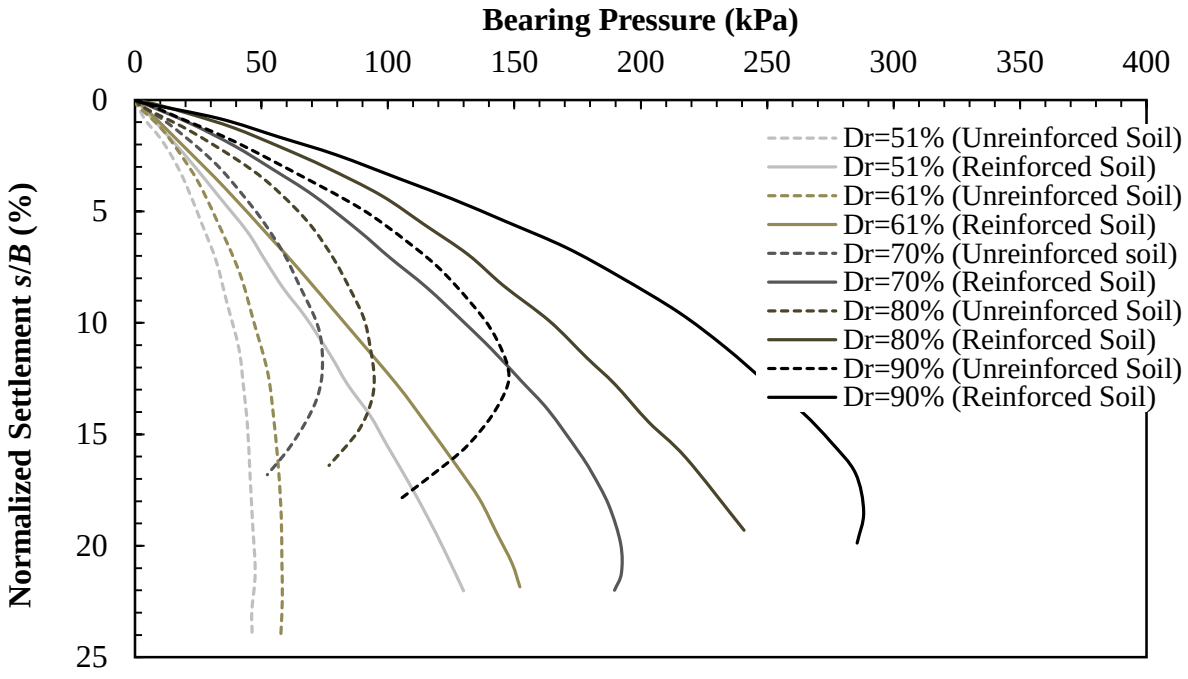

1 psi = 6.89 kPa

Note: This figure was created by FHWA after Fragaszy and Lawton.[53]

Figure 5. Graph. Load-settlement results on unreinforced and reinforced sand.

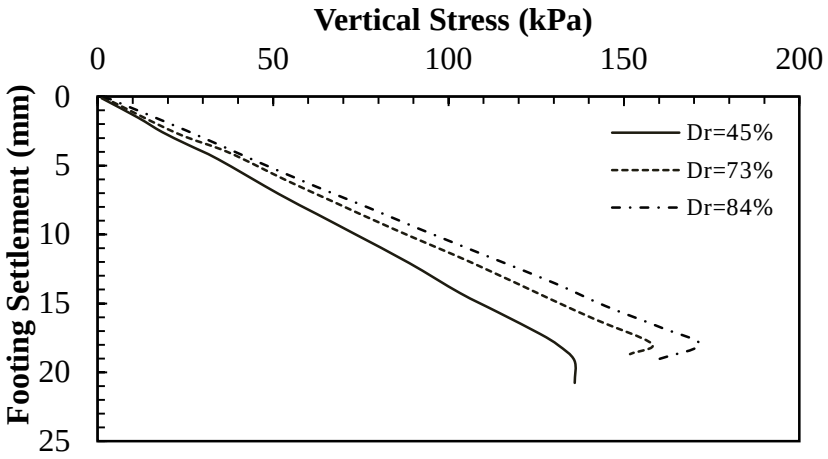

1 inch = 25.4 mm
1 psi = 6.89 kPa
Note: This figure was created by FHWA after Basudhar et al.[54]

Figure 6. Graph. Load-settlement results for different relative densities.

Effect of *N* on Settlement of Shallow Foundations

Omar et al. conducted a series of laboratory model tests on strip and square foundations supported by sand reinforced with geogrid layers.[55] As their results in figure 7 and figure 8 show, for similar values of applied load, the settlement of footings bearing on reinforced soil was lower than that on unreinforced soil. For tests with a strip foundation, when *N* increased from 1 to 3, the ultimate bearing load doubled, while the settlement at its respective ultimate load also almost doubled. At each applied pressure, the amount of settlement decreased with increasing *N*. for *N* greater than or equal to 4, the settlement at ultimate bearing load remained practically constant, indicating there is an optimum *N* beyond which the settlement at ultimate bearing load has insignificant improvement. It should be considered that based on the study by Omar et al., the effective depth of reinforcement is about 2*B* for strip foundations.[55] Therefore, in their experiment, by having $u/B = h/B = 0.33$ (the notations are shown in figure 4), reinforcements with *N* greater than or equal to 7 are placed out of the influence zone.

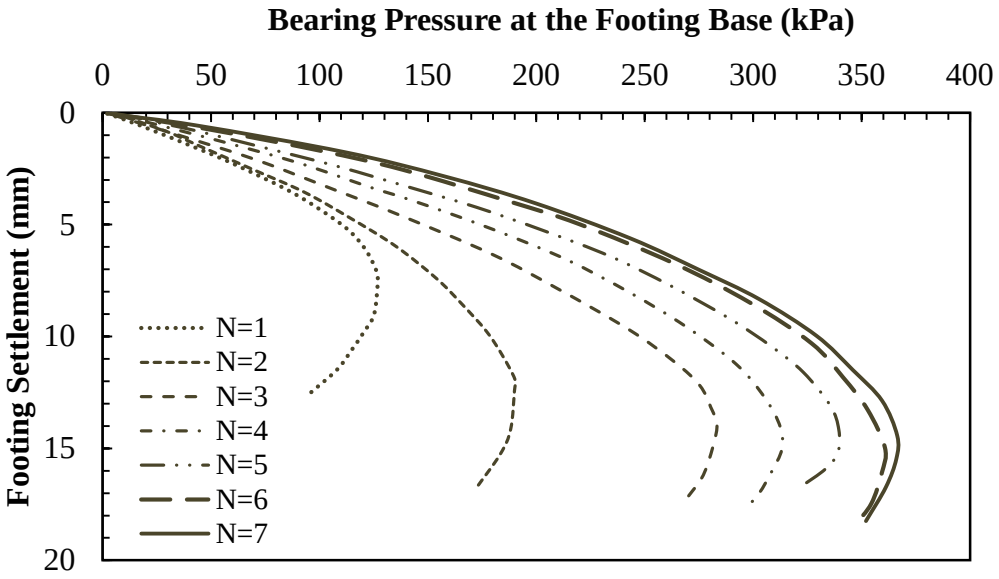

1 inch = 25.4 mm
1 psi = 6.89 kPa
Note: This figure was created by FHWA after Omar et al.[55]

Figure 7. Graph. Load-settlement results for strip footing for *u*/*B* = *h*/*B* = 0.333, *b*/*B* = 10.

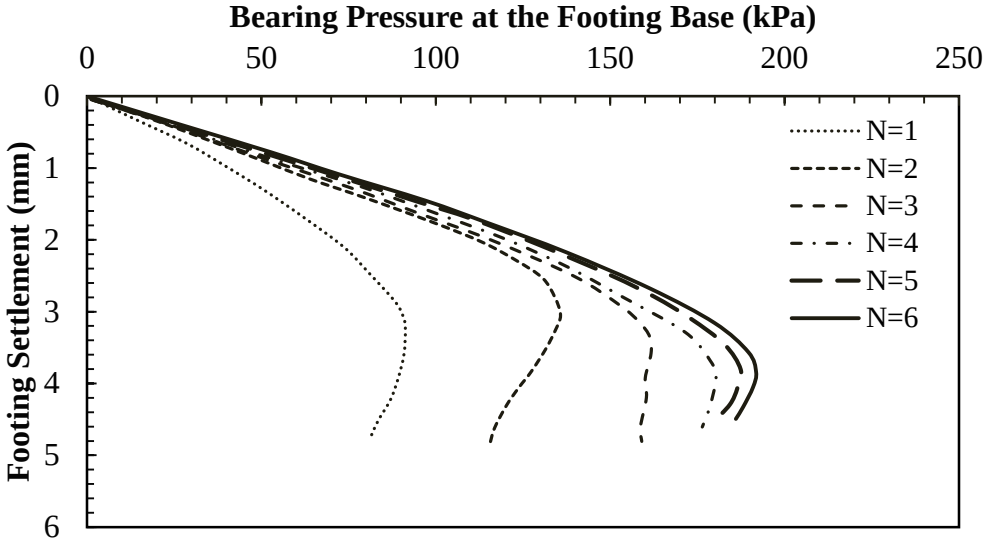

1 inch = 25.4 mm
1 psi = 6.89 kPa
Note: This figure was created by FHWA after Omar et al.[55]

Figure 8. Graph. Load-settlement results for square footing for *u/B* = *h/B* = 0.333, *b/B* = 6.

Chen et al. investigated the behavior of square foundations on geosynthetic-reinforced clayey soil with a PI of 15 percent using laboratory model footing tests.[56] The model footings used in the tests were steel plates with dimensions of 5.98 by 5.98 by 1 inch (152 by 152 by 25.4 mm) (width by length by thickness). The model tests were conducted in a 4.92- by 2.98- by 2.98-ft (1.5- by 0.91- by 0.91-m) (length by width by depth) steel test box. The testing procedure was

performed according to the ASTM D 1196-93, where the load increments were applied and maintained until the rate of settlement was less than 0.001 inch/min (0.03 mm/min) for 3 min consecutively.[57] The results, plotted in figure 9, show that by increasing *N*, the amount of settlement at each applied pressure decreased up to *N* = 4. For *N* greater than or equal to 4, settlement of square foundations did not increase with additional reinforcement layers. This again indicates there is an optimum *N* beyond which the settlement has insignificant improvement. It should be noted that based on Chen et al., the effective depth of reinforcement is about 1.5*B* for geogrid reinforced clay.[56] Therefore, in the experiment by Chen et al., by having $u/B = h/B = 0.33$, reinforcements with *N* greater than or equal to 7 are placed out of the influence zone.[56]

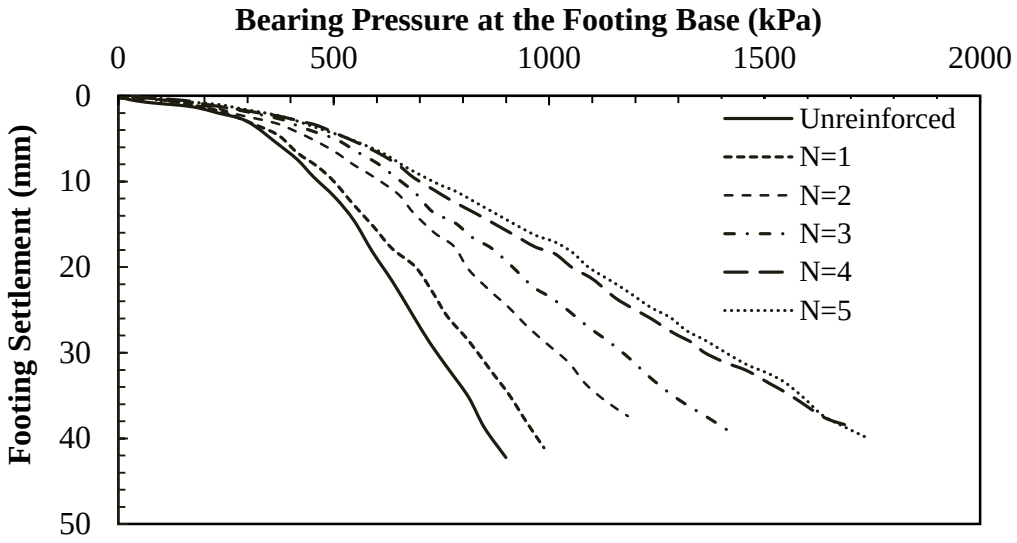

1 inch = 25.4 mm
1 psi = 6.89 kPa
Note: This figure was created by FHWA after Chen et al.[56]

Figure 9. Graph. Load-settlement results for square footing on unreinforced and reinforced soil with polypropylene (PP) geogrid layers.

Das et al. conducted laboratory model tests to investigate the ultimate bearing capacity of surface strip foundations on geogrid reinforced sand and clay.[58] Each foundation was made of an aluminum plate with dimensions of 3 by 12 inches (76.2 by 304.8 mm) ($B \times L$). Bearing capacity tests were conducted in two boxes, each with internal dimensions of 3.61 by 0.98 by 2.95 ft (1.1 by 0.3 by 0.9 m) (length by width by depth). The results show that the inclusion of geogrid reinforcement increased the load per unit area that could be carried by a foundation at any given settlement level. This is true for the tests in both sand and clay. As figure 10 shows, the foundation settlement decreased with the increase of reinforcement layer until *N* = 5. When *N* was greater than 5, the foundation settlement no longer decreased with an increase of the reinforcement layers. The results may be due to the fact that additional reinforcement layers were placed below the effective depth of reinforcement that was about 2*B* for strip footing in sandy soil.

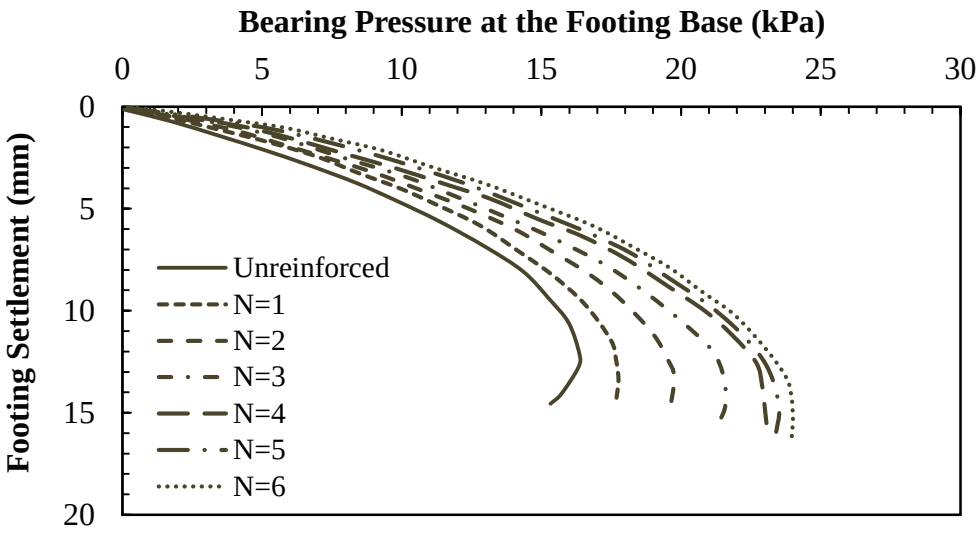

1 inch = 25.4 mm
1 psi = 6.89 kPa
Note: This figure was created by FHWA after Das et al.[58]

Figure 10. Graph. Load-settlement results for sandy soil for *u*/*B* = 0.4, *h*/*B* = 0.33, and *b*/*B* = 4.

Basudhar et al. conducted an experimental study on circular footings resting on sand reinforced with geotextiles.[54] They concluded that with an increase in *N*, the settlement gradually decreased in rate. As figure 11 shows, when *N* is greater than or equal to 2, the foundation settlement no longer decreased with an increase of the reinforcement layers, with the exception of the settlement at ultimate capacity. For the test with three layer of reinforcement, the geotextile was placed at depths of 0.25*B*, *B*, and 2*B* below the base of the footing. By considering the results presented in section, the effective depth of reinforcement was less than 2*B* for square foundation; therefore, layer 3 and the additional layers were placed outside the influence zone and no longer affected the foundation settlement.

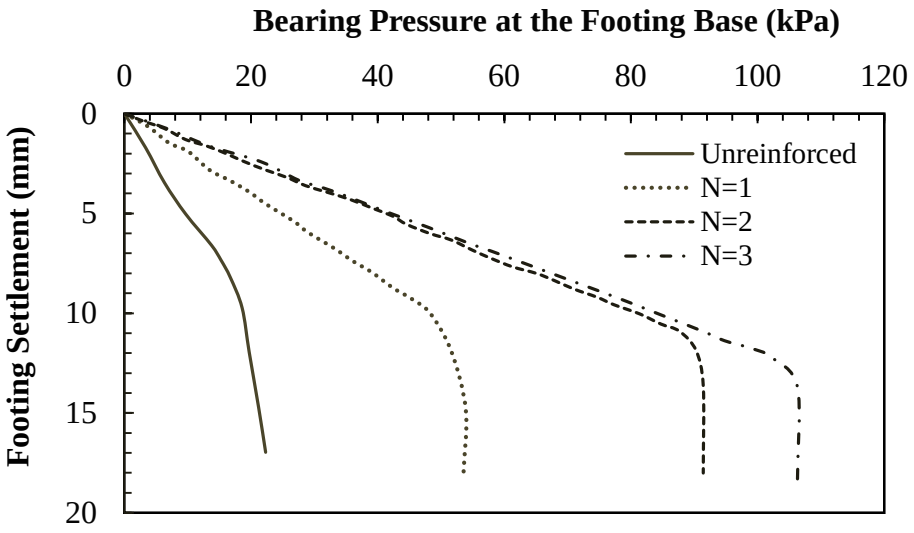

1 inch = 25.4 mm
1 psi = 6.89 kPa
Note: This figure was created by FHWA after Basudhar et al.[54]

Figure 11. Graph. Load-settlement results for 1.18-inch (30-mm)-diameter circular footing.

Phanikumar el al. performed a series of laboratory plate load tests on geogrid reinforced sand beds.[59] Properties of the test sands are presented in table 5. Figure 12 shows that at certain settlements, the bearing load needed to reach that settlement was also affected by *N* and soil types.

Table 5. Properties of test sands.[59]

Property	Fine Sand	Medium Sand	Coarse Sand
Dry unit weight (at D_R = 50 percent) (kN/m^3)	15.2	14.9	14.7
Maximum aggregate size (d_{max}) (mm)	0.425	2.36	4.75
Particle diameter at which 10 percent of the sample is finer, by mass (D_{10}) (mm)	0.25	0.59	1.3
Internal f* (degree)	32	35	40
Coefficient of uniformity	1.4	1.995	2.07
Coefficient of curvature	1.17	1.12	1.25

1 kN/m^3 = 6.37 lbf/ft^3
1 inch = 25.4 mm
*The internal f of the test sands was determined by performing direct shear tests. The test sands were compacted at their respective dry unit weights corresponding to a relative density of 50 percent.

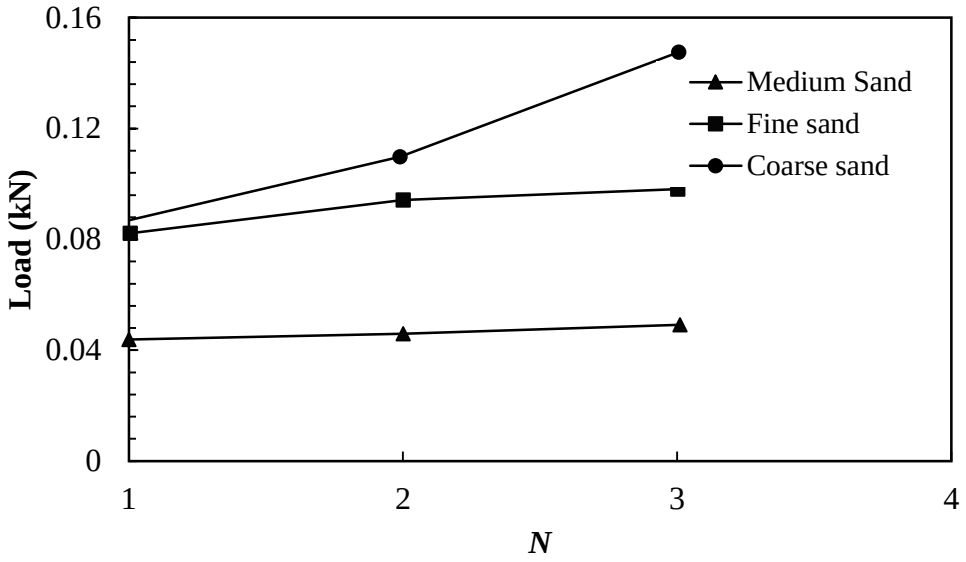

1 lbf = 0.0044 kN
Note: This figure was created by FHWA after Phanikumar et al.[59]

Figure 12. Graph. Effect of number of geogrids on the load required for a settlement of 0.02 inch (0.5 mm).

Results of the effect of different numbers of reinforcement on the behavior of foundation placed on reinforced sand with phosphor-bronze layers are plotted in figure 13.[60] The results also show the decreasing trend of settlement with the increasing *N* at two ratios of reinforcement: *L* versus *B*.

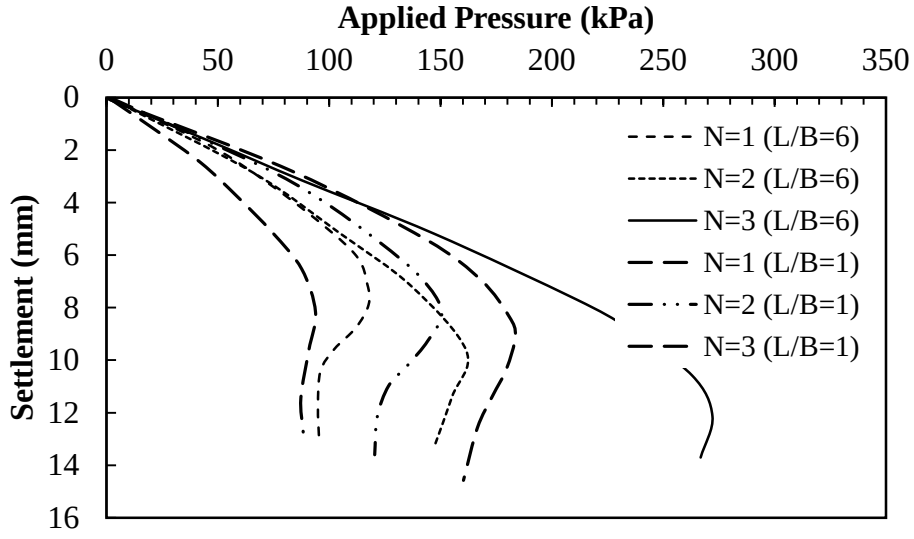

1 inch = 25.4 mm
1 psi = 6.89 kPa
Note: This figure was created by FHWA after Huang and Tatsuoka.[60]

Figure 13. Graph. Load-settlement results for different numbers of metallic reinforcement.

Effect of L and T_f of Reinforcement on Settlement of Shallow Foundations

Results from laboratory model tests conducted by Latha and Somwanshi are plotted in figure 14.[61] The results show that with an increase in *b*, the magnitude of ultimate bearing capacity of foundations on reinforced soil increased, and settlement decreased.

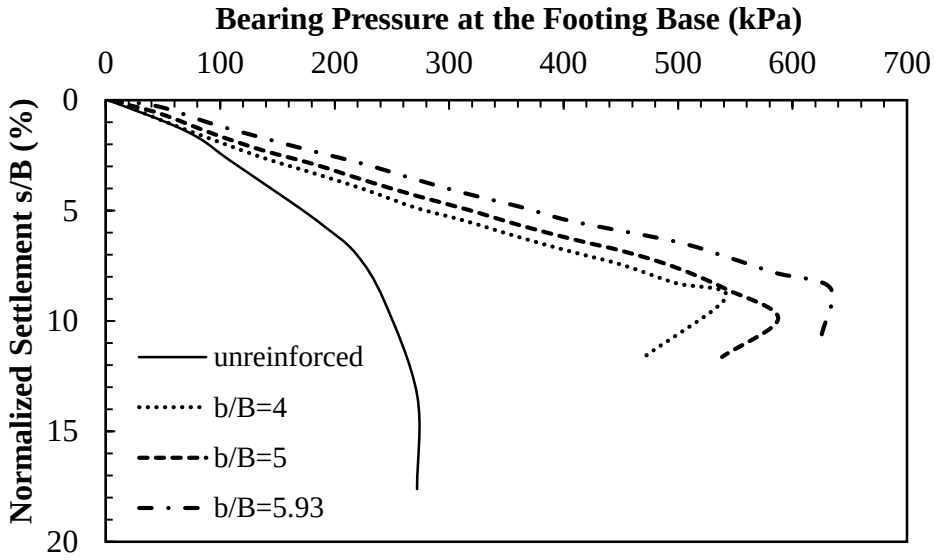

1 psi = 6.89 kPa
Note: This figure was created by FHWA after Latha and Somwanshi.[61]

Figure 14. Graph. Load-settlement results for different widths of geonet (N = 4, d = 2B).

Elton and Patawaran conducted an experimental study on reinforced soil specimens to evaluate the effects of T_f of geotextiles on the stress-strain relationship of reinforced soil.[62] The properties of the six geotextile used in their experiments are presented in table 6. Figure 15 shows the unconfined compression test results. Three transducers on top of the steel loading plate measured vertical displacements. As the results show, the curve initially reached its peak strength at approximately 3 to 8 percent strain, had a decrease in some strength, and then gradually increased back to reach a second peak before finally decreasing sharply. The peak strength and the corresponding strain of the specimens increased as reinforcement strength increased.

Table 6. Geotextile properties.[62]

Property	Geotextile Type (G)					
	G4	G6	G8	G12	G16	G28
Mass per area (g/m^2)	135.64	203.46	271.28	406.92	542.56	949.48
Wide-width machine direction strength (kN/m)	9.0	14.0	14.5	18.6	20.1	24.9
Wide-width cross-machine direction strength (kN/m)	14.4	19.3	19.8	20.3	22.9	21.7

1 g/m^2 = 2.05 ´ 10^{-4} lb/ft^2
1 kN/m = 68.5 lbf/ft

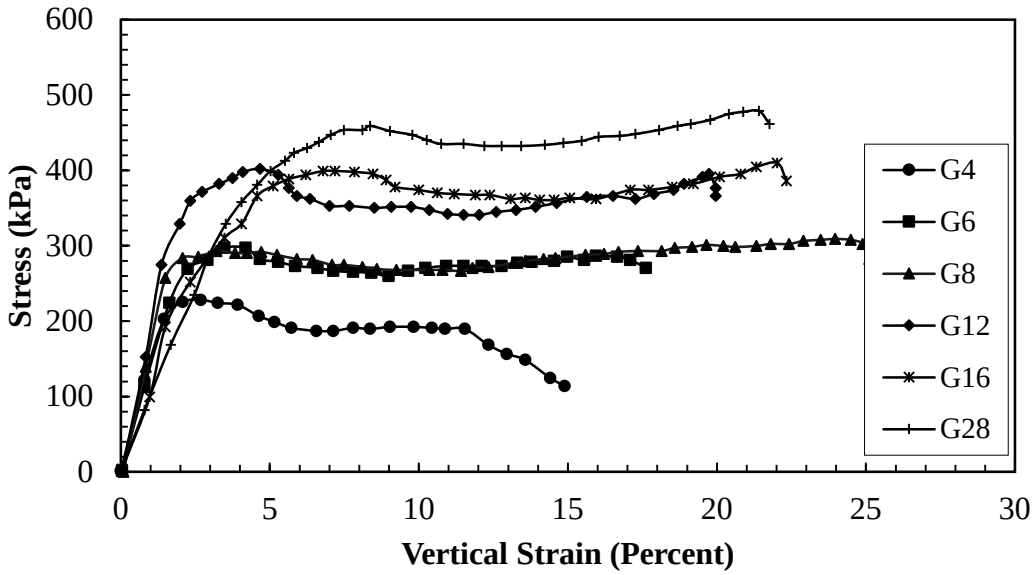

1 psi = 6.89 kPa
Note: This figure was created by FHWA after Elton and Patawaran.[62]

Figure 15. Graph. Stress-strain relationship of reinforced soil.

Adams and Collin conducted five laboratory experiments on reduced-scale piers as part of an FHWA research project.[41] Of the five experiments, one was unreinforced, and the others were reinforced with different reinforcement spacing and T_f. As the results in figure 16 show, the specimen with spacing of 0.66 ft (0.2 m) and lower wide width strength of 1,439 lbf/ft (21 kN/m) could withstand higher stresses compared to the specimen with 1.31-ft (0.4-m) spacing and higher wide width strength of 4,797 lbf/ft (70 kN/m) at any given strain. Therefore, they concluded that the reinforcement spacing played a more important role than the reinforcement strength.

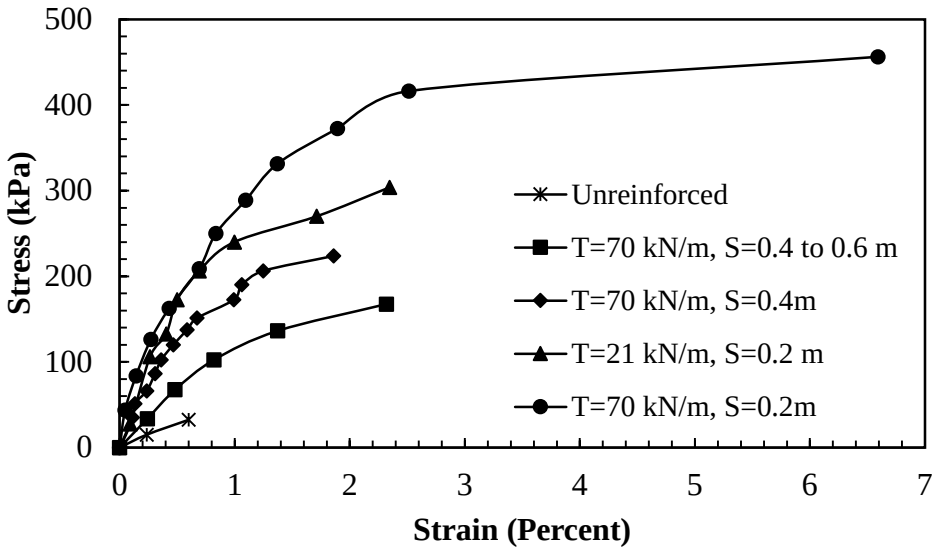

1 psi = 6.89 kPa
1 kN/m = 68.5 lbf/ft
1 ft = 0.305 m
Note: This figure was created by FHWA after Adams and Collin.[41]

Figure 16. Graph. Stress-strain relationship of the mini-pier experiments.

Abu-Hejleh et al. conducted an assessment of the new Founders/Meadows Bridge near Denver, CO, which was completed in July 1999.[63,64] The study focused on the performance and behavior of the GRS system under service loads. Three sections of the GRS system were instrumented to measure movements of the front GRS wall, settlement of the bridge footing, and differential settlements between the bridge abutment and the approaching roadway. The backfill soil used in this project was a mixture of gravel (35 percent), sand (54.4 percent), and fine-grained soil (10.6 percent). The backfill soil was classified as well-graded silty sand per ASTM D 2487 and as stone fragments, gravel, and sand (A-1-B (0)) per AASHTO M145-91.[65,66] The average unit weight and dry unit weight of the compacted backfill soil as measured during construction were 140.6 and 133.7 lb/ft^3 (22.1 and 21 kN/m^3), respectively, and the water content was 5.6 percent. Results of large direct shear and large triaxial tests showed a f of 47.7 and 39.5 degrees and c of 16.06 and 5.73 psi (110.7 and 39.5 kPa), respectively, for the direct shear and triaxial tests. Three grades of geogrid reinforcements were used in this project: uniaxial (UX) 6 below the foundation and UX 3 and UX 2 behind the abutment wall. Table 7 summarizes the ultimate strength and the long-term design strength (LTDS) for these geogrids.

Table 7. Placed geogrid strength.[64]

Geogrid Type and Notation	Ultimate Strength (kN/m)	LTDS (kN/m)
UX 6	157.3	27
UX 3	64.2	11
UX 2	39.3	6.8

1 kN/m =68.5 lbf/ft

Data were collected during construction of the GRS walls, during placement of the bridge superstructure, and during the 18 mo after opening the bridge to traffic. The results are presented in table 8 and show excellent performance of the GRS structure. The monitored overall displacements were smaller than those expected in the design and allowed by performance requirements, there were no signs for development of the bridge bump problem or of any structural damage, and post-construction movements became negligible within a year after opening the bridge to traffic.

Table 8. Summary of the maximum displacements of the front wall facing and of the settlements of the bridge abutment footing.

Types of Maximum Movements	Induced Only by GRS Wall Construction	Induced Only by Placement of Bridge Superstructure (115-kPa Surcharge)	Induced Only While Bridge in Service (150-kPa Surcharge)		
			6 Mo	12 Mo	18 Mo
Maximum outward displacement of the front wall facing (mm)	12	10	8	12	13
Maximum settlement of the leveling pad supporting the front wall facing (mm)	8	7	4	5	5
Maximum bridge abutment footing settlement (mm)		13	7	11	10
Percent maximum settlement of bridge abutment of wall height (percent)		0.29			0.17

1 kPa = 0.145 psi
1 inch = 25.4 mm
Note: This table was created by FHWA after Abu-Hejleh et al.[64] Blank cells indicate no value was recorded.

Huang and Tatsuoka used different types of metal strips to reinforce the soil beneath a shallow foundation.[60] Figure 17 shows the results from laboratory model tests reinforced with phosphor-bronze strips. The results show that with an increase in *L*, the magnitude of the settlement in each applied load decreased. However, this decrease was not proportional to the increase in *L*. For example, under 4,177 psf (200 kPa) of applied pressure, the settlement of the foundation was the same for two different reinforcement lengths of *L/B* = 3.5 and *L/B* = 6.

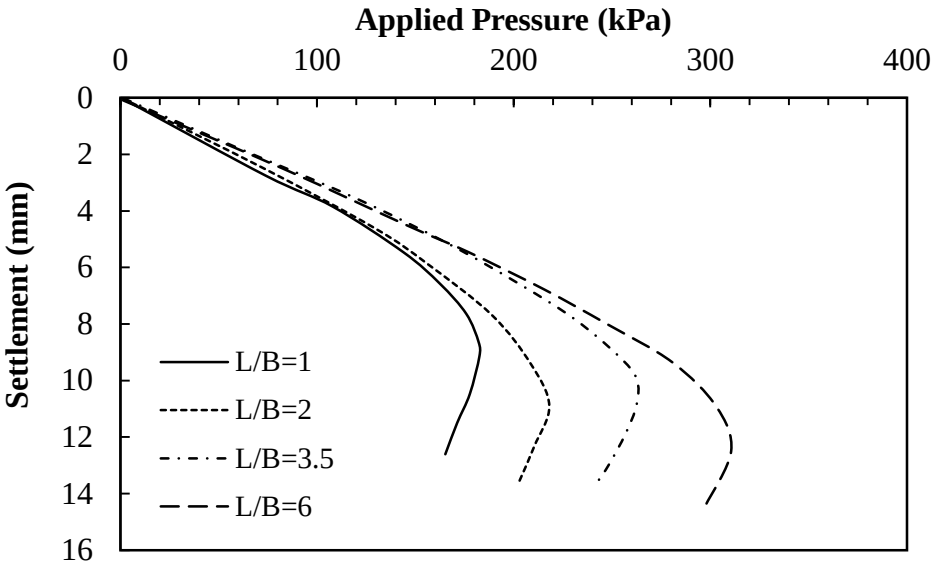

1 inch = 25.4 mm
1 psi = 6.89 kPa
Note: This figure was created by FHWA after Huang and Tatsuoka.[60]

Figure 17. Graph. Load-settlement results for different reinforcement lengths (*N* = 3).

Effect of *B* on Settlement of Shallow Foundations

Das and Omar conducted an experimental study on surface strip foundations on geogrid-reinforced sand.[67] As shown in figure 18, they concluded that the settlement at the ultimate bearing capacity increased with a decrease in *B*. The figure also revealed insignificant effects of footing size on settlement under bearing pressures less than approximately 6,266 psf (300 kPa). It is noted that these observations were obtained in small-scale experiments.

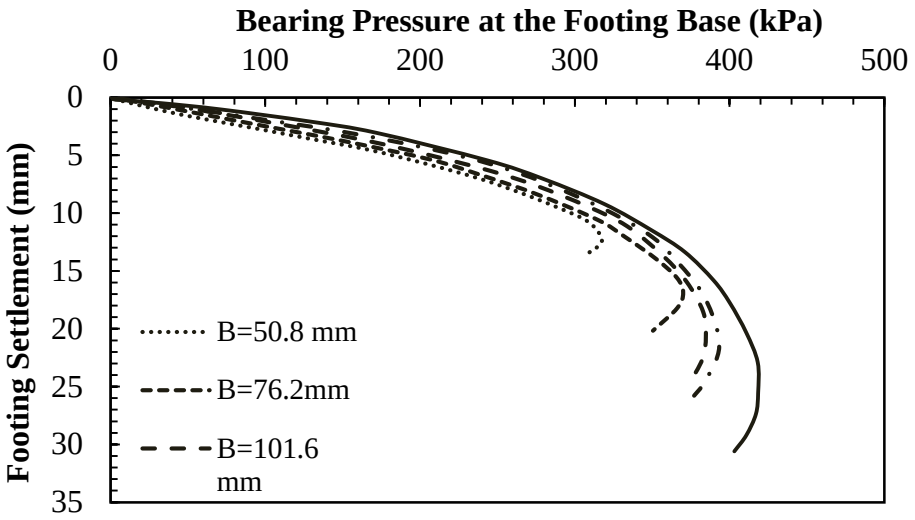

1 inch = 25.4 mm
1 psi = 6.89 kPa
Note: This figure was created by FHWA after Das and Omar.[67]

Figure 18. Graph. Load-settlement results in reinforced sand (D_R = 75 percent).

Effect of Embedment Depth of Top Reinforcement Layer on Settlement of Shallow Foundations

Mandal and Sah conducted bearing capacity tests on model footings on clay subgrades reinforced with geogrids.[68] Their results, plotted in figure 19, show that the maximum percentage reduction in settlement with the use of geogrid reinforcement within the compacted and saturated clay was about 45 percent, and it occurred at a depth of 0 to 0.25*B* below the base of the square foundation.

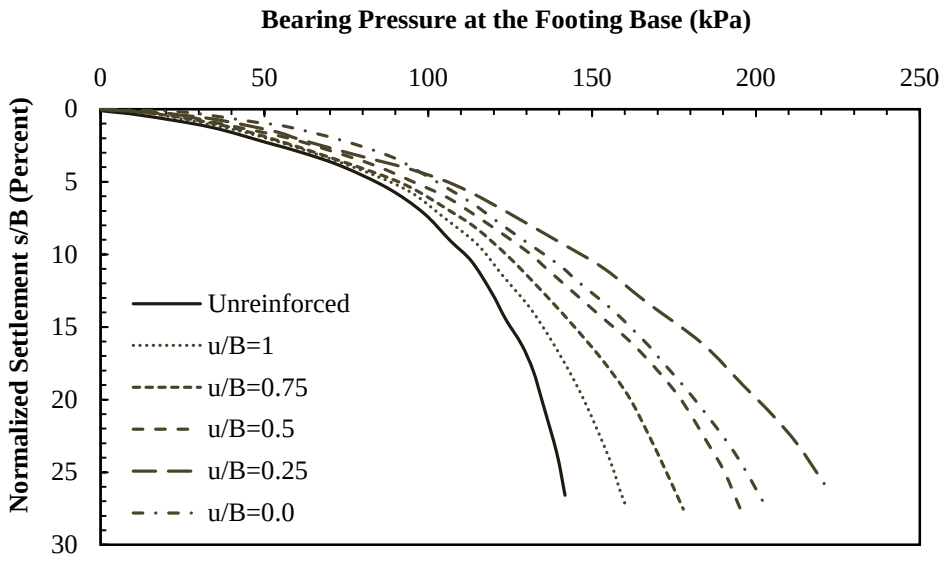

1 psi = 6.89 kPa
Note: This figure was created by FHWA after Mandal and Sah.[68]

Figure 19. Graph. Load-settlement results of model footings on clay subgrade reinforced with geogrid.

Binquet and Lee conducted a series of experiments on strip footing 2.99 inches (76 mm) wide placed on sandy soil reinforced with metal strips.[69] Figure 20 shows the results of the studies on the effect of u of the top reinforcement layer on the settlement of a foundation. They concluded that the optimum location of the top layer was at $u/B = 1.3$. Furthermore, based on experimental results obtained from foundations placed on reinforced soil with geogrid, it was concluded that the optimum depth for placing the top layer of reinforcement was within $0.25B$ below the base of the foundation. Therefore, the top layer of the metal strip could be located at a lower depth compared to geogrid reinforcement in order to have the minimum amount of settlement under each applied load.

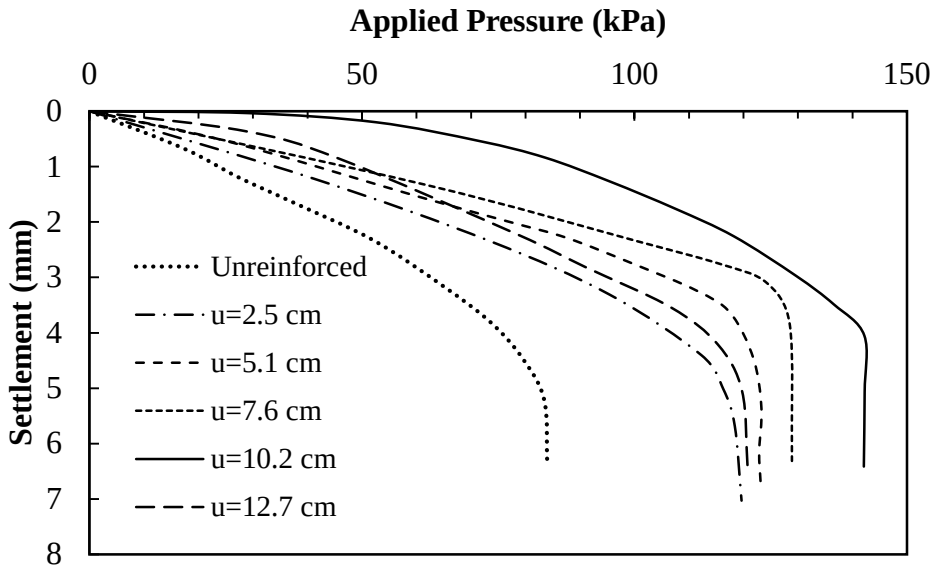

1 inch = 25.4 mm = 2.54 cm
1 psi = 6.89 kPa
Note: This figure was created by FHWA after Binquet and Lee.[69]

Figure 20. Graph. Load-settlement results for different depth of top layer of metallic reinforcement (*N* = 3).

Effect of Vertical Spacing of Reinforcement (S_v) Layers on Settlement of Shallow Foundations

Chen et al. investigated the behavior of square foundations on geosynthetic reinforced clayey soil of low to medium plasticity using laboratory model footing tests.[56] As figure 21 shows, by decreasing *h* between the three reinforcement layers (placed within the zone of influence below the footing), the amount of settlement at each applied load pressure decreased.

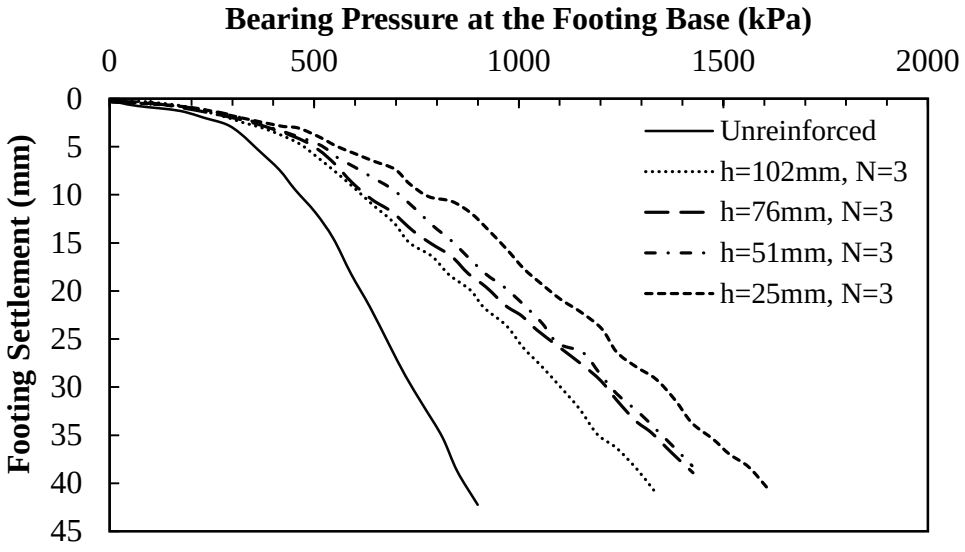

1 inch = 25.4 mm
1 psi = 6.89 kPa
Note: This figure was created by FHWA after Chen et al.[56]

Figure 21. Graph. Load-settlement results for square footing tests with three layers of geogrids placed at different vertical spacing.

Effect of Covering Ratio (CR) of Metallic Strip Reinforcement on Settlement of Shallow Foundations

An effective parameter for the load-settlement behavior of foundation on soil reinforced with metallic strips is the CR of reinforcement in each layer. Figure 22 shows the experimental results of the settlement of a foundation placed on reinforced soil with phosphor-bronze strip layers.[60] The figure shows by increasing CR, the settlement at each applied pressure decreases. From the results, it can be concluded that the decrease in settlement was not proportional to CR. This suggests that there is an upper bound in CR, above which a decrease in settlement with the increase in CR may not be expected.

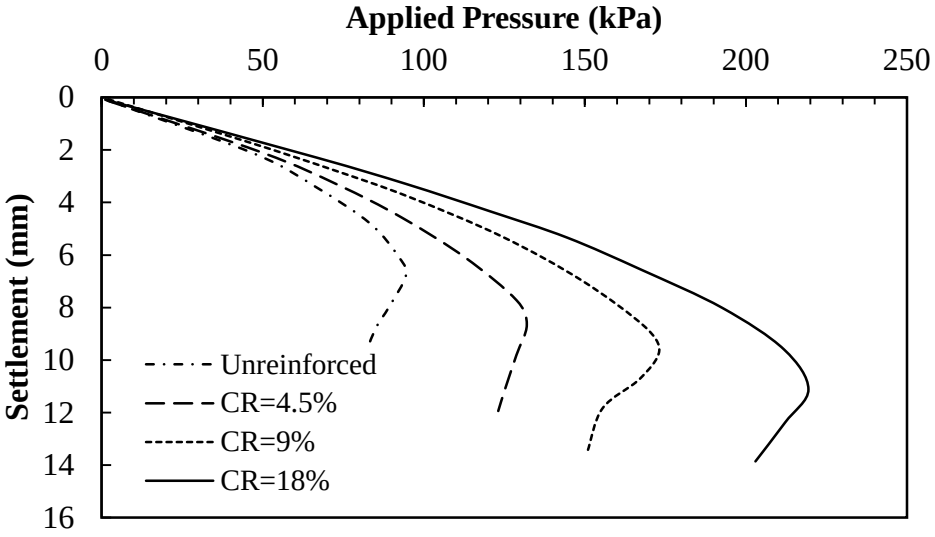

1 inch = 25.4 mm
1 psi = 6.89 kPa
Note: This figure was created by FHWA after Huang and Tatsuoka.[60]

Figure 22. Graph. Load-settlement results for different CRs of reinforcement (*L* = 2*B*, *N* = 3).

3.3 SYNTHESIS OF LOAD DEFORMATION RELATIONSHIPS OF BRIDGE ABUTMENTS AND PIERS

Effect of Soil Parameters on Load Deformation Relationships

Adams and Nicks conducted an experimental study to investigate secondary deformation characteristics of GRS as bridge piers under service load conditions.[27] Load-settlement behaviors of four GRS piers built using two types of soils and woven geotextiles were monitored under 30.45 psi (210 kPa) of pressure. The characteristics of the materials used and results presented by Adams and Nicks are shown in table 9.[27] The results show that under service load conditions, there was no significant increase in settlement for the pier with the weak geotextile (pier A). Also, the piers with open-graded #8 aggregates experienced slightly more compression (about 5 percent higher) compared to well-graded A-1-a backfill soil. The results from the pier deformation survey over 4 mo indicated that secondary settlement occurred in granular material, but it was still within typical tolerable limits for bridges of up to 2 percent vertical strain over the life of the bridge.[32]

Table 9. GRS pier materials and results recorded from vertical deformation survey.

Measurement Categories	Material Properties and Specific Field Surveys	Pier A	Pier B	Pier C	Pier D
Backfill material properties	AASHTO soil type	#8	A-1-a	A-1-a	#8
	f (degrees)	55	54	54	55
	c (kPa)	0	5.5	5.5	0
Reinforcement properties	T_f (kN/m)	35	70	70	70
	Minimum average roll value strength at 2 percent strain (kN/m)	3.5	19.3	19.3	19.3
Survey results	GRS composite settlement 105 days after load placement (mm)	24	23.6	22.5	24.8
	Vertical strain in GRS composite (percent)	1.03	1.01	0.97	1.07

1 psi = 6.89 kPa
1kN/m = 68.5 lbf/ft
1 inch = 25.4 mm
Note: This table was created by FHWA after Adams and Nicks.[27]

Nicks et al. conducted 19 GRS PTs as a part of FHWA research that investigated axial load versus vertical deformation characteristics of GRS piers.[42] A total of 5 tests were conducted at the Defiance County (DC), OH, highway maintenance facility, and 14 were conducted at the Turner-Fairbank Highway Research Center (TFHRC). The parameters that varied among tests were reinforcement spacing, geotextile strength, soil type, and frictionally connected facing element. The parameters of piers tested to investigate the effect of aggregate type on load-deformation characteristics of the piers and the test results are shown in table 10 and figure 23. The applied pressure was calculated as the average of the measured values over the period of loading, and the vertical strain was calculated as the averages of the four linear voltage displacement transducers (LVDTs) and potentiometers (POTs) located on the footing at the end of each load increment. Based on the results, the pier built with the largest aggregate tested (#57 stone) had the lowest service limit of all the tests, indicating more deformation under an applied load. In addition, the pier built with rounded pea gravel had a lower strength and service limit than the more angular aggregate meeting the same gradation specifications for an AASHTO #8 material.

Table 10. Parametric study on aggregate size.

Test No.	Backfill				Reinforcement		Facing
	Type	f (degree)	c (kPa)	Aggregate Size (mm)	T_f (kN/m)	S_v (mm)	
DC-1	8	54	0	12.7	70	194	CMU
DC-2	8P	46	0	19.05	70	194	CMU
DC-3	57	52	0	25.4	70	194	CMU
DC-4	9	49	0	9.525	70	194	CMU

1 psi = 6.89 kPa
1kN/m = 68.5 lbf/ft
1 inch = 25.4 mm
CMU = Concrete Masonry Unit.
Note: This table was created by FHWA after Nicks et al.[42]

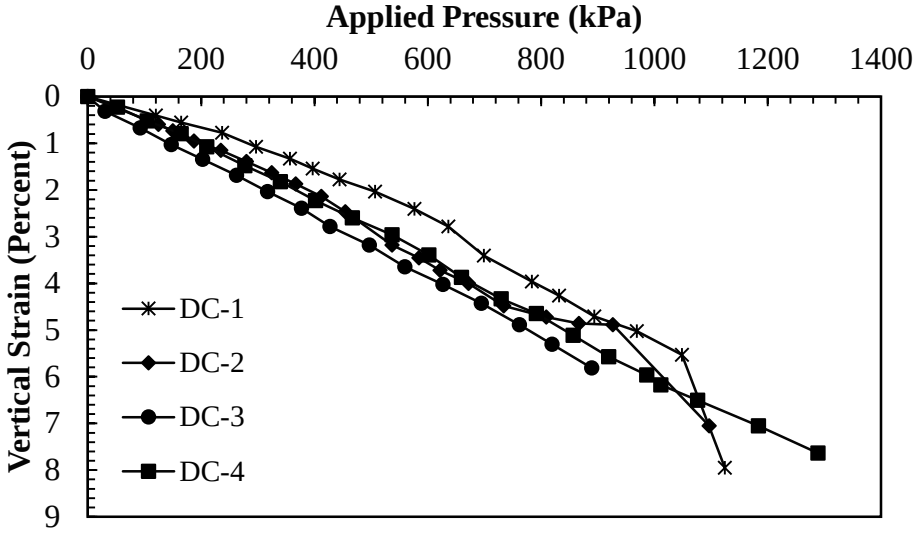

1 psi = 6.89 kPa
Note: This figure was created by FHWA after Nicks et al.[42]

Figure 23. Graph. Load-deformation behavior from PTs on GRS piers using five types of DC backfills.

By comparing identical piers that were similar in all of their characteristics except their gradation, Nicks et al. concluded that the use of well-graded material resulted in a considerably stiffer load-deformation response than that observed when open-graded material was used.[42]

Helwany et al. conducted finite element analyses (FEAs) of two full-scale loading tests on GRS bridge abutments and performed a parametric study to investigate the performance of the modular block facing of GRS bridge abutments subjected to live and dead loads from the bridge superstructure.[70] They concluded that more favorable deformation response was attained when using soil types that have higher internal f and corresponding higher bulk and shear moduli. figure 24 shows that when f increased from 34 to 40 degrees, the vertical displacement at the abutment seat decreased from 1.89 to 1.18 inches (48 to 30 mm) at applied pressure of 4,177 psf

(200 kPa), while vertical displacement showed little variation at a lower applied pressure of 2,088 psf (100 kPa).

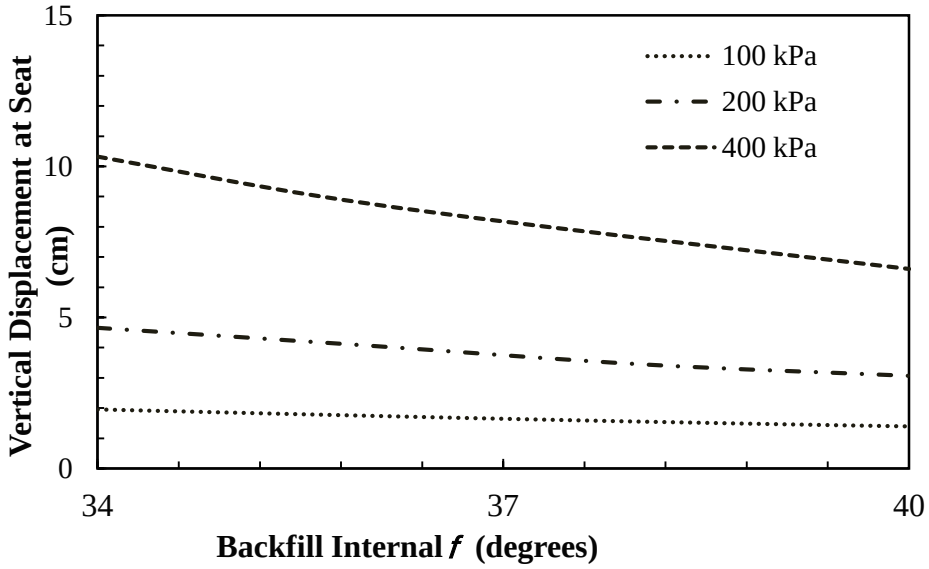

1 inch = 2.54 cm
1 psi = 6.89 kPa
Note: This figure was created by FHWA after Helwany et al.[70]

Figure 24. Graph. Effects of backfill internal f on vertical displacement at abutment seat (reinforcement spacing = 7.87 inches (20 cm)).

Helwany et al. also concluded that by using soil types that had higher internal f and higher bulk and shear moduli, a more favorable deformation response was attained for horizontal displacement at the abutment seat and for maximum lateral displacement of the segmental facing (see figure 26).[70] At applied pressure of 4,177 psf (200 kPa), by increasing the internal f from 34 to 40 degrees, the horizontal displacement at seat decreased by about 14 percent. As figure 26 shows, at different applied pressures, the maximum lateral displacement of the segmental facing decreased in a linear manner with increasing f.

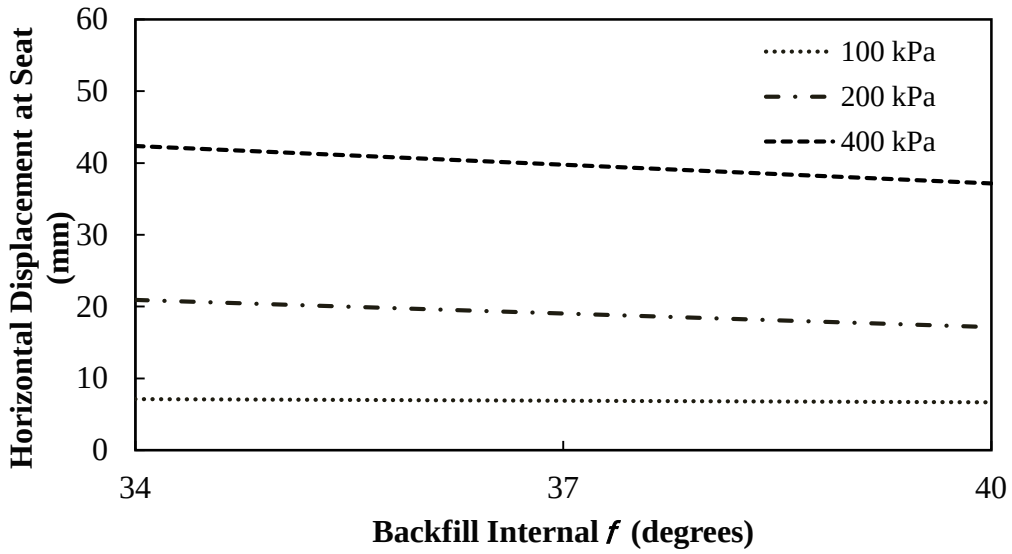

1 inch = 25.4 mm
1 psi = 6.89 kPa
Note: This figure was created by FHWA after Helwany et al.[70]

Figure 25. Graph. Effects of backfill internal f (reinforcement spacing = 7.87 inches (20 cm)) on horizontal displacement at abutment seat.

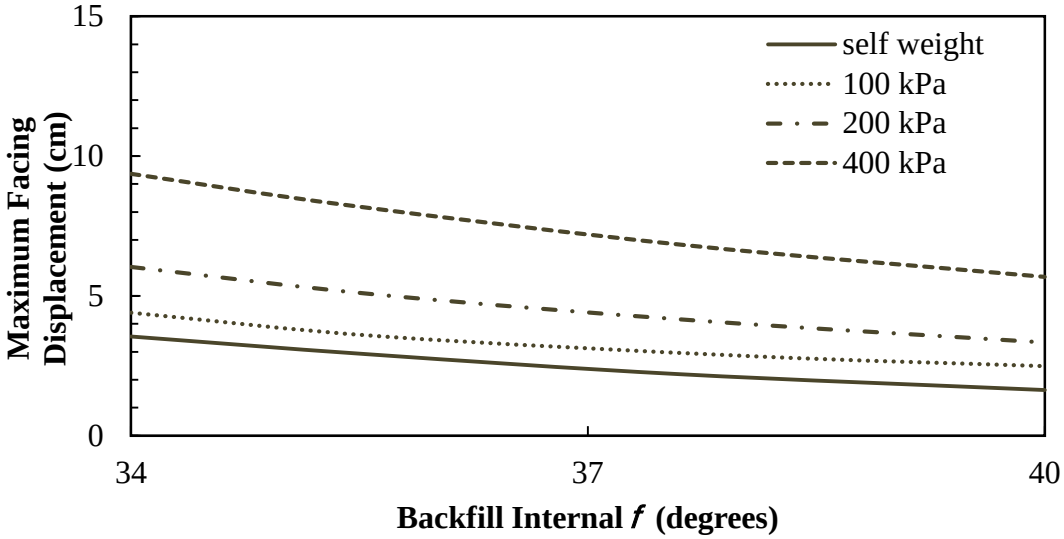

1 inch = 2.54 cm
Note: This figure was created by FHWA after Helwany et al.[70]

Figure 26. Graph. Effects of backfill internal f (reinforcement spacing = 7.87 inches (20 cm)) on the maximum lateral displacement of the facing.

Hatami and Bathurst investigated the influence of backfill type on the performance of reinforced soil segmental retaining walls (SRWs) under working stress conditions at the end of construction (EOC) using a finite difference numerical modeling.[71] As figure 27 shows, facing deflections diminished in magnitude as soil shear strength increased due to an increase in f, an increase in apparent *c*, or both. The pattern of deflected shape was also influenced by the increase of

apparent *c*. An increase of apparent *c* moved the location of maximum wall deflection lower down the wall and was particularly effective in reducing deflections at the wall crest. The results also show the different influences of f and *c*.

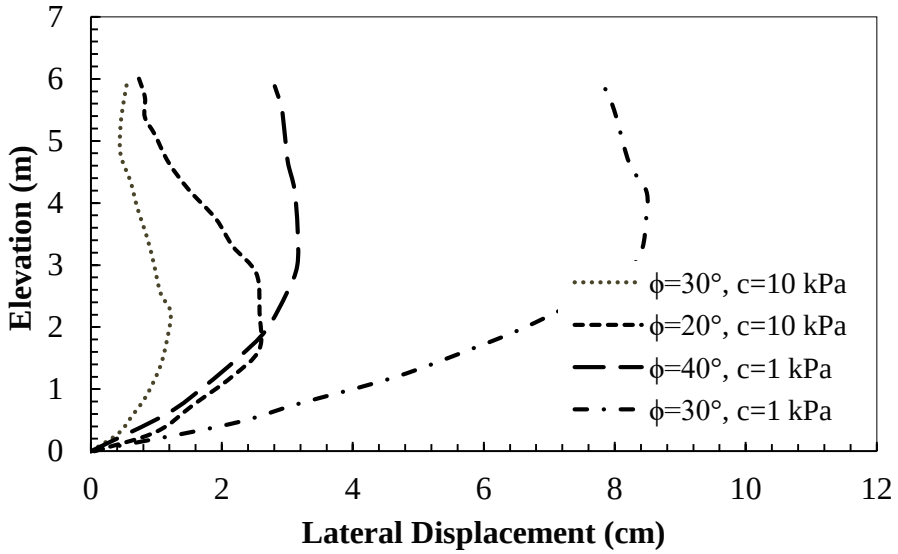

1 ft = 0.305 m
1 inch = 2.54 cm
Note: This figure was created by FHWA after Hatami and Bathurst.[71]

Figure 27. Graph. Influence of apparent *c* and f on lateral displacement of the wall.

Results plotted in figure 28 show that reinforcement loads were greater for the walls with weaker backfills, and the distribution of maximum load along the wall height varied between a parabolic shape for granular backfill and a linear shape when the backfill had higher value of apparent *c* and was more cohesive.[71]

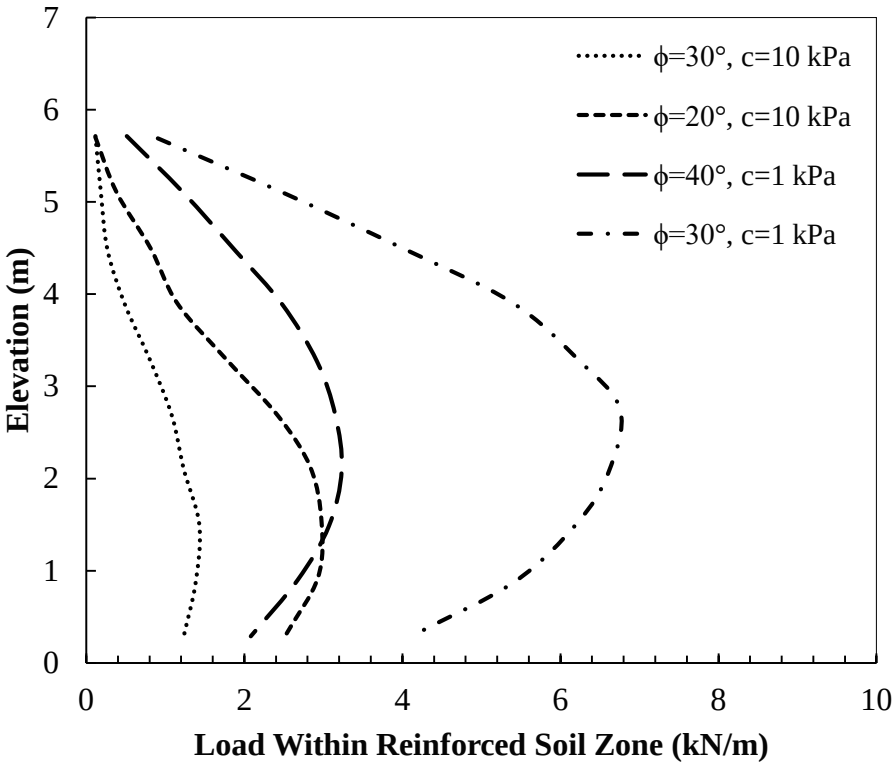

1 ft = 0.305 m
1kN/m = 68.5 lbf/ft
Note: This figure was created by FHWA after Hatami and Bathurst.[71]

Figure 28. Graph. Influence of backfill apparent *c* and *f* values on maximum reinforcement loads in wall models at EOC.

Skinner and Rowe numerically investigated the short- and long-term behaviors of a 19.68-ft (6-m)-high segmental block-faced geosynthetic reinforced retaining wall constructed on a rigid base; they also studied two 32.8-ft (10-m)-thick clayey foundations to investigate the effect of yielding in the foundation on the stability of the wall.[72] The horizontal displacements of the wall face calculated for the rigid foundation and the two clayey foundations are plotted in figure 29. Clayey foundations are significantly more compressible than the rigid foundation. The figure shows that the deformations at the face and base of the wall were considerably higher for soils 1 and 2 than for the rigid foundation. The increased foundation deformation contributed significantly to the facing displacement. For the lower viscosity soil 1, there was no significant change in behavior between the time of 95 percent consolidation (reached 1 year after EOC) and subsequent time (e.g., 7 years). The more viscous soil 2 reached approximately 20 percent consolidation 1 year after EOC and approximately 95 percent consolidation 7 years after EOC. The slight backward rotation of the wall face from EOC to 7 years (95 percent consolidation) for soil 1 was caused by local displacements at the face and especially at the toe of the wall.

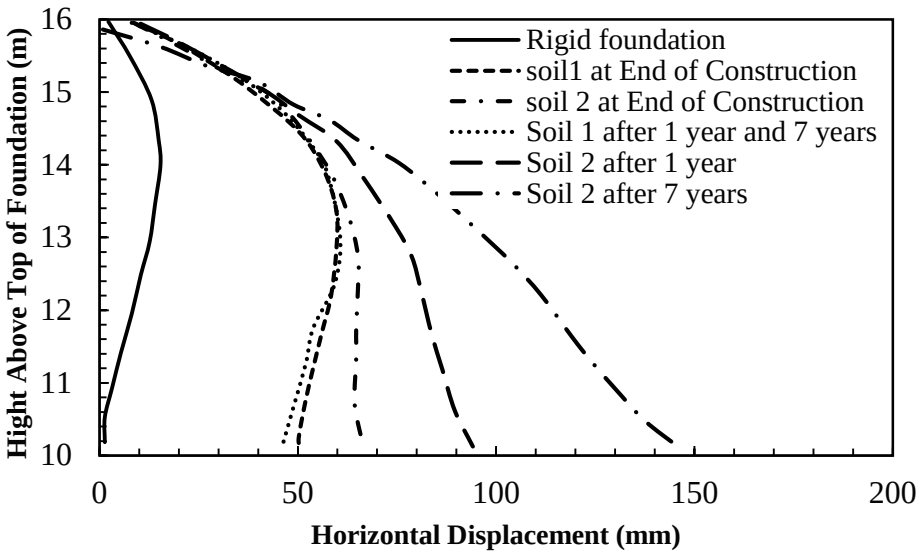

1 ft = 0.305 m
1 inch = 25.4 mm
Note: This figure was created by FHWA after Skinner and Rowe.[72]

Figure 29. Graph. Horizontal displacements at wall face.

Helwany et al. conducted FEAs to investigate the effect of backfill type and reinforcement strength on the behavior of GRS retaining walls.[73] A total of 3 different reinforcement stiffness values and 16 different backfill materials were implemented in the analyses of 3 walls with different heights to produce 144 analysis combinations. The GRS retaining walls were under 15.23-psi (105-kPa) surcharge pressure. The dimensions and the properties of the different soils are presented in table 11 and table 12, and the results are plotted in figure 30 through figure 33.

Table 11. GRS retaining wall dimensions.

Wall Height (m)	Depth of Backfill (m)	Length of Geotextile (m)	*N*
3	3.7	1.8	10
4.5	5.5	2.7	15
6	7.3	3.7	20

1 ft = 0.305 m
Note: This figure was created by FHWA after Helwany et al.[73]

Table 12. Representative soil parameters.

Soil Type Based on Unified Soil Classification	Backfill Designation Number	RC Based on Percent of Standard Proctor	Moist Unit Weight (kN/m^3)	f for Confining Pressure = 1 Atmosphere Pressure (degrees)	Reduction in f for a 10-Fold Increase in Confining Pressure (degrees)	c (kN/m^2)
Well-graded gravel, poorly graded gravel, well-graded sand, poorly graded sand	1	105	23.6	42	9	0
	2	100	22.8	39	7	0
	3	95	22.1	36	5	0
	4	90	21.3	33	3	0
Silty sand	5	100	21.3	36	8	0
	6	95	20.5	34	6	0
	7	90	19.7	32	4	0
	8	85	18.9	30	2	0
Silty clayey sand	9	100	21.3	33	0	24
	10	95	20.5	33	0	19
	11	90	19.7	33	0	14
	12	85	18.9	33	0	10
Low plasticity clay	13	100	21.3	30	0	19
	14	95	20.5	30	0	14
	15	90	19.7	30	0	10
	16	85	18.9	30	0	5

1 kN/m^3 = 6.37 lbf/ft^3
1kN/m^2 = 20.89 lb/ft^2
Note: This table was created by FHWA after Helwany et al.[73]

Figure 30 through figure 33 all show that the type of backfill had the most effect on the behavior of the GRS retaining wall. They concluded that the stiffness of the geosynthetic reinforcement had a considerable effect on the behavior of the GRS retaining wall when the backfill was of lower stiffness and shear strength. For example, the 9.84-ft (3-m)-high GRS retaining walls made of soils #15 and #16 (lower stiffness and shear strength) exhibited significant improvement when a stiffer geosynthetic was utilized. When the 9.84-ft (3-m)-high GRS retaining wall was made of soils #13 and #14 (higher stiffness and shear strength), it exhibited relatively small improvements when the geosynthetic stiffness was increased.

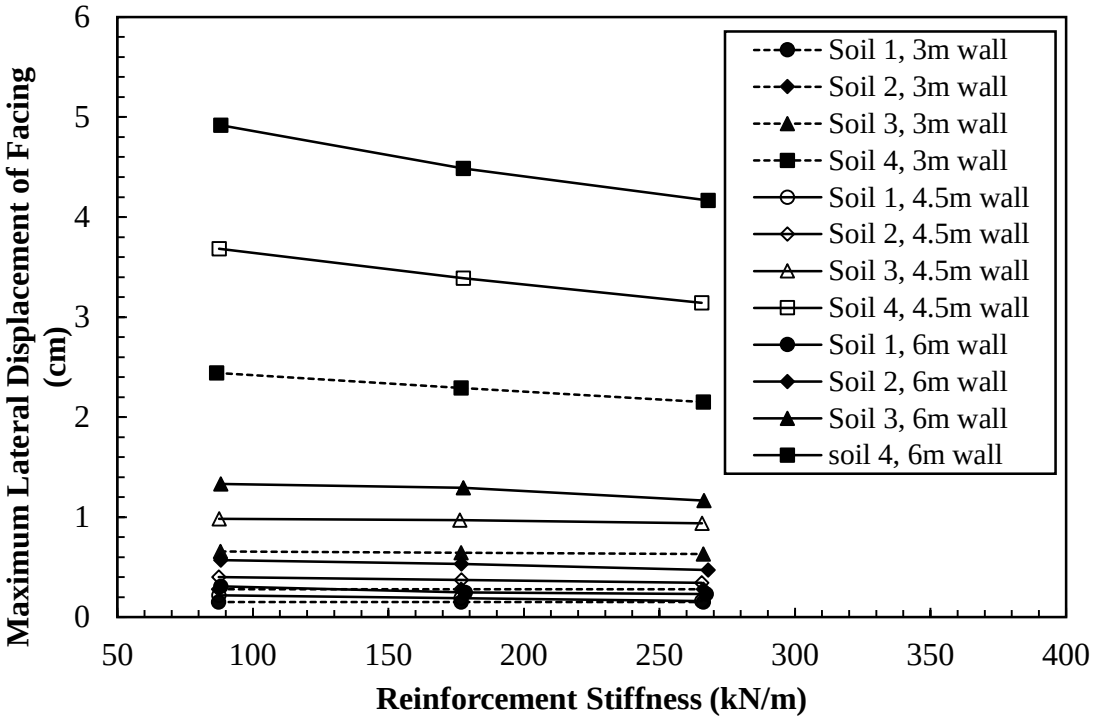

1 inch = 2.54 cm
1 ft = 0.305 m
1kN/m = 68.5 lbf/ft
Note: This figure was created by FHWA after Helwany et al.[73]

Figure 30. Graph. Maximum lateral displacement versus geosynthetic stiffness for soils 1–4.

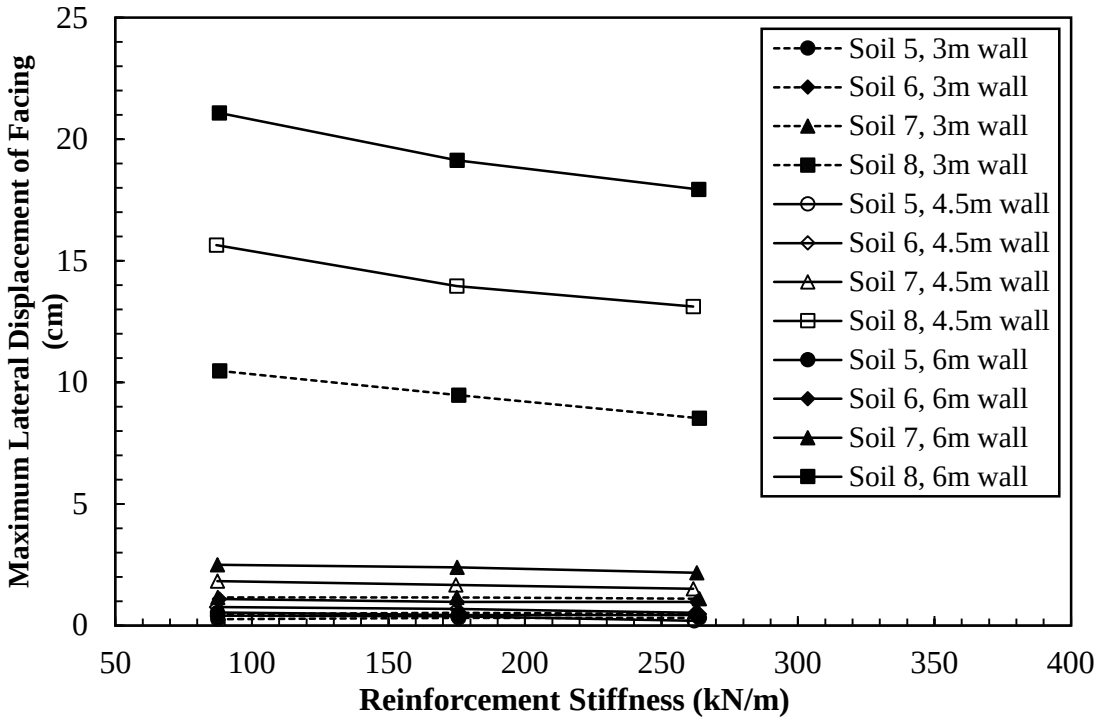

1 inch = 2.54 cm
1 ft = 0.305 m
1kN/m = 68.5 lbf/ft
Note: This figure was created by FHWA after Helwany et al.[73]

Figure 31. Graph. Maximum lateral displacement versus geosynthetic stiffness for soils 5–8.

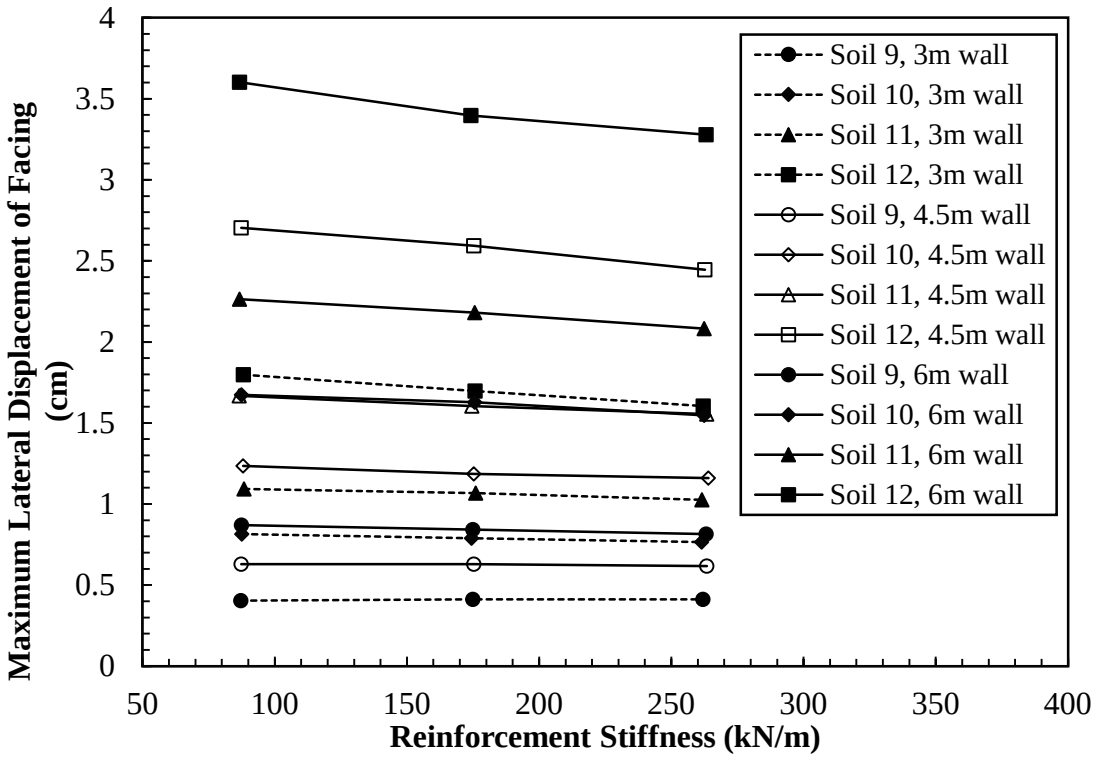

1 inch = 2.54 cm
1 ft = 0.305 m
1kN/m = 68.5 lbf/ft
Note: This figure was created by FHWA after Helwany et al.[73]

Figure 32. Graph. Maximum lateral displacement versus geosynthetic stiffness for soils 9–12.

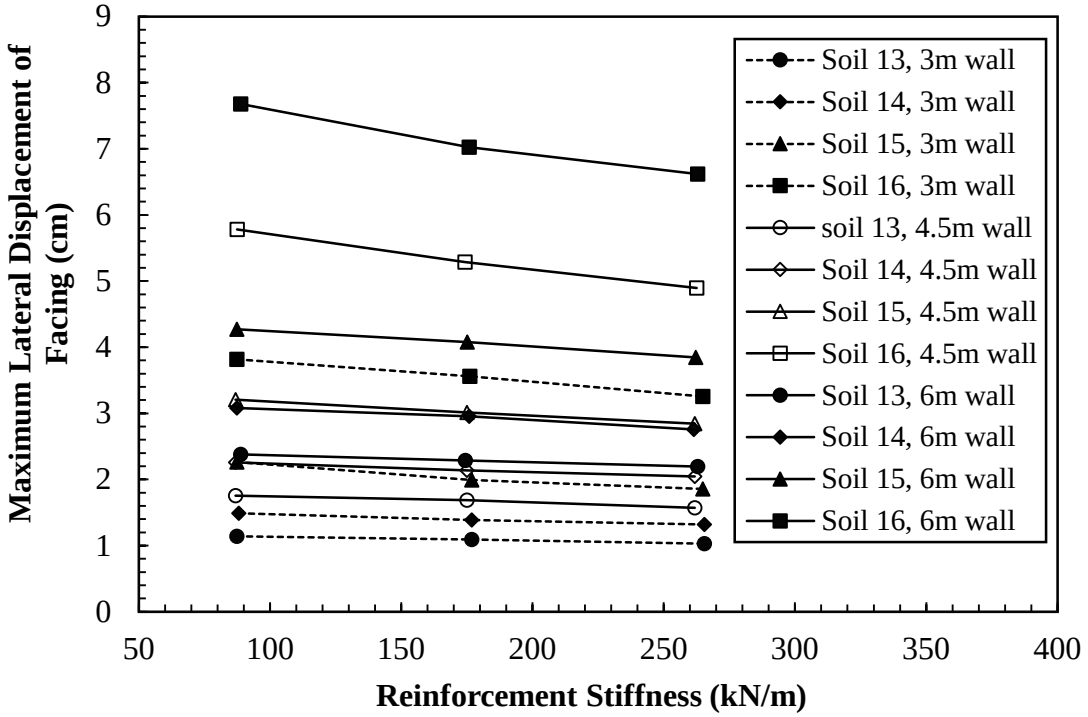

1 inch = 2.54 cm
1 ft = 0.305 m
1kN/m = 68.5 lbf/ft
Note: This figure was created by FHWA after Helwany et al.[73]

Figure 33. Graph. Maximum lateral displacement versus geosynthetic stiffness for soils 13–16.

Effect of Reinforcement Characteristics on Load Deformation Relationships

Figure 34 and figure 35 show the results from two PTs conducted by Nicks et al. to investigate the effect of bearing bed reinforcement on load deformation characteristics of bridge piers.[42] Bearing bed reinforcement placed directly underneath the beam seat was recommended in at least the top five courses of CMU facing elements for GRS abutments to support the increased loads due to the bridge and should be, at a minimum, half the primary spacing.[32] The two piers were identical except one pier (Turner-Fairbank (TF)-8) had two courses of bearing bed reinforcement in addition to the primary reinforcement of 7.87-inch (20-cm) spacing, and the other pier (TF-7) had no bearing bed reinforcement with only primary reinforcement. The applied pressure was calculated as the average of the measured values over the period of loading, and the vertical strain was calculated as the averages of the four LVDTs and POTs located on the footing at the end of each load increment. The axial deformations plotted in figure 34 indicate that the bearing bed provided marginally higher vertical capacity; however, vertical deformation was not improved at low strain levels. Figure 35 shows that at service loads (3,550-psf (170-kPa) applied vertical pressure), the lateral deformation of the top 1.31-ft (0.4-m)-thick bearing bed reduced by more than 50 percent due to inclusion of two courses of reinforcement.

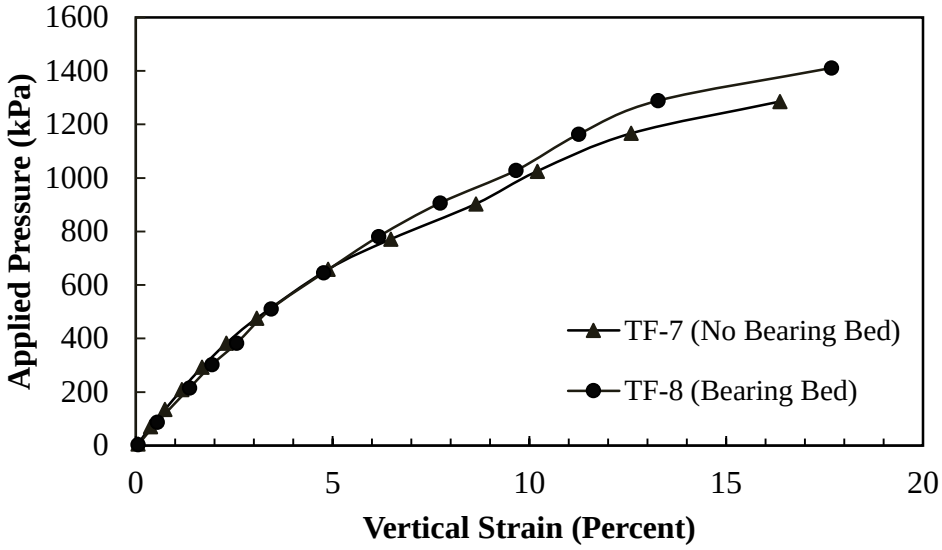

1 psi = 6.89 kPa
Note: This figure was created by FHWA after Nicks et al.[42]

Figure 34. Graph. Effect of bearing bed reinforcement for TF-7 and TF-8.

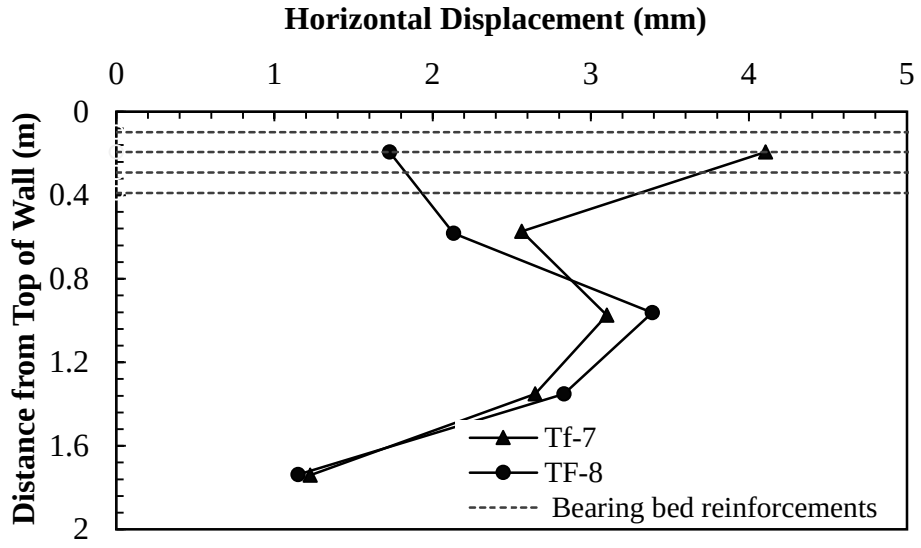

1 ft = 0.305 m
1 inch = 25.4 mm
Note: This figure was created by FHWA after Nicks et al.[42]

Figure 35. Graph. Measured lateral deformation at 3,600 psf (172.5 kPa) applied pressure for TF-7 (no bearing bed reinforcement) and TF-8 (two courses of bearing bed reinforcement).

Wu et al. conducted a series of generic soil geosynthetic composite (GSGC) laboratory tests to investigate the composite behavior of GRS mass with varying spacing and T_f of reinforcement.[74] The test program comprised five GSGC tests. The specimen height was 6.56 ft (2 m) with a square cross section of 4.59 ft (1.4 m). The test conditions and a summary of the

results are presented in table 13. The vertical movement was measured along the top surface of the concrete pad placed on top of the specimen before loading. Test 1 was conducted as a baseline for the other four tests. The specimen was loaded to 36.26 psi (250 kPa) (nearly up to 1 percent vertical strain), then unloaded to 0 psi (0 kPa) load and reloaded until failure. Other tests were loaded to the failure directly. A prescribed confining pressure of 4.93 psi (34 kPa) was applied on the entire surface area of the test specimens for tests 1 through 4. Figure 36 shows the load deformation behavior of the five GSGC tests. By comparing the results from tests 2 and 3, it can be concluded that the ultimate applied pressure increased by about 35 percent by doubling the reinforcement strength. By comparing tests 2 and 4, it can be concluded that by changing the reinforcement spacing from 1.31 to 0.66 ft (0.4 m to 0.2 m), the ultimate applied pressure increased by more than 50 percent. Therefore, compared to the T_f of reinforcement, the spacing of the reinforcement layers plays a more significant role in improving load-settlement behavior of a reinforced soil mass. Figure 37 shows lateral displacement of the test specimens at failure and at applied pressure of 87.02 psi (600 kPa). Test 2, which was a confined specimen with 0.66-ft (0.2-m) reinforcement spacing, demonstrated the highest ultimate capacity and least lateral deformation.

Table 13. Test conditions and results summary of GSGC tests.

Parameters	Test 1	Test 2	Test 3	Test 4	Test 5
Wide-width tensile ultimate strength (kN/m)	No reinforcement	70	140	70	70
Reinforcement spacing (m)	No reinforcement	0.2	0.4	0.4	0.2
Confining pressure (kPa)	34	34	34	34	0
Ultimate applied pressure (kPa)	770	2,700	1,750	1,300	1,900
Vertical strain at failure (percent)	3	6.5	6.1	4	6
Maximum lateral displacement at failure (mm)	47	60	54	53	Not measured

1 kN/m = 68.5 lbf/ft
1 ft = 0.305 m
1 psi = 6.89 kPa
1 inch = 25.4 mm
Note: This table was created by FHWA adopted from Wu et al.[74]

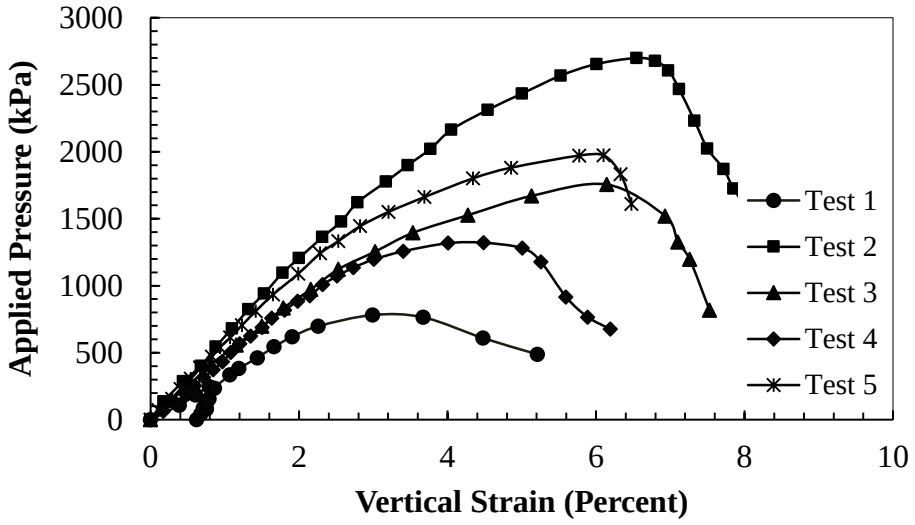

1 psi = 6.89 kPa
Note: This figure was created by FHWA after Wu et al.[74]

Figure 36. Graph. Load-deformation behaviors for GSGC tests.

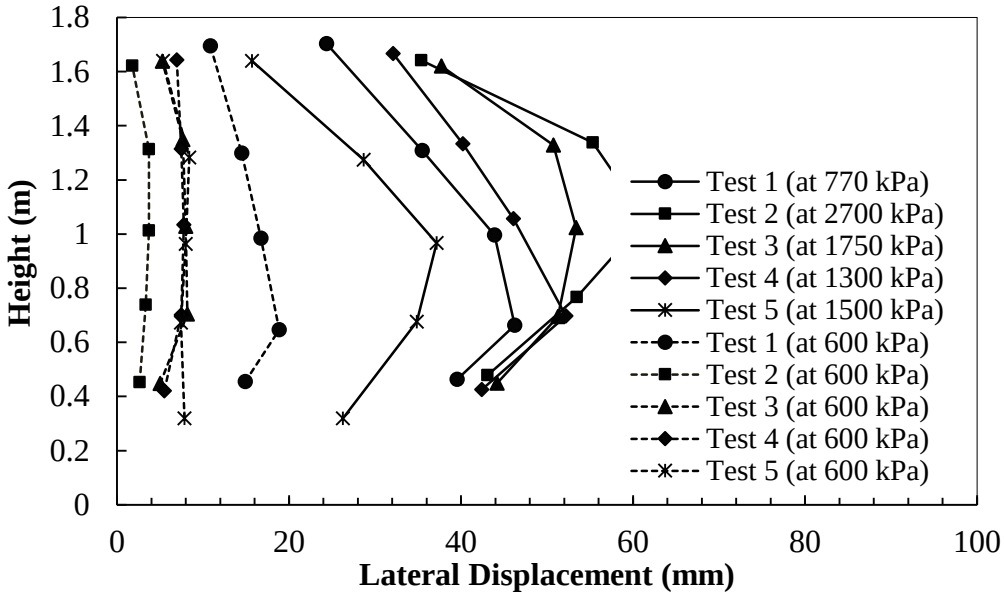

1 ft = 0.305 m
1 inch = 25.4 mm
1 psi = 6.89 kPa
Note: This figure was created by FHWA after Wu et al.[74]

Figure 37. Graph. Lateral deformation of test specimens at 12,531 psf (600 kPa) and the ultimate applied pressure.

Helwany et al. conducted FEAs to investigate the effects of geosynthetic stiffness on the performance of GRS abutment.[70] The stiffness of the base case was assumed to be 36,305 lbf/ft (530 kN/m). Results plotted in figure 38 show that the vertical displacement of the abutment seat for the base case (for an applied pressure of 4,177 psf (200 kPa)) was reduced by 43 percent when the geosynthetic stiffness increased by 10 times to 363,050 lbf/ft (5,300 kN/m).

Conversely, a drastic increase of 250 percent in displacement was noted when the geosynthetic stiffness was reduced to 3,603.5 lbf/ft (53 kN/m). Vertical displacement at the abutment seat increased drastically when axial stiffness of the geosynthetic dropped below a critical value, and the trend became more pronounced with an increase in applied pressure.

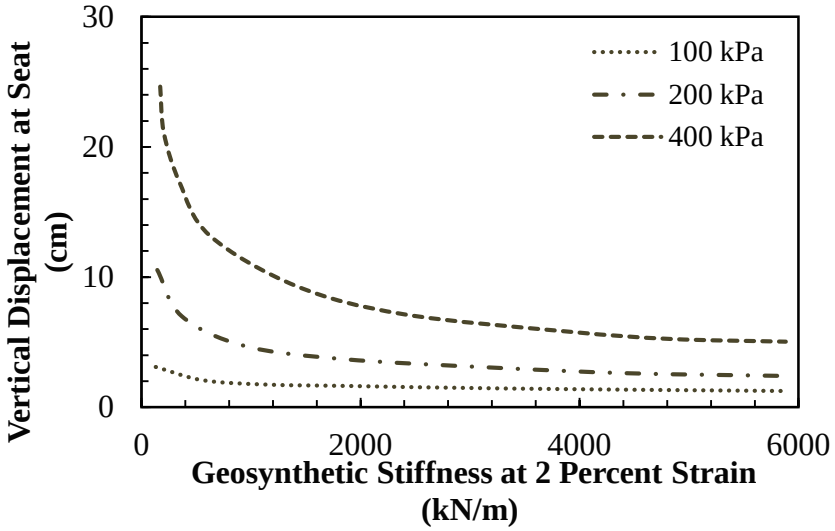

1 inch = 2.54 cm
1 psi = 6.89 kPa
1 kN/m = 68.5 lbf/ft
Note: This figure was created by FHWA after Helwany et al.[70]

Figure 38. Graph. Effect of geosynthetic stiffness (reinforcement spacing = 7.87 inches (20 cm)) on vertical displacement at abutment seat.

Helwany et al. concluded that the vertical displacement at the abutment seat increased when the vertical spacing between reinforcements increased at a high pressure of 58 psi (400 kPa).[70] Figure 39 shows that the increase in vertical displacement became more significant as the applied pressure increased. At an applied pressure of 4,177 psf (200 kPa), an increase of 40 percent in the vertical displacement was observed when the reinforcement vertical spacing increased from 7.87 to 23.62 inches (20 to 60 cm).

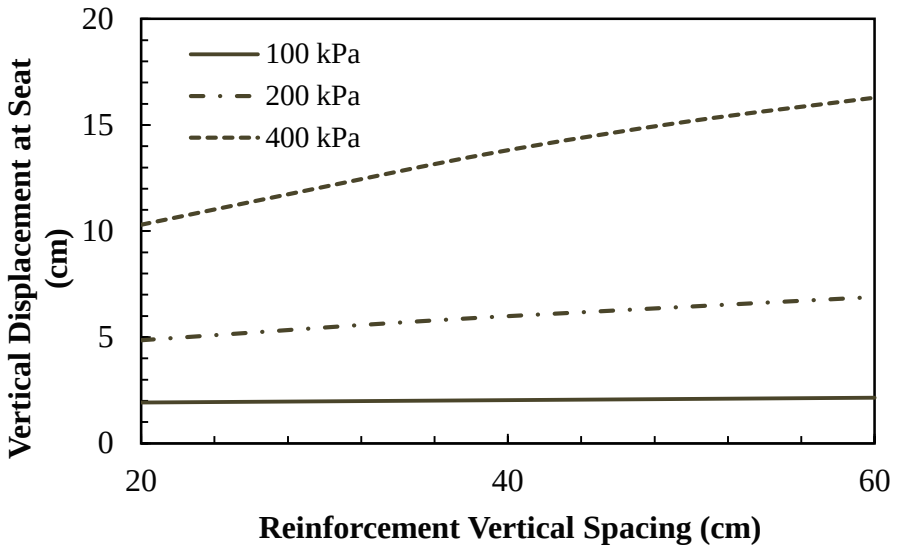

1 inch = 2.54 cm
1 psi = 6.89 kPa
Note: This figure was created by FHWA after Helwany et al.[70]

Figure 39. Graph. Effect of geosynthetic spacing on vertical displacement at abutment seat.

Figure 40 and figure 41 show that the horizontal displacements of the abutment seat and the maximum lateral displacement of the segmental wall decreased when the geosynthetic stiffness increased to 363,050 lbf/ft (5,300 kN/m) from the base case. Conversely, a drastic increase in displacements occurred when the geosynthetic stiffness was reduced to 3,630.5 lbf/ft (53 kN/m).

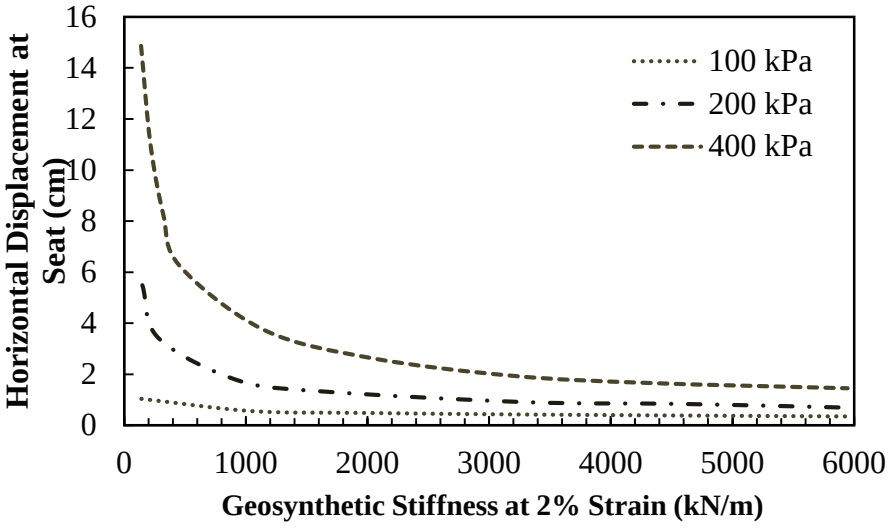

1 inch = 2.54 cm
1 psi = 6.89 kPa
1 kN/m = 68.5 lbf/ft
Note: This figure was created by FHWA after Helwany et al.[70]

Figure 40. Graph. Effect of geosynthetic stiffness (reinforcement spacing = 7.87 inches (20 cm)) on horizontal displacement at abutment seat.

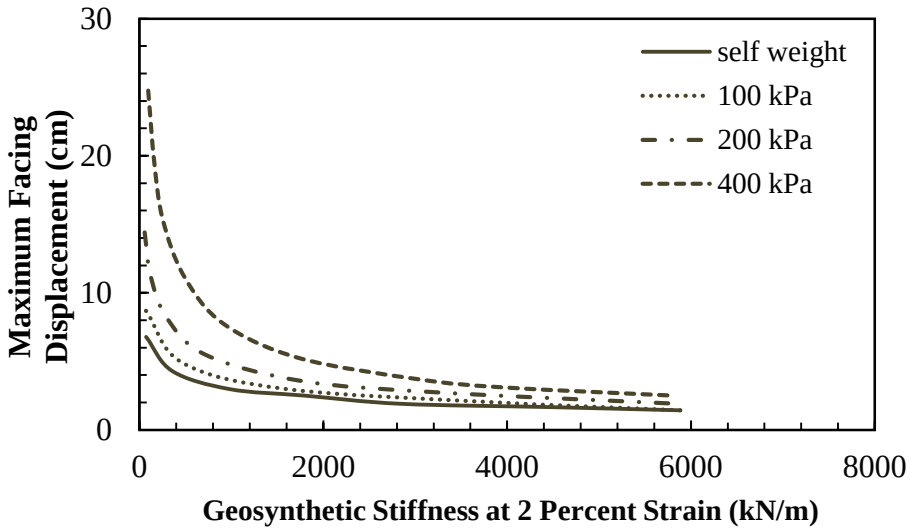

1 inch = 2.54 cm
1 psi = 6.89 kPa
1 kN/m = 68.5 lbf/ft
Note: This figure was created by FHWA after Helwany et al.[70]

Figure 41. Graph. Effect of geosynthetic stiffness (reinforcement spacing = 7.87 inches (20 cm)) on the maximum lateral displacement of the facing.

Based on the FEA of two full-scale loading tests of GRS bridge abutments as well as a parametric study to investigate the performance of GRS bridge abutments, Helwany et al. concluded that the horizontal displacement at the abutment seat and the maximum lateral displacement of the segmental facing increased with an increase in reinforcement spacing (see figure 42 and figure 43).[70] As figure 42 shows, at applied pressure of 29 psi (200 kPa), an increase of 52 percent in the horizontal displacement was observed when reinforcement vertical spacing increased from 7.87 to 23.62 inches (20 to 60 cm). At a lower applied pressure of 14.50 psi (100 kPa), the vertical spacing had a minimum effect on horizontal displacement. As shown in figure 43, at an applied pressure of 29 psi (200 kPa), by increasing the reinforcement spacing from 7.87 to 23.62 inches (20 to 60 cm), the maximum facing displacement increased by about 50 percent.

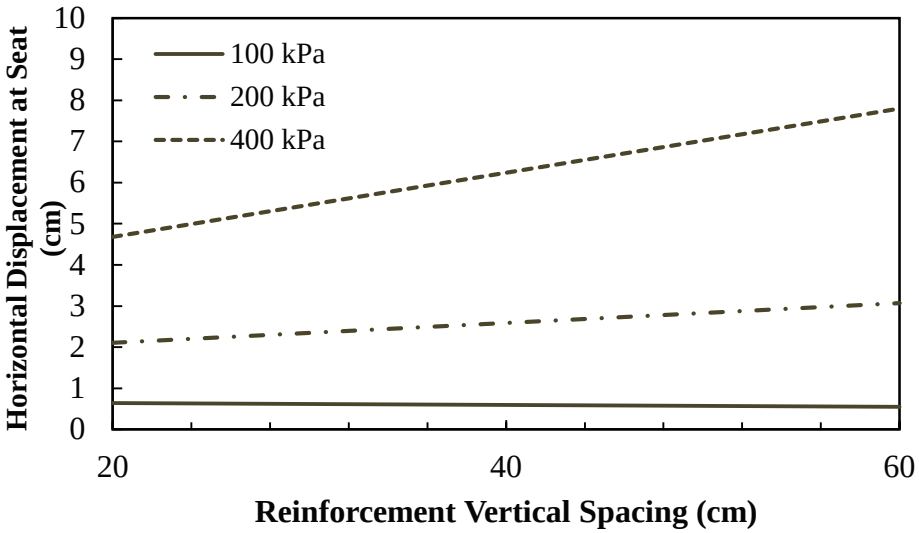

1 inch = 2.54 cm
1 psi = 6.89 kPa
Note: This figure was created by FHWA after Helwany et al.[70]

Figure 42. Graph. Effect of geosynthetic spacing on horizontal displacement at abutment seat.

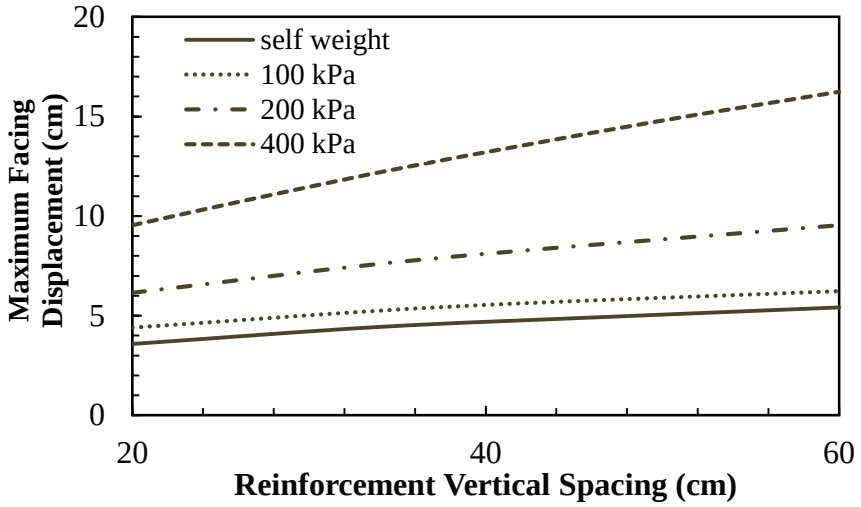

1 inch = 2.54 cm
1 psi = 6.89 kPa
Note: This figure was created by FHWA after Helwany et al.[70]

Figure 43. Graph. Effect of geosynthetic spacing on the maximum lateral displacement of the facing.

Gotteland et al. performed experimental and numerical studies on two reinforced walls: one was reinforced with a non-woven geotextile (represented by NW) and the other with a woven geotextile (represented by W) (see figure 44 and figure 45).[75] The non-woven geotextile was 3.5 times more extensible than the woven one and approximately half as strong in terms of T_f. After construction, the reinforced walls were loaded in the same way as a bridge deck through a foundation slab until failure occurred. The 3.28-ft (1-m)-wide foundation was located 4.92 ft

(1.50 m) from the edge of the facing. As figure 44 shows, the abutment with woven geotextile had a higher ultimate bearing capacity, and its settlement was less compared to the non-woven one. The results in figure 45 show that lateral deformation of the wall face with woven geotextile was less than that with non-woven geotextile.

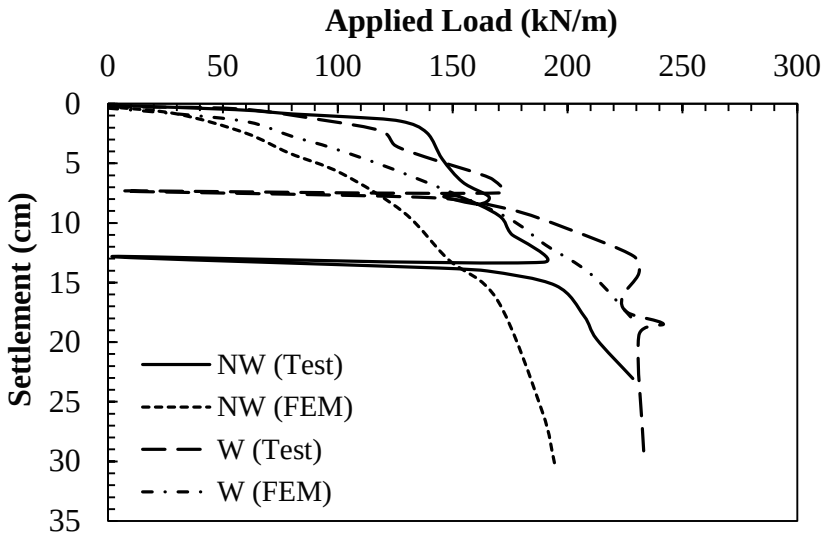

1 inch = 2.54 cm
1 kN/m = 68.5 lbf/ft
FEM = Finite element method.
Note: This figure was created by FHWA after Gotteland et al.[75]

Figure 44. Graph. Central settlement of the foundation versus applied load.

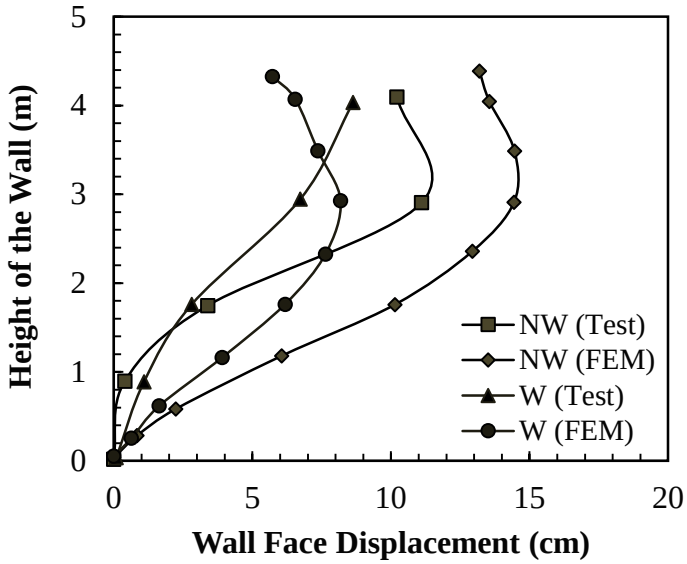

1 ft = 0.305 m
1 inch = 2.54 cm
Note: This figure was created by FHWA after Gotteland et al.[75]

Figure 45. Graph. Wall face displacement at applied pressure of 3,969.1 lb/ft^2 (190 kN/m^2) for non-woven and woven reinforcement.

Bathurst et al. conducted experiments on four full-scale modular block walls that were constructed with reinforcement layers with different tensile stiffnesses.[76] The walls were 11.81 ft (3.6 m) high. Two of the walls (walls 1 and 2) were reinforced with two different PP geogrid reinforcements, wall 3 was reinforced with a polyester (PET) geogrid, and wall 4 was reinforced with a welded wire mesh (WWM). Walls 1 and 2 were compacted using vibrating plate equipment, and walls 3 and 4 were compacted by a vibrating rammer. Figure 46 shows measured relative horizontal displacements recorded at monitored points on the wall facing column shortly after EOC. Each elevation point has a local datum corresponding to the time when each row of displacement POTs were installed.

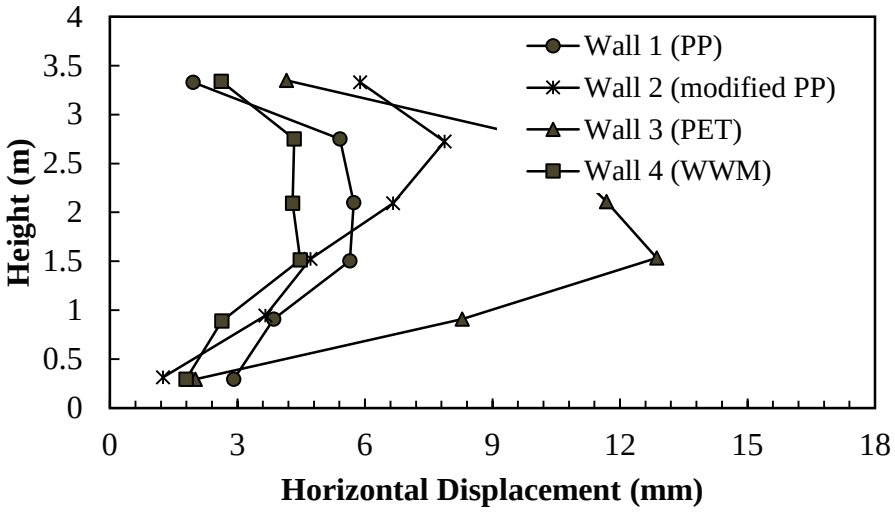

1 ft = 0.305 m
1 inch = 25.4 mm
Note: This figure was created by FHWA after Bathurst et al.[76]

Figure 46. Graph. Relative horizontal displacement of wall facing recorded at EOC.

Hatami and Bathurst investigated the influence of reinforcement properties on the performance of reinforced soil SRWs using a finite difference numerical model.[71] They concluded that the deformation response of the model wall with a pinned (fully fixed) reinforcement condition was very close to that of the model with interface stiffness between backfill soil and reinforcement layers (k_b) ≥ 145 lbf/inch/inch (1,000 kN/m/m). As figure 47 shows, for values of $k_b \leq$ 145 lbf/inch/inch (1,000 kN/m/m), the lower k_b, the greater the wall deformation. The wall deformation magnitude increased by a factor of two when the value of k_b was reduced by two orders of magnitude from k_b = 145 lbf/inch/inch (10^3 kN/m/m) to k_b = 1.45 lbf/inch/inch (10 kN/m/m).

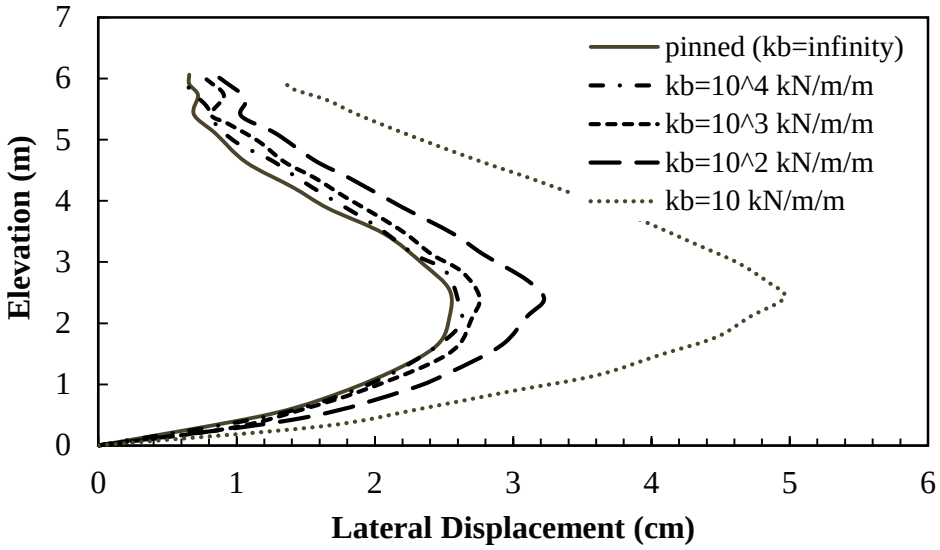

1 ft = 0.305 m
1 inch = 2.54 cm
1 kN/m/m = 0.145 lbf/inch/inch
Note: This figure was created by FHWA after Hatami and Bathurst.[71]

Figure 47. Graph. Influence of soil-reinforcement interface stiffness value on lateral displacement of the wall.

Zevgolis and Bourdeau simulated the performance of MSE abutments with metal strips to investigate the effects of different parameters such as the elastic modulus of reinforcement (E_R), H, magnitude of the applied load, and foundation soil type on the behaviors of the abutments.[4] They defined five case studies; H1-L3-S2, H1-L3-S3, H2-L1-S3, H2-L2-S2, and H3-L1-S2, where H1, H2, and H3 stand for the abutments that were 19.66, 22.97, and 26.24 ft (6, 7, and 8 m) tall, respectively; L1, L2, and L3 stand for supported spans that were 59.06, 78.74, and 9,843 ft (18, 24, and 30 m) long with total applied load of 18,152, 22,262, and 26,372 lbf/ft (265, 325, and 385 kN/m), respectively; and S2 and S3 represent different foundation soil types. For S2, f was 30 degrees, c was 104 lb/ft^2 (5 kPa), and the unit weight was 121 lb/ft^3 (19 kN/m^3). For S3, f was 20 degrees, c was 835 lb/ft^2 (40 kPa), and the unit weight was 108 lb/ft^3 (17 kN/m^3). As figure 48 shows, by increasing Young's modulus of reinforcement from 3.63 to 7.25 ksi (25 to 50 MPa), the maximum vertical deformation of the abutment decreased at least 42 percent, and by increasing Young's modulus of reinforcement from 7.25 to 14.50 ksi (50 to 100 MPa), the maximum vertical deformation decreased at least 36 percent. Moreover, the results indicate that higher MSE abutment had more vertical displacement that that of a lower one.

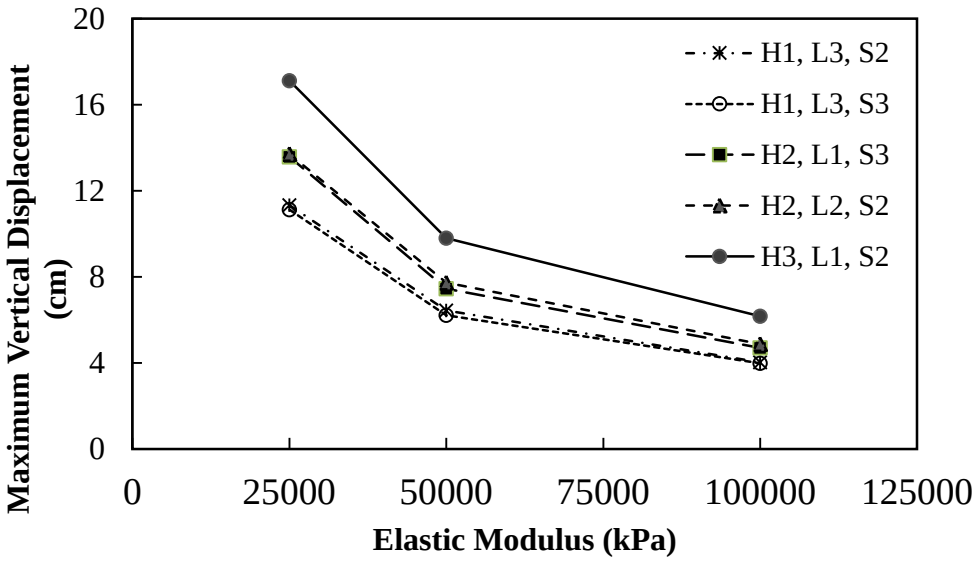

1 inch = 2.54 cm
1 psi = 6.89 kPa

Figure 48. Graph. Effect of E_R on the maximum vertical displacement of MSE abutments with metal strips.[(4)]

Tatsuoka et al. and Tateyama performed a series of plane strain model tests of metal strip-reinforced sand retaining walls with three different numbers of reinforcement layers (N = 2, 5, and 10).[(77,78)] The reinforcement layers were made of phosphor-bronze strips. The model wall was 33.07 inches (84 cm) wide, 15.55 inches (39.5 cm) long, and 20.47 inches (52 cm) tall. As the results plotted in figure 49 show, by increasing N, the vertical displacement of the foundation placed on top of abutment under each applied load decreased. For instance, by increasing N from 2 to 5, the settlement under applied pressure of 1.02 psi (7 kPa) decreased about 70 percent, and by increasing N from 5 to 10, the settlement decreased 53 percent under applied pressure of 2.03 psi (14 kPa). Cao and Peng simulated these experiments through a nonlinear FEM analysis and obtained similar results.[(79)] The results showed that the peak footing load of reinforced retaining walls increased significantly with an increase in the number of reinforced layers. The experimental results were obtained by Tateyama, and the FEM results were obtained by Cao and Peng.[(78,79)]

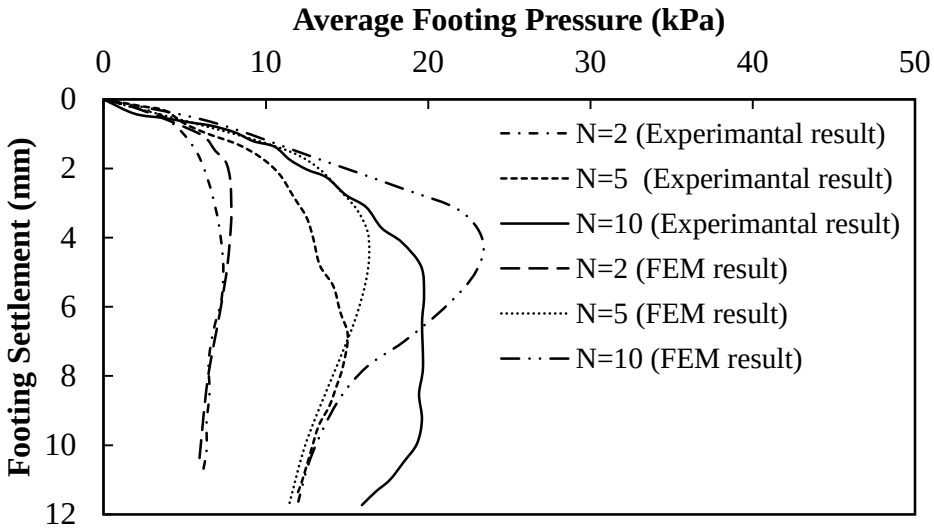

1 inch = 25.4 mm
1 psi = 6.89 kPa
Note: This figure was created by FHWA after Zevgolis and Bourdeau.[4]

Figure 49. Graph. Load-settlement results for the foundation on top of MSE abutment.

Effect of Facing Blocks on Load Deformation Relationships

Nicks et al. conducted five pairs of tests as a part of an FHWA research study to investigate the effects of facing elements on load deformation behavior of bridge piers (see figure 50).[42] They concluded that the ultimate capacity of pier increased when a facing element was present; however, the magnitude of strain at failure, which was measured through LVDTs and POTs on the footing, was similar for a given GRS composite with or without a facing.

For figure 50, the following parameters were used:

- TF-2 and TF-3 with S_v = 7.64 inches (19.4 cm) and T_f = 2,398 lb/ft (35 kN/m).
- TF-6 and TF-7 with S_v = 7.64 inches (19.4 cm) and T_f = 4,795 lb/ft (70 kN/m).
- TF-9 and TF-10 with S_v = 15.24 inches (38.7 cm) and T_f = 4,795 lb/ft (70 kN/m).
- TF-12 and TF-11 with S_v = 3.82 inches (9.7 cm) and T_f = 1,404 lb/ft (20.5 kN/m).
- TF-14 and TF-13 with S_v = 11.26 inches (28.6 cm) and T_f = 3,596 lb/ft (52.5 kN/m).

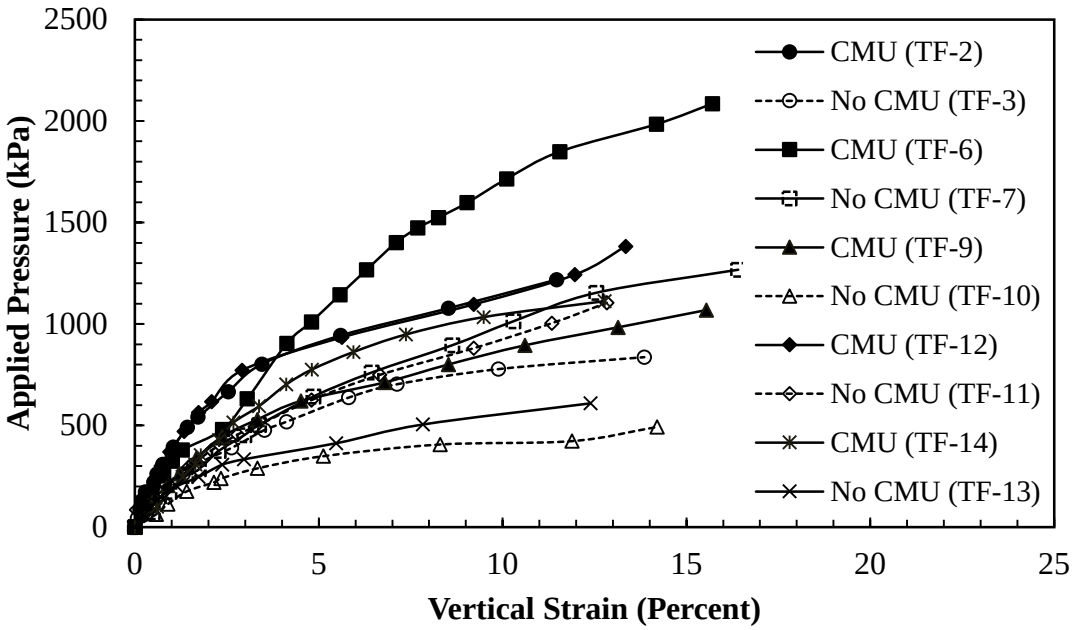

1 psi = 6.89 kPa
Note: This figure was created by FHWA after Nicks et al.[42]

Figure 50. Graph. Stress-strain response for different piers.

Effect of Prestraining on Load Deformation Relationships

A full-scale GRS bridge pier load test was conducted at FHWA's TFHRC in 1996.[22,23] The GRS pier was prestrained (preloaded) using hydraulic jacks and a specially designed reaction system. Results obtained from this instrumented bridge pier show that the prestraining reduced vertical settlement of the pier by approximately 50 percent (see figure 51). Figure 52 shows that prestraining did not reduce lateral deformation except for near the top of the pier where the lateral movement reduced significantly.

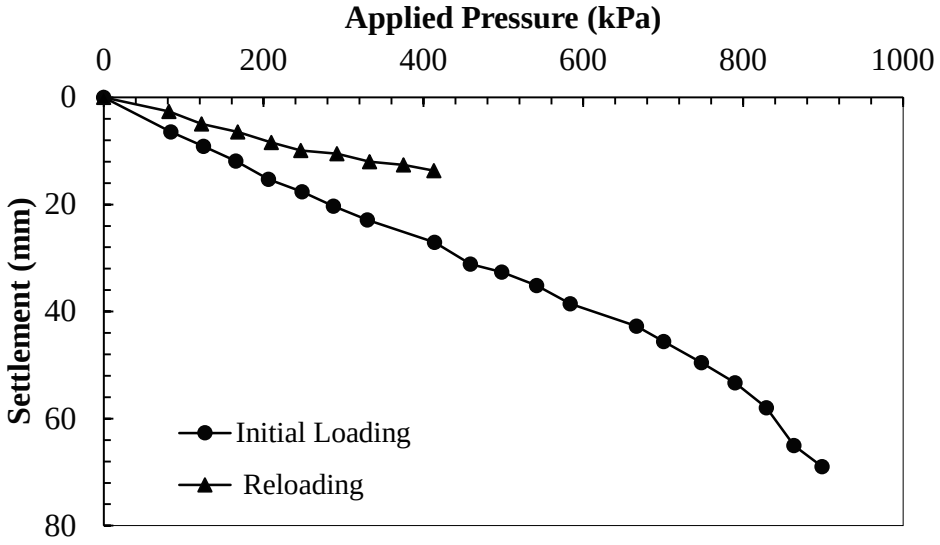

1 inch = 25.4 mm
1 psi = 6.89 kPa
Note: This figure was created by FHWA after Adams and Wu et al.[22,23]

Figure 51. Graph. Load-settlement curves for the pier.

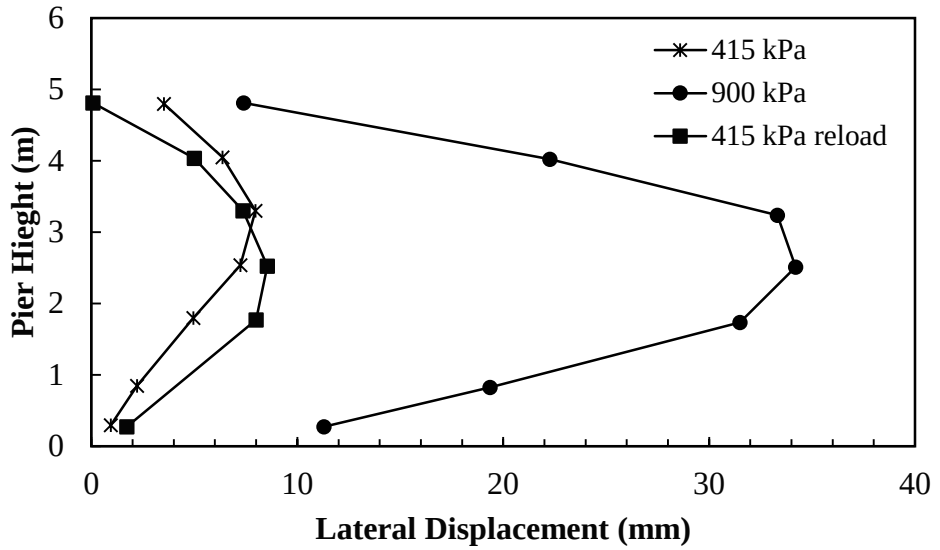

1 ft = 0.305 m
1 inch = 25.4 mm
1 psi = 6.89 kPa
Note: This figure was created by FHWA after Adams and Wu et al.[22,23]

Figure 52. Graph. Lateral displacement measured by LVDT.

Two GRS bridge abutments were built in Black Hawk, CO, in 1997 to support a steel bridge.[23] Because the thickness of the reinforced soil abutment were different beneath the four footings directly supporting the weight of the bridge, the GRS abutment was preloaded to reduce the differential settlement between adjacent footings. The abutment was preloaded up to 35.53 psi (245 kPa) (1.6 times the design load of 21.76 psi (150 kPa)) for the square footing and

11.60 psi (80 kPa) (2 times the design load of 5.80 psi (40 kPa)) for the rectangular footing. It was found that preloading substantially reduced the differential settlement. The differential settlements at 21.76 psi (150 kPa) of the preloading cycle for the two abutments were 0.33 and 0.85 inch (8.4 and 21.6 mm). At 21.76 psi (150 kPa) in the reloading cycle, the differential settlement of both abutments was less than 0.039 inch (1 mm).[23] Measured results by Wu et al. also show that preloading reduced the lateral movement of GRS abutments (see figure 53 and figure 54).[23] At 21.76 psi (150 kPa) in the preloading cycle, the maximum lateral displacements in the west abutment (8.86 ft (2.7 m) tall) and the east abutment (17.72 ft (5.4 m) tall) were 0.06 and 0.52 inch (1.5 and 13.2 mm), respectively. These displacement values were reduced to 0.02 and 0.18 inch (0.6 and 4.5 mm), respectively, at 21.76 psi (150 kPa) in the reloading cycle. After the first reloading cycle, there was no significant reduction in the magnitude of the lateral and vertical deformations of the GRS abutments in the subsequent reloading cycles.[23]

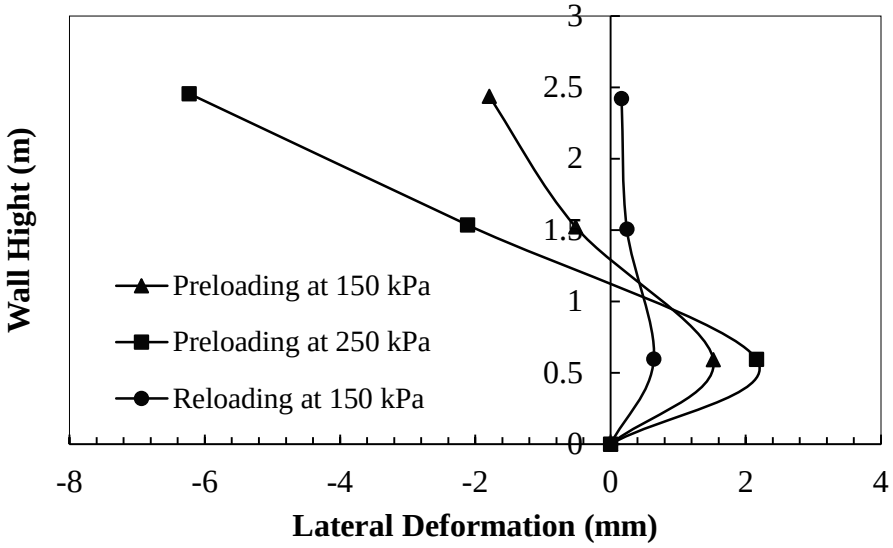

1 ft = 0.305 m
1 inch = 25.4 mm
1 psi = 6.89 kPa
Note: This figure was created by FHWA after Wu et al.[23]

Figure 53. Graph. Lateral deformation profiles of the west abutment.

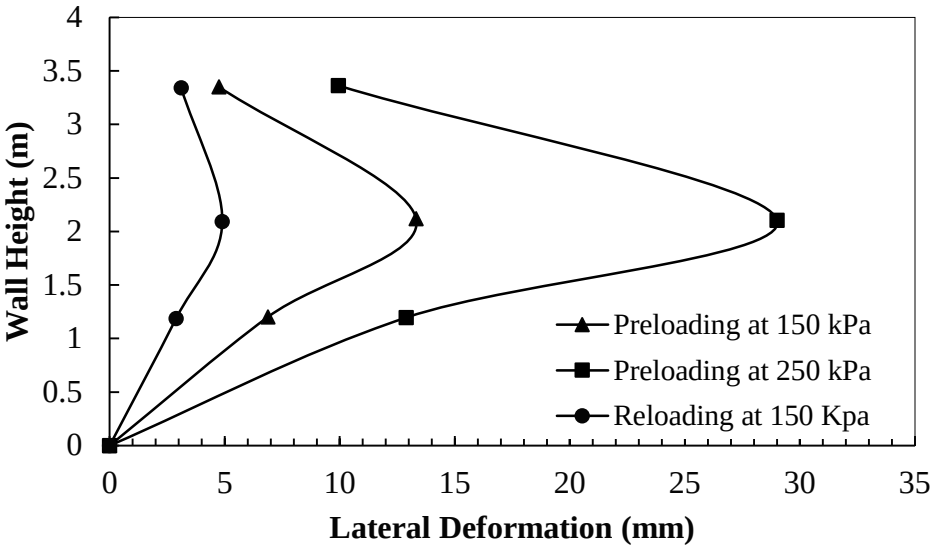

1 ft = 0.305 m
1 inch = 25.4 mm
1 psi = 6.89 kPa
Note: This figure was created by FHWA after Wu et al.[23]

Figure 54. Graph. Lateral deformation profiles of the east abutment.

3.4 EFFECTS OF TRANSIENT LOADS ON DEFORMATIONS OF BRIDGE SUPPORTS ON GRANULAR SOILS

Live loads may include traffic load and compaction-induced load. Few research studies have investigated the effect of live loads on bridge supports using engineered fills. Based on a three-dimensional (3D) numerical study on an integral abutment bridge, Olson et al. concluded that superstructure deflections related to live load had a secondary effect on the abutment displacement but substantially changed their rotation.[80] As a result, the critical moments at the connection between superstructure and foundation were exacerbated by live load in thermal expansion and improved in thermal contraction conditions. Chapter 10 of *AASHTO LRFD Bridge Design Specifications* specification states, "Transient load may be omitted for settlement analysis for cohesive soils subjected to time-dependent consolidation settlement."[8] However, for cohesionless soils (including engineered fills), transient load may be considered in the deformations of shallow foundations and abutments and piers of bridges. For retaining walls and bridge abutments, the traditional approach is to add the live load to the dead load and consider the combined loads as a permanent dead load. For example, through analytical studies, Kim and Barker and Esmaeili and Fatollahzadeh investigated the equivalent surcharge for truck load and train load, respectively, on retaining walls and bridge abutments.[81,82] Presently, the dynamic effect of transient load on bridge supports using engineered fills has not been investigated. Moreover, there is a lack of literature on the time-dependent and live (transient) load on the stress-deformation behaviors of bridge supports in engineered fills.

3.5 DETERMINATION OF STRESS DISTRIBUTIONS IN GRANULAR SOILS UNDER SHALLOW FOUNDATIONS

Equations to compute vertical stresses at any point in a soil mass due to external vertical loadings have been developed based on the theory of elasticity. The formulas that are most widely used are the Boussinesq and Westergaard formulas.[83,84] They were first developed for point loads acting at the surface. These formulas have been integrated to obtain stresses below uniform strip loads and rectangular loads. In the practice, Boussinesq's formulas are often preferred, as they give conservative results.

The Boussinesq formulas are based on the following assumptions:[83]

- The soil mass is elastic, isotropic, and homogeneous.
- The soil is semi-infinite.
- The soil is weightless.

In the Westergaard formulas, the material is isotropic with finite and equal horizontal and vertical normal moduli and Poison's ratios but with infinite horizontal shear modulus.[84] The assumptions for Westergaard's formulas are as follows:

- The soil is elastic and semi-infinite.
- The soil is composed of numerous closely spaced horizontal layers of negligible thickness of an infinite rigid material.
- The rigid material permits only the downward deformation of mass in which horizontal deformation is zero.

For engineered fills without reinforcement, the Boussinesq and Westergaard formulas can be used to determine the stress distributions inside the soil mass. In reinforced engineered fills that are used as bridge supports, the reinforced soils are no longer isotropic or homogeneous. Therefore, the Boussinesq and Westergaard formulas may not be applicable. In such a case, numerical simulations (such as FEM or finite difference method) may be used. Many past researches have studied the strain and stress distributions of the reinforcements within geosynthetic-reinforced walls. (See references 85–88.) For metallic-reinforced soils, there are three common methods used in North American practice for estimating reinforcement loads: the AASHTO coherent gravity method, the FHWA structure stiffness method, and the AASHTO simplified method. (See references 52, 89, and 36.) Limited studies have been conducted on stress distributions in reinforced soils as bridge supports, particularly in SLS. Rowe and Ho studied a continuous full-facing panel wall with a hinged toe and reinforced with extensible reinforcement in a granular backfill resting on a rigid foundation.[90] This numerical study concluded that among the parameters examined, the distribution of force was most affected by the reinforcement stiffness, density, the external f between facing and soil, the backfill soil internal f, and the rigidity of the facing.

The stress distribution can be influenced by various soil conditions (i.e., grain size distribution, strength parameters, relative density, and fine content), reinforcement characteristics (i.e., T_f, stiffness, N, and S_v), and loading conditions, some of which were investigated by Rowe and Ho.[90] However, the literature search conducted by the authors of this report suggests there is a lack of documentation and understanding of the effects of various parameters on the stress distribution in reinforced engineered fills as bridge supports in SLS.

CHAPTER 4. EVALUATION OF PREDICTION METHODS FOR DEFORMATIONS OF BRIDGE SUPPORTS ON GRANULAR SOILS

In this chapter, methods that are widely accepted and routinely used to calculate immediate and long-term settlement of shallow foundations of bridges, vertical deformation of GRS abutments, and lateral displacement of GRS abutments are evaluated. Available methods for long-term deformations of shallow foundations on granular soils are also presented.

4.1 METHODS FOR IMMEDIATE SETTLEMENT OF SHALLOW FOUNDATIONS OF BRIDGES ON GRANULAR SOILS

Various methods are available to calculate the immediate (elastic) settlement of shallow foundations. Das provided a critical review of 12 common methods on elastic settlement of shallow foundations on granular soil.[91] He grouped the methods into three categories: methods based on observed settlement of structures and full scale prototypes, semi-empirical methods based on a combination of field observations and theoretical studies, and methods based on theoretical relationships derived from the theory of elasticity. In this section, the following five methods are presented and evaluated:

- Modified Schmertmann method.[92,93]
- Hough method.[94]
- Peck and Bazaraa method.[95]
- Burland and Burbidge method.[96]
- D'Appolonia method.[97,98]

These five methods were evaluated in previous FHWA studies and a SHRP2 study.[3,12,10] The *AASHTO LRFD Bridge Design Specifications* recommends the use of the Hough method, which has the smallest coefficient of variance.[8,94] However, the Hough method is conservative by a factor of approximately two, which often leads to unnecessary use of deep foundations instead of spread footings to meet tolerable deformation criteria. FHWA recommends the use of the method proposed by Schmertmann because it is a rational method that considers not only the applied stress and its associated strain influence distribution with depth for various footing shapes but also the elastic properties of the foundation soils, even if they are layered. (See references 6, 7, 92, 93, and 10.)

Modified Schmertmann Method

To estimate settlements of footings in structural fills by the Schmertmann method, an assumption must be made about the standard penetration test (SPT) blow count for an SPT sampler to penetrate the second and third 6 inches into the subsoil (*N*-value) that is representative of the engineered fill.[92,93] The FHWA report, *Spread Footings for Highway Bridges* used an SPT *N*-value of 32 blows/ft (32 blows/0.305 m) corrected for overburden pressure as a representative value for estimating settlement in structural fills.[3] This SPT *N*-value corresponds to a relative

density of approximately 85 percent at an overburden stress of about 2,000 psf (95.8 kPa) and approximately 97 percent RC based on the modified Proctor compaction energy.[3,18] Under such compacted conditions, and in the absence of other SPT data in structural fills, the settlement of a footing supported on structural fill can be estimated by using an assumed corrected SPT blow count ($(N_1)_{60}$) of 32. However, engineered fills are often compacted to a RC of 95 percent based on the modified Proctor compaction energy. For this case, $(N_1)_{60}$ of 23 is more appropriate.[18]

Based on the modified Schmertmann method, the immediate settlement of spread footing can be estimated by the equations found in figure 55 through figure 57.[93]

$$S_i = C_1 C_2 \Delta p \sum_{i=1}^{n} \left(H_i \left(\frac{I_z}{XE_i} \right) \right)$$

Figure 55. Equation. Immediate settlement of spread footing based on modified Schmertmann method.

Where:

Si = Immediate settlement.
C_1 = Correction factor for strain relief due to soil excavation for foundation embedment, which is defined in figure 56.
C_2 = Correction factor to consider creep as the time-dependent increase in settlement for t time (i.e., number of years) after construction, which is defined in figure 57.
Δp = Net uniform pressure applied at the foundation depth.
H_i = Thickness of each soil layer.
I_z = Strain influence factor.
X = Factor used to determine the value of elastic modulus.
E_i = Elastic modulus of layer i in the vertical direction.

$$C_1 = 1 - 0.5 \left(\frac{p_0}{\Delta p} \right) \geq 0.5$$

Figure 56. Equation. Correction factor to consider foundation embedment depth.

Where p_0 = Initial effective stress at the foundation depth.

$$C_2 = 1 + 0.2 \log_{10} \left(\frac{t(\text{years})}{0.1} \right)$$

Figure 57. Equation. Correction factor to consider creep.

Hough Method

The original Hough method was used to estimate immediate settlement of embankments.[84] It was based on uncorrected SPT N-values and included recommendations for cohesionless as well as cohesive soils such as sandy clay and remolded clay, respectively. AASHTO modified the Hough method and used $(N_1)_{60}$ to eliminate the recommendations for sandy clay and remolded clay.[9,84] However, the settlements estimated by the modified Hough method are usually overestimated by a factor of 2 or more based on the data in the FHWA report, *Spread Footings for Highway Bridges*.[3] Such conservative estimates may be excessive with respect to the

behavior of the structures founded within, under, or near the embankment. In cases where structures are affected by embankment settlement, more refined estimates of the immediate settlements are warranted.

In the Hough method, the immediate settlement of sand under a shallow foundation is calculated by taking the summation of settlement of subdivided layers of 10 ft (3.05 m) that are influenced by the foundation load. The settlement (ΔH) of each soil layer is calculated using the following:

$$\Delta H = H_i \left(\frac{1}{C}\right) \log_{10} \left(\frac{\sigma'_0 + \Delta\sigma'_v}{\sigma'_0}\right)$$

Figure 58. Equation. Immediate settlement of each soil layer based on the Hough method.

Where:

C = Bearing Capacity Index.
σ'_0 = Initial average effective stress of the subdivided soil layer.
$\Delta\sigma'_v$ = Vertical stress increase in the subdivided soil layer due to applied foundation load.

Peck and Bazaraa method

The Peck and Bazaraa method is based on the original Terzaghi and Peck empirical equation.[95,99] The SPT blow count is corrected for overburden pressure to reflect the relative density of the soil. The immediate settlement of a footing on sand is calculated as follows:

$$S = C_w C_D \frac{2p}{(N_1)_{60}} \left(\frac{B}{B + 0.3}\right)^2$$

Figure 59. Equation. Immediate settlement of footing based on Peck and Bazaraa method.

Where:

S = Settlement of footing.
C_w = Water table correction factor at depth of $B/2$ below footing bearing level.
C_D = Embedment correction factor.
p = Footing bearing pressure.

$(N_1)_{60}$ can be estimated using the equations in figure 60 and figure 61 as follows:

$$(N_1)_{60} = \frac{4N_{60}}{1 + 0.04\sigma'_0} \text{ (for } \sigma'_0 \leq 1{,}566 \text{ lb/ft}^2 \text{ (75 kN/m}^2\text{))}$$

Figure 60. Equation. SPT blow count corrected for overburden pressure less than or equal to 1,566 lb/ft^2 (75 kPa).

Where N_{60} = Standard penetration number that is corrected based on the field conditions.

$$(N_1)_{60} = \frac{4N_{60}}{3.25 + 0.01\sigma'_0} \text{ (for } \sigma'_0 > 1{,}566 \text{ lb/ft}^2 \text{ (75 kN/m}^2\text{))}$$

Figure 61. Equation. SPT blow count corrected for overburden pressure greater than 1,566 lb/ft^2 (75 kPa).

Burland and Burbidge Method

The Burland and Burbidge method is an empirical relationship between average SPT blow count, foundation width, and foundation subgrade compressibility.[96] It is based on regression analysis of case studies. The immediate settlement of a footing on granular soil is given by the following:

$$S = f_s f_l f_t \left[\left(q' - \frac{2}{3}\sigma'_0 \right) B^{0.7} I_c \right]$$

Figure 62. Equation. Immediate settlement of a footing based on Burland and Burbidge method.

Where:

f_s = Shape correction factor.
f_l = Correction factor for thickness of sand or gravel layer.
f_t = Time factor, used if t ³ 3 years.
q¢= Average gross applied pressure.
I_c = Compressibility Index.

D'Appolonia Method

The D'Appolonia method is based on the elastic theory.[97,98] The immediate settlement of a footing on sand is given by the following:

$$S = \frac{pB}{M}\mu_0\mu_1$$

Figure 63. Equation. Immediate settlement of a footing based on D'Appolonia method.

Where:

M = Modulus of compressibility of sand; it is determined using the empirical chart based on SPT results for both normally consolidated and over-consolidated sand; the SPT blow count in the chart is the average blow count in the depth B below the footing bearing level.[97]
μ_0 = Embedment correction factor, using the chart by Christian and Carrier.[100]
μ_1= Correction factor for thickness of sand layer, using the chart by Christian and Carrier.[100]

4.2 LONG-TERM SETTLEMENT OF SHALLOW FOUNDATIONS ON GRANULAR SOILS

Long-term, or time-dependent, settlement of shallow foundations on granular soils is also known as "creep" or "secondary settlement." Crouse and Wu conducted a study to examine the long-term (greater than 6 mo) performance of seven full-scale GRS walls in the United States and Canada.[101] The walls ranged from 15 to over 40 ft (4.6 to over 12.2 m) in height and typically

included surcharge loads from earth fills or highway loads. The geosynthetics were geogrid or geotextiles, and the facing consisted of concrete modular blocks, panels, or exposed surface. The creep rate of reinforcement ranged from 0.4 to 0.7 percent, with one GRS wall at 1.5 percent. Although quantitative creep rate of the GRS walls was not reported, it was found that creep rate decreased with time at a decreasing rate.[102] Adams and Nicks conducted a full-scale study on the secondary settlement of four GRS piers.[27] The results indicate that secondary settlement does occur in granular material, but the amount with GRS is still within typical tolerable limits for bridges.

Empirical equations have been proposed by previous researchers to evaluate long-term settlement of granular soils due to creep. This section presents four methods. Due to the limited data on long-term settlement of shallow foundations on granular soils, evaluation of these methods was not conducted.

The modified Schmertmann method considered creep as the time-dependent increase in settlement after construction, as shown in figure 57.[92,93]

Terzaghi, Peck, and Mesri presented the following equation for settlement due to creep (S_{creep}):[103]

$$S_{creep} = \left(\frac{0.1}{\bar{q}_c}\right) z_0 \log\left(\frac{t_{\text{days}}}{1\text{ day}}\right)$$

Figure 64. Equation. Settlement due to creep.

Where:

$\bar{q}_c$ = Weighted mean value of measured static cone resistance of cone penetration test (q_c) between $z = 0$ to z_0, where z is depth from the ground surface, and z_0 is the depth under consideration.

Wu reported the following creep rate equation by assuming a linear relationship between the log scale of creep rate and log scale of time:[102]

$$\frac{d\varepsilon_c}{dt} = A(t)^m$$

Figure 65. Equation. Creep rate of shallow foundations.

Where:

ε_c = Creep strain (percent).
A = Reference creep rate; ($d\varepsilon_c/dt$) at $t = 1$ day (percent/day).
m = Creep modulus (equal to slope of $\log(d\varepsilon_c/dt)$ versus $\log(t)$ line; it may be obtained from PTs.

Briaud and Garland and Briaud proposed an expression of time-dependent settlement of footings in sand as follows:[104,105]

$$\frac{s(t)}{s(t_t)} = \left(\frac{t}{t_1}\right)^n$$

Figure 66. Equation. Time-dependent settlement of footings in sand.

Where:

$s(t)$ = Settlement at time t.
$s(t_1)$ = Settlement at time t_1, where t_1 is the reference time (1 min).
n = Time dependency exponent.

Briaud reported that the model identified in figure 66 fit well with a large-scale footing test and the n value typically varied from 0.005 to 0.03 for sands.[105,106] Briaud recommended obtaining site-specific n values by creep pressure meter testing.[105] If this is not available, a value of 0.03 seems conservative for sand in most cases.

4.3 VERTICAL DEFORMATION OF GRS ABUTMENTS

The approach for determining vertical deformation of a GRS abutment involves empirically finding the strain from an applicable PT curve.[32] The vertical strain of a GRS abutment is found from the intersection of the applied vertical stress due to the dead load and the PT design envelope for vertical strain. The vertical strain should be limited to 0.5 percent unless additional deformation is permitted.[32] The lateral strain can be then determined analytically assuming no volume change in the abutment.

The vertical displacement (ρ) of a GRS abutment with a strip footing is given by the equation in figure 67.[42] This equation is based on a solution for a relative displacement between the center of the strip footing and any arbitrary point assuming a constant stiffness with depth and a Poisson's ratio of 0.5 for the GRS material.[107]

$$\rho = \frac{3qb'}{4\pi E_{GRS}}\left[\frac{1}{2}\left(1+\frac{a+\frac{b'}{2}}{\frac{b'}{2}}\right)\ln\left(\frac{H^2+\left(a+\frac{b'}{2}\right)^2}{\left(\frac{b'}{2}\right)^2}\right)+\frac{1}{2}\left(1-\frac{a+\frac{b'}{2}}{\frac{b'}{2}}\right)\ln\left(\frac{H^2+a^2}{\left(\frac{b'}{2}\right)^2}\right)+\frac{H}{a}\tan^{-1}\left(\frac{a+b'}{H}\right)+\frac{H}{a}\tan^{-1}\left(\frac{-b'}{H}\right)\right]$$

Figure 67. Equation. Vertical displacement of a GRS abutment with a strip footing.

Where:

$\pi \approx 3.1415926$.
E_{GRS} = Young's elastic modulus of the GRS composite.
q = Applied pressure.
a = Setback distance between the face of the wall and the applied load.
b' = Width of facing block.

4.4 LATERAL DISPLACEMENT OF GRS WALLS AND ABUTMENTS

This section presents six methods for calculating lateral displacement of GRS walls and abutments. It is noted that these methods apply to GRS walls and abutments only. Their applicability to MSE walls or abutments remains to be verified.

For the lateral deformations of MSE walls and abutments, the FHWA specification, *Design and Construction of Mechanically Stabilized Earth Walls and Reinforced Soil Slopes* states the following:[37]

> "With respect to lateral wall displacements, no method is presently available to definitively predict lateral displacements, most of which occur during construction. The horizontal movements depend on compaction effects, reinforcement extensibility, reinforcement length, reinforcement-to-panel connection details, and details of the facing system. A rough estimate of probable lateral displacements of simple structures that may occur during construction can be made based on the reinforcement length to wall-height ratio and reinforcement extensibility as shown in Figure '2-15', for the serviceability limit check." (Chapter 2, pp. 40)[37]

FHWA Method

Christopher et al. correlated the ratio of reinforcement length and wall height (*L/H*) with the lateral displacement of a reinforced soil wall during construction.[89] This method is referred to as the "FHWA method." The FHWA method was developed empirically by determining a displacement trend from numerical analysis and adjusting the curve to fit with field-measured data. The method provides an estimate of the maximum lateral displacement. In this method, an empirically derived relative displacement coefficient (δ_R) was related graphically to *L/H*. Based on the graphical relationship, a fourth-order polynomial equation was derived for $0.3 < L/H < 1.175$ shown in figure 68.[74]

$$\delta_R = 11.81\left(\frac{L}{H}\right)^4 - 42.25\left(\frac{L}{H}\right)^3 + 57.16\left(\frac{L}{H}\right)^2 - 35.45\left(\frac{L}{H}\right) + 9.471$$

Figure 68. Equation. Displacement coefficient of a reinforced soil wall.

The maximum lateral deformation (δ_{max}) of a GRS wall is as follows:

$$\delta_{max} = \frac{\delta_R H}{250}$$

Figure 69. Equation. Maximum lateral deformation of a GRS wall with inextensible reinforcement (i.e., metallic reinforcement).

$$\delta_{max} = \frac{\delta_R H}{75}$$

Figure 70. Equation. Maximum lateral deformation of a GRS wall with extensible reinforcement (i.e., geosynthetic reinforcement).

Wu et al. stated that figure 70 has been corrected for a wall with a different height and surcharge.[74]

Geoservices Method

The Geoservices method relies on limit equilibrium analyses to calculate the length of the required reinforcement to satisfy a suggested factor of safety with regard to three presumed external failure modes (e.g., bearing capacity failure, sliding, and overturning).[108] The method provides a procedure for calculating the lateral wall displacement. The lateral displacement is calculated by first choosing a strain limit for the reinforcement. This strain limit is usually less than 10 percent and depends on a number of factors, such as the type of wall facing, the displacement tolerances, and the type of geosynthetic to be used as reinforcement. Concrete facing panels, for example, would not allow much lateral displacement without showing signs of distress. Therefore, a low strain limit (1 to 3 percent) should be selected.[74] Once the strain limit has been selected, the method assumes a distribution of strain in the reinforcement for calculating wall movement. The maximum horizontal displacement of a GRS wall or abutment, d_{max}, can be calculated as follows:

$$\delta_{max} = \frac{\varepsilon_d L}{2}$$

Figure 71. Equation. Maximum horizontal displacement of a GRS wall or abutment based on Geoservices method.

Where ε_d = Strain limit.

Colorado Transportation Institute (CTI) Method

In a study for CTI, Wu proposed a service load-based design method, referred to as the CTI method, to determine the maximum lateral displacement of a GRS wall or abutment.[109] In most cases, the designer may select a design limit strain (e_d) of 1 to 3 percent for the reinforcement for H less than or equal to 29.52 ft (9 m). d_{max} can be estimated by the following empirical equation in figure 72:

$$\delta_{max} = \varepsilon_d \left(\frac{H}{1.25} \right)$$

Figure 72. Equation. Maximum lateral displacement of a GRS wall or abutment based on CTI method.

If d_{max} exceeds a prescribed tolerance for the wall, a smaller e_d should be selected so that d_{max} of the wall will satisfy the performance requirement. Figure 72 applies only to walls with very small facing rigidity, such as wrapped-faced walls. Walls with significant facing rigidity have smaller maximum lateral displacement. For example, a modular block GRS wall has a $d_{\max}$ about 15 percent smaller than that calculated in figure 72.[74]

Jewell-Milligan Method

Jewell and Jewell and Milligan proposed a method for calculating wall displacement based on analysis of stresses and displacements in a reinforced soil mass.[110,111] This method only applies to a GRS wall with flexible facing (i.e., the rigidity of wall facing is ignored). Jewell and

Milligan provided graphical relationships between a dimensionless displacement factor, $\left(\frac{\delta_h K_{reinf}}{HP_{base}}\right)$ and depth below crest of wall $\left(\frac{Z}{H}\right)$ at various soils f and dilation angles. Where:[111]

d_h = Lateral displacement of a GRS wall or abutment with flexible facing.
K_{reinf} = Stiffness of reinforcement.
P_{base} = Reinforcement force at the base of the wall.
Z = Depth from the crest of the wall.

d_h varies with wall depth, and d_{max} occurs in the middle of H. Based on the Jewell and Milligan method, Wu et al. derived the following analytical expression of the lateral displacement of a GRS wall:[74]

$$\delta_h = \left(\frac{1}{2}\right)\left(\frac{P_{rm}}{K_{reinf}}\right)(H - z_i)\left[\tan\left(45^o - \frac{\psi}{2}\right) + \tan\left(90^o - \phi_{ds}\right)\right]$$

Figure 73. Equation. Lateral displacement of a GRS wall or abutment with flexible facing.

Where:

P_{rm} = Maximum reinforcement force at depth of influence zone (z_i).
K_{reinf} = Stiffness of the reinforcement.
f_{ds} = Friction angle of soil based on direct shear test.
y = Dilation angle of soil.

Wu Method

Following the theory for the Jewell and Milligan method, Wu et al. proposed an analytical model for calculating the lateral movement of a GRS wall with modular block facing.[74] This method, referred to as the "Wu method," considers the rigidity of wall facing. Figure 74 shows the lateral displacement of a GRS wall with modular block facing, and figure 75 shows the lateral displacement of a GRS wall with modular block facing while ignoring the effect of fiction between the back of the modular block and soil.

$$\Delta_i = 0.5\left(\frac{K_h\left(\gamma_s Z + q\right)S_v - \gamma_s b' S_v \tan\delta(1 + \tan\delta\tan\beta)}{K_{reinf}}\right)(H - Z)\left[\tan\left(45^o - \frac{\psi}{2}\right) + \tan\left(90^o - \phi_{ds}\right)\right]$$

Figure 74. Equation. Lateral movement of a GRS wall with modular block facing.

Where:

D_i = Lateral movement of a GRS wall with modular block facing.
K_h = Horizontal earth pressure coefficient.
g_s = Unit weight of soil.
Z = Depth from the wall crest.
g_b = Unit weight of modular block facing.
d = Friction angle between modular block facing elements.
b = Friction angle between back face of wall and soil.

$$\Delta_i = 0.5\left(\frac{\left(K_h\left(\gamma_s Z + q\right)S_v - \left(\gamma_b b' S_v\right)\tan\delta\right)}{K_{reinf}}\right)(H - Z)\left[\tan\left(45^o - \frac{\psi}{2}\right) + \tan\left(90^o - \phi_{ds}\right)\right]$$

Figure 75. Equation. Lateral movement of a GRS wall with modular block facing (no friction between wall and soil).

Adams Method

Adams et al. presented a method for calculating lateral displacement of GRS abutments in response to a vertical load.(32) The method, referred to as the "Adams method," conservatively assumes no volume change in a GRS abutment, which represents a worst-case scenario. The composite behavior of a properly constructed GRS mass is such that both the reinforcement and soil deform laterally together at the same strain. This composite behavior can be used to predict both the maximum lateral reinforcement strain and the maximum face deformation at a given load. The maximum lateral displacement of an abutment face can be estimated using figure 76. The lateral strain is then found using figure 77 and should be limited to 1 percent.(32)

$$D_L = \frac{2b_{q,vol}D_v}{H}$$

Figure 76. Equation. Lateral displacement of GRS abutments in response to a vertical load.

Where:

D_L = Lateral displacement of GRS abutments in response to a vertical load.
$b_{q,vol}$ = Width of the load along the top of the wall (including the setback).
D_v = Vertical settlement in the GRS abutment.

$$\varepsilon_L = \frac{D_L}{b_{q,vol}} = \frac{2D_v}{H} = 2\varepsilon_v$$

Figure 77. Equation. Lateral strain of GRS abutments in response to a vertical load.

Where:

ε_L = Lateral strain.
ε_v = Vertical strain at the top of the wall.

Note that figure 76 and figure 77 are based on the assumption of a triangular lateral deformation and a uniform vertical deformation; this assumption is based on observed deformation behavior of GRS.(32)

4.5 EVALUATION OF THE DEFORMATION PREDICTION METHODS

In this section, experimental data in the literature are applied to the deformation prediction methods presented in this chapter for evaluation purposes. In the evaluation, bias (denoted as λ), which is defined as the ratio of the measured value to the predicted value, is analyzed as a statistical variable. A λ value of 1.0 represents the prediction is the same as the measured (observed) deformation.

The arithmetic mean of λ (m) can be calculated as follows:

$$\mu_\lambda = \frac{\sum \lambda_i}{N_0}$$

Figure 78. Equation. Arithmetic mean value.

Where:

m = Arithmetic mean of λ.
λ_i = Sampled λ value.
N_0 = Total number (population) of values.

The standard deviation of λ (s_l) can be calculated as follows:

$$\sigma_\lambda = \sqrt{\frac{\sum(\lambda_i - \mu_\lambda)^2}{N_0 - 1}}$$

Figure 79. Equation. Standard deviation.

The coefficient of variation (COV) of λ can be calculated as follows:

$$COV = \frac{\sigma}{\mu}$$

Figure 80. Equation. COV.

Where:

s = Standard deviation.
m= Mean value.

Each prediction method is evaluated using the following three criteria:

- **Conservativeness**: A prediction method with λ less than 1.0 represents a conservative prediction method, while a prediction method with λ greater than 1.0 represents an unconservative prediction method.

- **Accuracy**: Accuracy of a prediction method is represented by the deviation of mean λ from unity; a mean λthat is much larger or smaller than unity represents a less accurate prediction method.

- **Reliability**: The reliability of a prediction method is indicated by COV; a large COV value represents a prediction method that is unreliable.

Immediate Settlement

Laboratory and field observations of immediate settlements are used to evaluate the five immediate settlement methods presented in this chapter. Table 14 shows the soil and foundation parameters of the case histories used in the evaluation.

Table 14. Soil and foundation parameters for the case histories.

Case History No.	B (m)	L (m)	Total Unit Weight of Soil (kN/m^3)	Depth from Ground Surface to Groundwater Table (m)	D_f (m)	H_{inc} (m)	q_c (kN/m^2)	N	Reference Number	Abutment/ Pier Designation in the Reference
1	1.0	1.0	15.65	4.9	0.71	11.0	2,500–18,800	16–24	106	None
2	1.5	1.5	15.65	4.9	0.76	11.0	2,500–18,800	16–24	106	None
3	2.5	2.5	15.65	4.9	0.76	11.0	2,500–18,800	16–24	106	None
4	3.0	3.0	15.65	4.9	0.76	11.0	2,500–18,800	16–24	106	None
5	3.0	3.0	15.65	4.9	0.89	11.0	2,500–18,800	16–24	106	None
6	5.2	28.0	18.85	1.2	2.3	14.2	11,768	42*	112	Gentbrugge Ghent abutment
7	7.0	36.0	18.85	1.2	2.3	14.2	11,768	42*	112	Gentbrugge Brussels abutment
8	6.0	52.5	18.85	1.2	2.8	$> z_i$	11,768	42*	112	Gentbrugge pier A
9	6.0	52.5	18.85	2.5	3.6	$> z_i$	11,768	42*	112	Gentbrugge pier B
10	5.0	8.5	18.85	5.0	2.5	$> z_i$	8,336	24*	113	
11	3.0	10.0	18.85	4.6	3.0	$> z_i$	12,749	50*	114	Loopem pier
12	5.8	24	18.85	2.0	2.5	$> z_i$	6,865	17*	112	Denys-Westrem abutment
13	2.6	21.0	18.85	2.0	2.0	$> z_i$	6,276	9*	114	Denys-Westrem pier

1 ft = 0.305 m
1 kN/m^3 = 6.37 lbf/ft^3
1 kN/m^2 = 20.89 lbf/ft^2
* Indicates that the SPT blow count (N-value) corrected for overburden per Peck and Bazaraa.[(94)]
H_{inc} = Depth below footing to (relatively) incompressible stratum ($H_{inc} > z_i$ indicates that the incompressible layer is located below z_i).

Modified Schmertmann Method

Table 15 lists the predicted and measured values of immediate settlements of shallow foundations and λ and standard normal variable (z) for each measured data point. Based on the results, the mean λ is 0.49, s is 0.54, and COV is 1.10.

Table 15. Predicted and measured immediate settlements of shallow foundations using the modified Schmertmann method.

Case History No.	Applied Pressure (kPa)	Measured Immediate Settlement (mm)	Predicted Immediate Settlement (mm)	/ (Measured/ Predicted)	z
1	315.2	4.3	19.0	0.23	0
	496.4	7.4	34.0	0.22	-0.19
2	235.6	3.1	18.6	0.17	-0.73
	348.0	5.9	30.5	0.19	-0.61
	444.9	10.6	41.7	0.25	0.29
3	188.2	2.4	20.0	0.12	-1.41
	292.0	5.5	34.9	0.16	-0.87
	395.8	10.2	51.1	0.20	-0.5
	488.3	16.9	66.5	0.25	0.19
4	130.7	1.6	14.3	0.11	-1.75
	390.7	11.4	56.6	0.20	-0.39
	490.9	18.1	75.3	0.24	0.1
5	90.7	1.2	8.3	0.14	-1.2
	194.7	3.6	22.9	0.16	-1.02
	290.7	7.9	38.0	0.21	-0.29
	390.9	14.9	55.1	0.27	0.39
	487.3	25.9	72.6	0.36	0.5
6	95.8	9.9	6.1	1.62	1.41
7	131.7	11.9	12.1	0.98	0.87
8	158.0	7.9	14.4	0.55	0.61
9	214.5	4.1	18.8	0.22	-0.1
10	181.9	11.9	17.9	0.66	0.73
11	230.8	21.1	10.6	1.99	1.75
12	72.8	11.9	9.3	1.28	1.02
13	196.3	33.0	22.1	1.49	1.2

1 psi = 6.89 kPa
1 inch = 25.4 mm

Figure 81 shows the frequency of occurrence histogram of λ. The probability plot for λ is depicted in figure 82. The curve follows a lognormal distribution.

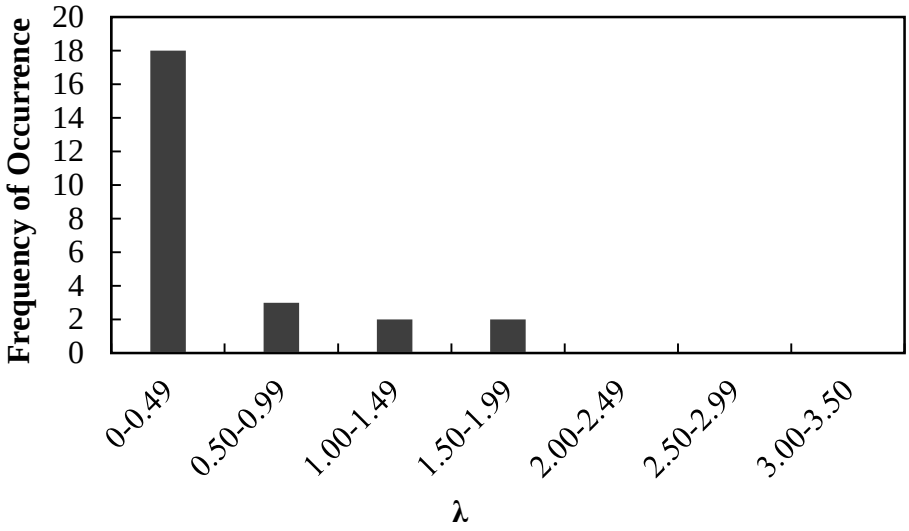

Figure 81. Graph. Frequency of occurrence histogram of / for immediate settlements of shallow foundations using the modified Schmertmann method.

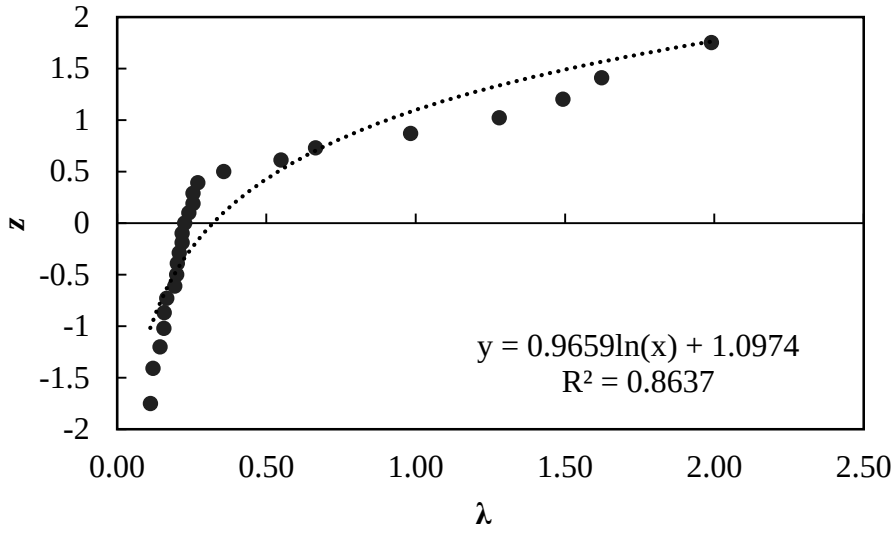

Figure 82. Graph. Probability plot for measured and predicted settlements using the modified Schmertmann method.

Conclusion:

Any interpretations of the results in this study should consider that the number of measured data points is statistically small. With this limitation, it was observed that the low mean λ (0.49) of the modified Schmertmann method indicates this method is highly conservative, and the prediction method overestimates immediate settlement of a shallow foundation by a factor of 2.04. The relatively high COV value (1.10) indicates the method has relatively low reliability.

Hough Method

Table 16 lists the predicted and measured values of immediate settlement of shallow foundations as well as λ and *z* for each measured data point. Based on the results, the mean λ is 0.49, s is 0.31, and COV is 0.63.

Table 16. Predicted and measured immediate settlements of shallow foundations using the Hough method.

Case History No.	Applied Pressure (kPa)	Measured Immediate Settlement (mm)	Predicted Immediate Settlement (mm)	/ (Measured/ Predicted)	*z*
1	315.2	4.3	29.2	0.15	-1.75
	496.4	7.4	38.7	0.19	-1.02
2	235.6	3.1	19.2	0.16	-1.2
	348.0	5.9	25.4	0.23	-0.73
	444.9	10.6	30.0	0.35	-0.29
3	188.2	2.4	10.4	0.23	-0.87
	292.0	5.5	14.9	0.37	-0.19
	395.8	10.2	18.9	0.54	0.5
	488.3	16.9	22.1	0.76	0.87
4	130.7	1.6	6.2	0.26	-0.61
	390.7	11.4	15.8	0.72	0.73
	490.9	18.1	18.9	0.96	1.2
5	90.7	1.2	4.6	0.26	-0.5
	194.7	3.6	9.2	0.39	-0.1
	290.7	7.9	13.0	0.61	0.61
	390.9	14.9	16.5	0.90	1.02
	487.3	25.9	19.6	1.32	1.75
6	95.8	9.9	19.9	0.50	0.39
7	131.7	11.9	27.2	0.44	0.19
8	158.0	7.9	26.4	0.30	-0.39
9	214.5	4.1	29.5	0.14	-1.41
10	181.9	11.9	27.9	0.43	0.1
11	230.8	21.1	19.2	1.10	1.41
12	72.8	11.9	28.7	0.41	0
13	196.3	33.0	67.0	0.49	0.29

1 psi = 6.89 kPa
1 inch = 25.4 mm

Figure 83 shows the frequency of occurrence histogram of λ. The probability plot for λ is depicted in figure 84. The curve follows a lognormal distribution.

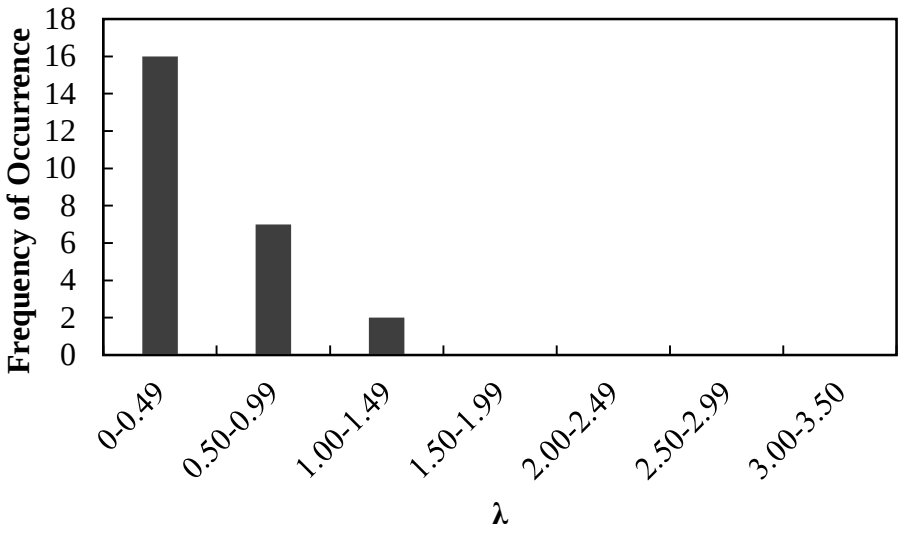

Figure 83. Graph. Frequency of occurrence histogram of / for immediate settlements of shallow foundations using the Hough method.

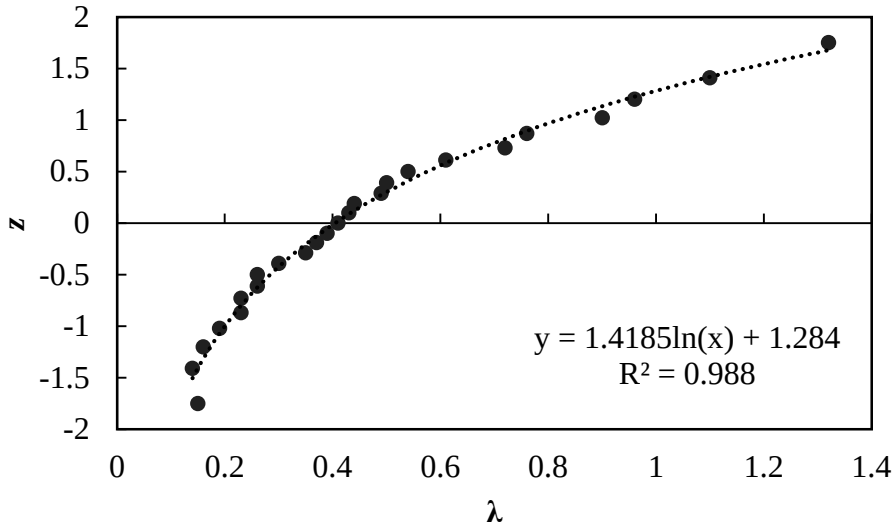

Figure 84. Graph. Probability plot for measured and predicted settlement using the Hough method.

Conclusion:

Any interpretations of the results in this study should consider that the number of measured data points is statistically small. With this limitation, it was observed that the low mean λ (0.49) of the Hough method indicates this method is highly conservative, and the prediction method overestimates immediate settlement of a shallow foundation by a factor of 2.04. The relatively low COV value (0.63) indicates the method has fair reliability. The overestimation of the Hough method agrees with the conclusion from the FHWA report, *Spread Footings for Highway*

Bridges, which concluded that settlements estimated by the modified Hough method are usually overestimated by a factor of 2 or more.[3]

Peck and Bazaraa Method

Table 17 lists the predicted and measured values of immediate settlements of shallow foundations and λ and *z* for each measured data point. Based on the results, the mean λ is 0.79, s is 0.77, and COV is 0.97.

Table 17. Predicted and measured immediate settlements of shallow foundations using the Peck and Bazaraa method.

Case History No.	Applied Pressure (kPa)	Measured Immediate Settlement (mm)	Predicted Immediate Settlement (mm)	/ (Measured/ Predicted)	*z*
1	315.2	4.3	14.1	0.30	-0.87
	496.4	7.4	22.6	0.33	-0.39
2	235.6	3.1	12.2	0.25	-1.02
	348.0	5.9	18.3	0.32	-0.5
	444.9	10.6	23.7	0.45	0
3	188.2	2.4	11.1	0.22	-1.41
	292.0	5.5	17.5	0.31	-0.61
	395.8	10.2	24.1	0.42	-0.19
	488.3	16.9	29.9	0.57	0.19
4	130.7	1.6	7.8	0.21	-1.75
	390.7	11.4	24.6	0.46	0.1
	490.9	18.1	31.2	0.58	0.29
5	90.7	1.2	5.2	0.23	-1.2
	194.7	3.6	11.8	0.31	-0.73
	290.7	7.9	18.0	0.44	-0.1
	390.9	14.9	24.5	0.61	0.39
	487.3	25.9	30.8	0.84	0.5
6	95.8	9.9	4.7	2.11	1.41
7	131.7	11.9	7.1	1.68	1.02
8	158.0	7.9	7.0	1.13	0.87
9	214.5	4.1	10.1	0.41	-0.29
10	181.9	11.9	10.7	1.11	0.73
11	230.8	21.1	6.1	3.46	1.75
12	72.8	11.9	6.3	1.89	1.2
13	196.3	33.0	32.3	1.02	0.61

1 psi = 6.89 kPa
1 inch = 25.4 mm

Figure 85 shows the frequency of occurrence histogram of λ. The probability plot for λ is depicted in figure 86. The curve follows a lognormal distribution.

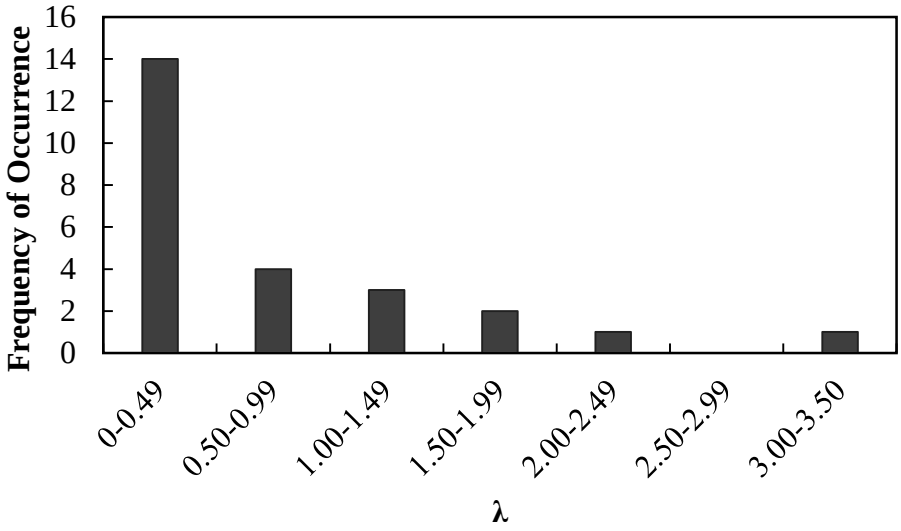

Figure 85. Graph. Frequency of occurrence histogram of / for immediate settlements of shallow foundations using the Peck and Bazaraa method.

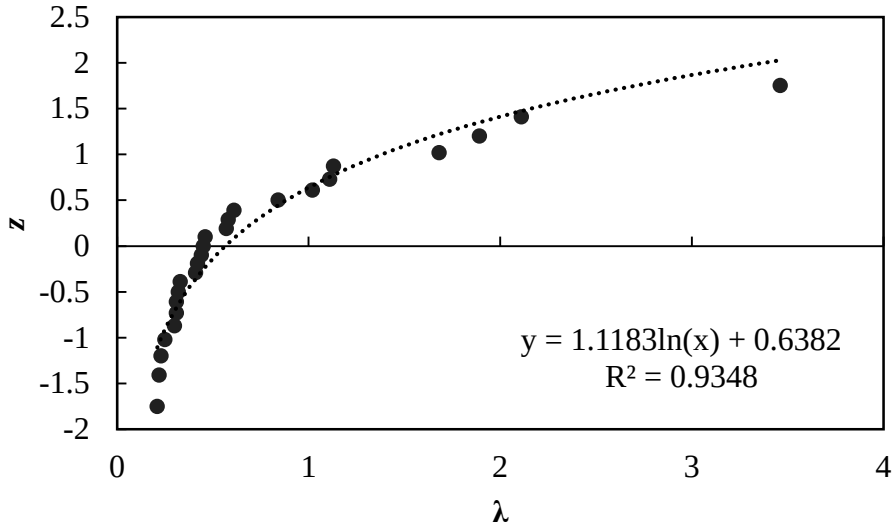

Figure 86. Graph. Probability plot for measured and predicted settlement using the Peck and Bazaraa method.

Conclusion:

Any interpretations of the results in this study should consider that the number of measured data points is statistically small. With this limitation, it was observed that the less-than-unity mean λ value (0.79) indicates the Peck and Bazaraa method is a conservative prediction method, and the prediction method overestimates the settlement of a shallow foundation by a factor of 1.26. The COV value of 0.97 indicates the method has relatively fair reliability.

Burland and Burbidge Method

Table 18 lists the predicted and measured values of immediate settlements of shallow foundations and λ and *z* for each measured data point. Based on the results, the mean λ is 0.62, s is 0.49, and COV is 0.79.

Table 18. Predicted and measured immediate settlements of shallow foundations using the Burland and Burbidge method.

Case History No.	Applied Pressure (kPa)	Measured Immediate Settlement (mm)	Predicted Immediate Settlement (mm)	/ (Measured/ Predicted)	*z*
1	315.2	4.3	10.0	0.43	-0.1
	496.4	7.4	15.7	0.47	0
2	235.6	3.1	9.9	0.31	-0.73
	348.0	5.9	14.6	0.40	-0.39
	444.9	10.6	18.7	0.57	0.29
3	188.2	2.4	11.3	0.21	-1.2
	292.0	5.5	17.5	0.31	-0.61
	395.8	10.2	23.8	0.43	-0.29
	488.3	16.9	29.3	0.58	0.39
4	130.7	1.6	8.9	0.18	-1.75
	390.7	11.4	26.6	0.43	-0.19
	490.9	18.1	33.5	0.54	0.1
5	90.7	1.2	6.2	0.19	-1.41
	194.7	3.6	13.3	0.27	-1.02
	290.7	7.9	19.8	0.40	-0.5
	390.9	14.9	26.6	0.56	0.19
	487.3	25.9	33.2	0.78	0.87
6	95.8	9.9	6.6	1.50	1.41
7	131.7	11.9	11.2	1.06	1.2
8	158.0	7.9	11.1	0.71	0.61
9	214.5	4.1	15.0	0.27	-0.87
10	181.9	11.9	17.4	0.68	0.5
11	230.8	21.1	8.6	2.45	1.75
12	72.8	11.9	11.9	1.00	1.02
13	196.3	33.0	43.3	0.76	0.73

1 psi = 6.89 kPa
1 inch = 25.4 mm

Figure 87 shows the frequency of occurrence histogram of λ. The probability plot for λ is depicted in figure 88. The curve follows a lognormal distribution.

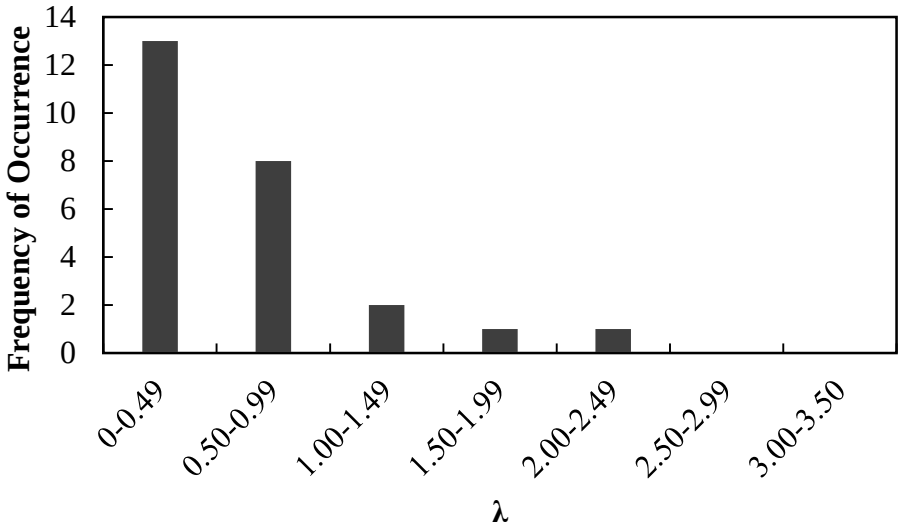

Figure 87. Graph. Frequency of occurrence histogram of / for immediate settlements of shallow foundations using the Burland and Burbidge method.

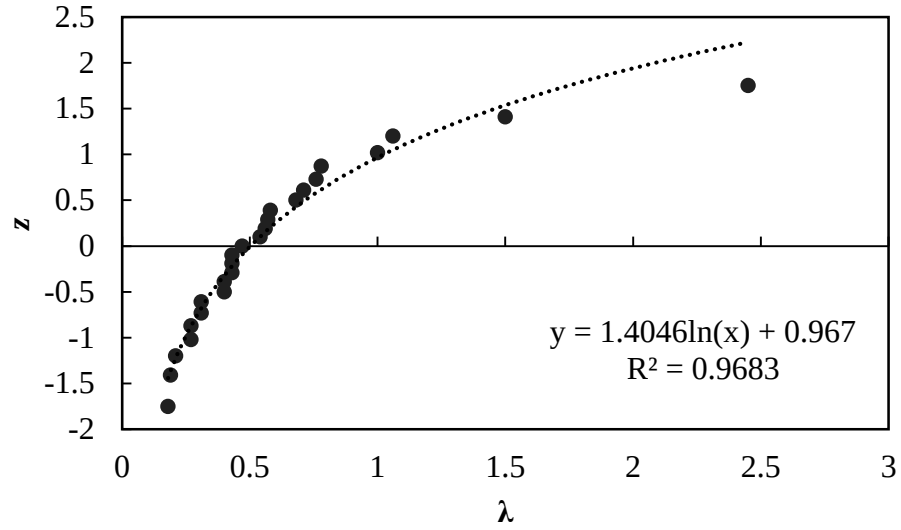

Figure 88. Graph. Probability plot for measured and predicted settlement using the Burland and Burbidge method.

Conclusion:

Any interpretations of the results in this study should consider that the number of measured data points is statistically small. With this limitation, it was observed that the less-than-unity mean λ value (0.62) indicates that the Burland and Burbidge method is a conservative prediction method, and the prediction method overestimates the settlement of a shallow foundation by a factor of 1.64. The relatively low COV value (0.79) indicates the method has fair reliability.

D'Appolonia Method

Table 19 lists the predicted and measured values of immediate settlement of shallow foundations and λ and *z* for each measured data point. Based on the results, the mean λ is 1.11, s is 0.85, and COV is 0.77.

Table 19. Predicted and measured immediate settlements of shallow foundations using the D'Appolonia method.

Case History No.	Applied Pressure (kPa)	Measured Immediate Settlement (mm)	Predicted Immediate Settlement (mm)	/ (Measured/ Predicted)	*z*
1	315.2	4.3	4.4	0.98	0.29
	496.4	7.4	6.9	1.07	0.5
2	235.6	3.1	5.0	0.62	-0.61
	348.0	5.9	7.4	0.80	-0.19
	444.9	10.6	9.5	1.12	0.61
3	188.2	2.4	6.8	0.35	-1.02
	292.0	5.5	10.5	0.52	-0.73
	395.8	10.2	14.3	0.71	-0.29
	488.3	16.9	17.6	0.96	0.19
4	130.7	1.6	5.6	0.29	-1.75
	390.7	11.4	16.6	0.69	-0.39
	490.9	18.1	20.9	0.87	0
5	90.7	1.2	3.8	0.32	-1.41
	194.7	3.6	8.1	0.44	-0.87
	290.7	7.9	12.0	0.66	-0.5
	390.9	14.9	16.2	0.92	0.1
	487.3	25.9	20.2	1.28	0.73
6	95.8	9.9	5.4	1.83	0.87
7	131.7	11.9	5.8	2.05	1.02
8	158.0	7.9	9.4	0.84	-0.1
9	214.5	4.1	12.0	0.34	-1.2
10	181.9	11.9	11.3	1.05	0.39
11	230.8	21.1	6.2	3.40	1.75
12	72.8	11.9	3.6	3.31	1.41
13	196.3	33.0	14.1	2.34	1.2

1 psi = 6.89 kPa
1 inch = 25.4 mm

Figure 89 shows the frequency of occurrence histogram of λ. The probability plot for λ is depicted in figure 90. The curve follows a lognormal distribution.

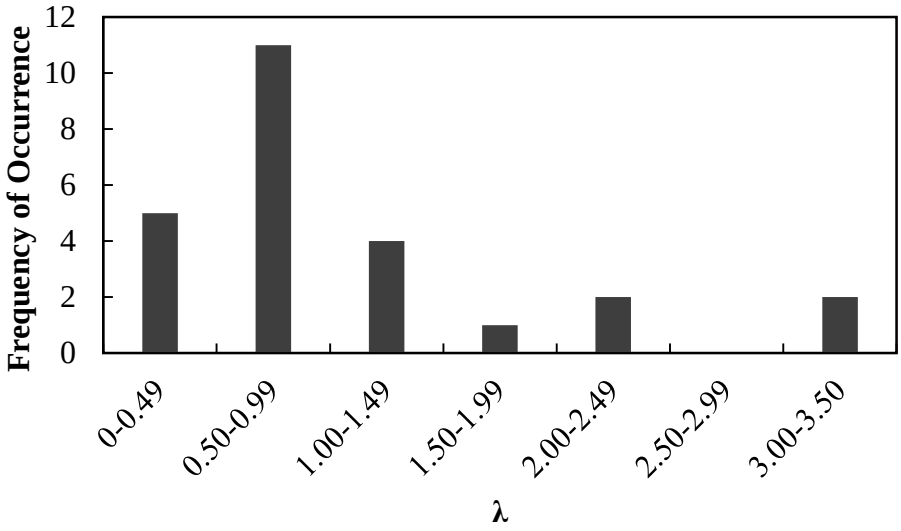

Figure 89. Graph. Frequency of occurrence histogram of / for immediate settlements of shallow foundations using the D'Appolonia method.

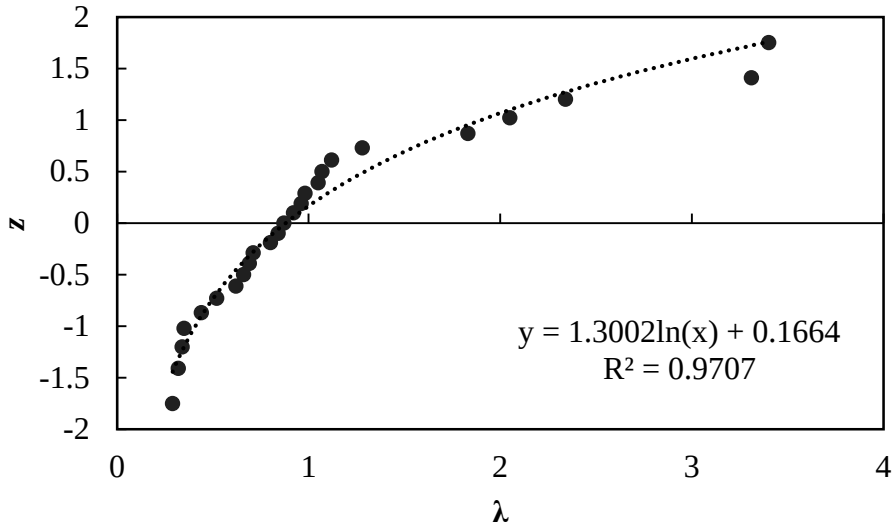

Figure 90. Graph. Probability plot for measured and predicted settlement using the D'Appolonia method.

Conclusion:

Any interpretations of the results in this study should consider that the number of measured data points is statistically small. With this limitation, it was observed that the slightly higher-than-unity mean λ value (1.11) indicates the D'Appolonia method is a slightly unconservative prediction method, and the predicted immediate settlement is on average 91 percent of the actually measured settlement of a shallow foundation. The relatively low COV value (0.77) indicates the method has fair reliability.

Comparison of the Five Prediction Methods for Immediate Settlement of Shallow Foundation on Granular Soils

Table 20 summarizes the statistical analyses of the five prediction methods for immediate settlement of shallow foundation on granular soils. Any interpretations of the results in this study should consider that the number of measured data points is statistically small. With this limitation, it was observed that four of the five methods (modified Schmertmann, Hough, Peck and Bazaraa, and Burland and Burbidge) overestimate immediate settlement, while the D'Appolonia method slightly underestimates immediate settlement. In comparison, the D'Appolonia method is the most accurate method with the mean λ the closest to unity and relatively small COV, followed by the Peck and Barazaa method and the Burland and Burbidge method. Both the modified Schmertmann method and the Hough method overestimate immediate settlement of shallow foundations on granular soils by a factor of approximately 2.

Table 20. Summary of the statistical analyses of the five prediction methods for immediate settlement of shallow foundations on granular soil, results from this study.

Statistical Parameters	Modified Schmertmann Method	Hough Method	Peck and Barazaa Method	Burland and Burbidge Method	D'Appolonia Method
Mean λ	0.49	0.49	0.79	0.62	1.11
s	0.54	0.31	0.77	0.49	0.85
COV	1.10	0.63	0.97	0.79	0.77

A similar FHWA study was conducted by Gifford to evaluate the five methods based on the observed deformations of 34 bridge foundations, and their statistical results are listed in table 21 for comparison.[3] With the acknowledgement of the statistically small data set, Gifford concluded the following:[3]

> "Three of the five methods (Burland and Burbidge, D'Appolonia, and Peck and Bazaraa) typically underpredicted settlement, while the other two (Hough and Schmertmann) typically overpredicted. The D'Appolonia method was the most accurate, on average, with Burland and Burbidge next. The Hough method provided the least accurate predictions."(pp. 75)[3]

Table 21. Summary of the statistical analyses of the five prediction methods for immediate settlement of shallow foundations on granular soil, results from Gifford.[3]

Statistical Parameters	Modified Schmertmann Method*	Hough Method**	Peck and Bazaraa Method*	Burland and Burbidge Method**	D'Appolonia Method*
Mean λ	0.74	0.69	1.21	1.14	1.33
s	0.28	0.49	0.55	1.69	0.94
COV	0.38	0.70	0.45	0.79	0.7

*Based on 10 bridge foundations.
**Based on 24 bridge foundations.

Vertical Deformations of GRS Walls and Abutments

In this section, the empirical equation by Adams et al. for predicting vertical deformation of GRS walls and abutments is evaluated using field observation data.[32] To calculate the vertical displacement of a GRS wall, the composite Young's modulus of the GRS wall (E_{GRS}) is needed. The equation by Holtz and Lee is used to calculate the GRS composite Young's modulus (see figure 91).[115] In deriving this equation for the GRS composite Young's modulus, it is assumed that the stress-strain behavior of the soil and reinforcement follows Hooke's Law and that the deformation of the composite material is uniform.

$$E_{GRS} = E_R \times \frac{t_R}{S_v} + E_s \times \frac{(S_v - t_R)}{S_v}$$

Figure 91. Equation. Elastic modulus of GRS composite.

Where:

E_s = Elastic modulus of soil.
t_R = Thickness of reinforcement.

Since $S_v - t_R \gg S_v$ and $E_R = J/t_R$, where J is the stiffness of the reinforcement, then figure 91 can be simplified as follows:

$$E_{comp} \approx \frac{J}{t_R} \times \frac{t_R}{S_v} + E_s \times \frac{S_v}{S_v} = \frac{J}{S_v} + E_s$$

Figure 92. Equation. Elastic modulus of GRS composite (modified equation).

Where E_{comp} is the elastic modulus of GRS composite. Given q, b', a, H, and E_{GRS}, the vertical displacement can be calculated using figure 67. Table 22 presents the parameters used for the evaluation.

Table 22. Abutment and GRS wall parameters in case histories.

No.	H (m)	a (m)	b' (m)	S_v (m)	E_{GRS} (kN/m^2)	Reference Number	Wall Designations in the References
1	4.65	0.15	0.91	0.2	62,731	70	Wall section A
2	4.65	0.15	0.91	0.2	62,669	70	Wall section B
3	4.35	1.5	1.0	0.3–0.6	20,253	75	Wall section nonwoven
4	4.35	1.5	1.0	0.3–0.6	20,653	75	Wall section woven
5	7.62	0.2	2.44	0.2	240,147	116	
6	5.9	1.35	3.81	0.4	62,700	63	Wall section 800
7	5.9	1.35	3.81	0.4	62,700	63	Wall section 400
8	4.5	1.35	3.81	0.4	62,700	63	Wall section 200

1 ft = 0.305 m
1 kN/m^2 = 20.89 lbf/ft^2

Table 23 lists the predicted and measured values of the vertical deformation predictions of GRS walls and abutments and λ and *z* for each data point. Based on the results, the mean λ is 7.31, s is 5.73, and COV is 0.78.

Table 23. Predicted and measured vertical displacements of abutments and GRS walls.

Case History No.	Applied Pressure (kPa)	Measured Vertical Displacement (mm)	Predicted Vertical Displacement (mm)	/ (Measured/ Predicted)	*z*
1	100	14.4	1.9	7.58	0
	200	32.7	3.9	8.38	0.11
	300	55.4	5.8	9.55	0.43
	400	75.5	7.8	9.68	0.55
2	100	25.6	1.9	13.47	0.97
	200	58.9	3.9	15.10	1.15
	300	103.1	5.8	17.78	1.38
	400	158.9	7.8	20.37	1.73
3	50	3.5	3.2	1.09	-1.38
	100	7.7	6.5	1.18	-1.15
	150	50.6	9.7	5.22	-0.21
	180	115.6	11.7	9.88	0.68
	200	161.5	13.0	12.42	0.81
4	50	4.5	3.2	1.41	-0.81
	100	18.2	6.3	2.89	-0.32
	150	60.4	9.5	6.36	-0.11
	180	95.8	11.4	8.40	0.21
	200	113.0	12.7	8.90	0.32
5	195	5.1	2.2	2.32	-0.55
	260	8.2	2.9	2.83	-0.43
6	115	3.0	5.4	0.56	-1.73
7	115	7.0	5.4	1.30	-0.97
8	115	7.0	4.6	1.52	-0.68

1 psi = 6.89 kPa
1 inch = 25.4 mm

Figure 93 shows the frequency of occurrence histogram of λ. The probability plot for λ is depicted in figure 94. The curve follows a lognormal distribution.

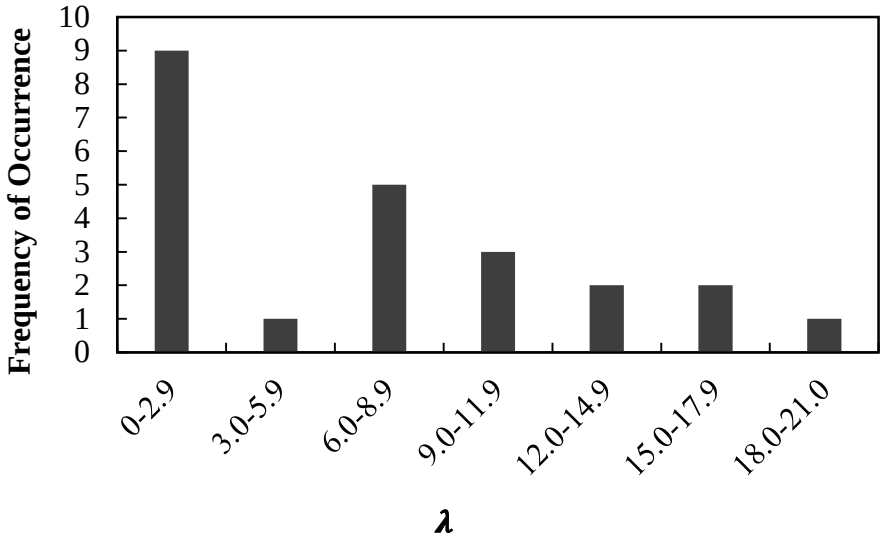

Figure 93. Graph. Frequency of occurrence histogram of / of vertical displacement of abutments and GRS walls.

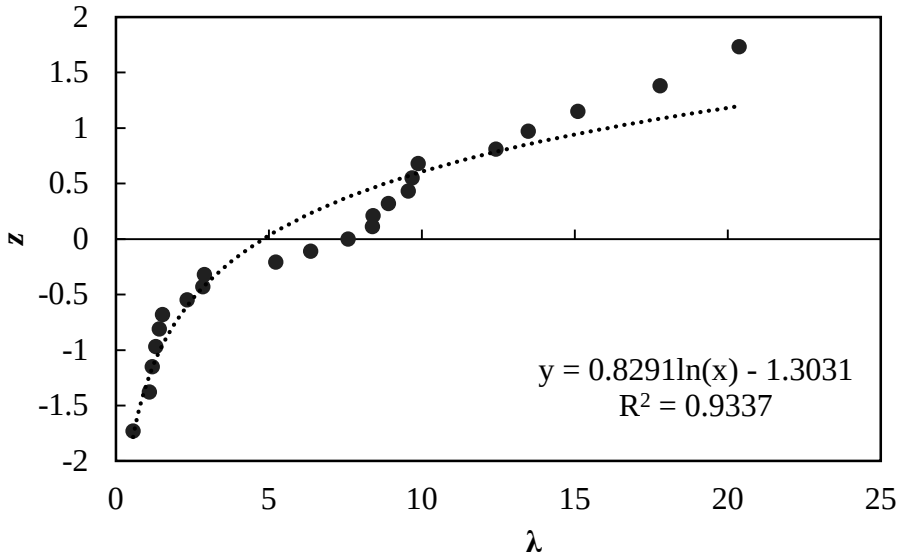

R^2 = Coefficient of determination.

Figure 94. Graph. Probability plot for measured and predicted vertical displacement of abutments and GRS walls.

Conclusion:

Any interpretations of the results in this study should consider that the number of measured data points is statistically small. With this limitation, it was observed that the high mean λ value (7.31) indicates this prediction method for vertical deformations of GRS walls and abutments is unconservative. It should be noted that the accuracy of this method is affected by the accuracy in determination of the Young's modulus of the composite material. Since the proposed equation by

Holtz and Lee (see figure 91) is associated with simplifying assumptions, its accuracy also depends on the accurate estimation of Young's moduli of the reinforcement and soil.[115] Any error in these estimations may lead to error in the prediction results.

Lateral Displacements of GRS Walls and Abutments

In this section, field observations of lateral displacements of GRS walls and abutments are applied to the six methods presented previously to evaluate their conservativeness, accuracy, and reliability. Table 24 presents the parameters used for the evaluation.

Table 24. Abutment and GRS wall parameters in case histories.

Case History No.	H (m)	L (m)	S_v (m)	f (Degree)	y (Degree)	Facing Type	Reference Number	Wall Designations in the References
1	3.6	2.5	0.6	41(DS)	11	CMU	71	Wall 1
2	3.6	2.5	0.6	41(DS)	11	CMU	71	Wall 2
3	3.6	2.5	0.9	41(DS)	11	CMU	71	Wall 3
4	4.0	3.0	0.4	32(DS)	14	Wrap around	117	N/A
5	6.0	3.6	0.6	40(PS)	11	CMU	118	Wall 1
6	6.0	3.6	0.6	30(PS)	11	CMU	118	Wall 2
7	6.0	3.6	0.6	30(PS)	11	CMU	118	Wall 3
8	6.0	3.6	0.6	20(PS)	11	CMU	118	Wall 4
9	4.0	3.0	0.4	33(TT)	3	Wrap around	119	N/A
10	3.6	2.5	0.6	41(DS)	11	CMU	76	Wall 5
11	5.3	2.0	0.5	40	10	Wrap around	120	N/A
12	7.62	3.2–4.4	0.2	—	—	CMU	116	N/A
13	4.35	1.3–3.6	0.3–0.6	—	—	CMU	75	Woven wall
14	4.35	2.7–3.6	0.3–0.6	—	—	CMU	75	Nonwoven wall
15	5.9	8–12	0.4	—	—	CMU	63	Wall section 800
16	5.9	8–12	0.4	—	—	CMU	63	Wall section 400
17	4.5	8–12	0.4	—	—	CMU	63	Wall section 200
18	4.65	3.15	0.2	—	—	CMU	70	Wall section A
19	4.65	3.15	0.2	—	—	CMU	70	Wall section B

1 ft = 0.305 m
— Indicates the values are not provided.
DS = Direct shear test.
PS = Plain strain test.
TT = Triaxial test.
N/A = No wall designation was provided.

FHWA Method

Table 25 lists the predicted and measured values of the lateral displacements of GRS walls and abutments and λ and z for each data point. Based on the results, the mean λ is 0.12, s is 0.10, and COV is 0.83.

Table 25. Predicted and measured maximum lateral displacements of GRS walls at EOC using the FHWA method.

Case History No.	Measured Maximum Lateral Displacement (mm)	Predicted Maximum Lateral Displacement (mm)	/ (Measured/ Predicted)	*z*
1	5.2	48.4	0.11	0.11
2	7.9	48.4	0.16	0.6
3	6.0	48.4	0.12	0.35
4	15.7	50.6	0.31	1.34
5	3.2	94.6	0.03	-0.6
6	8.4	94.6	0.09	-0.35
7	1.2	94.6	0.01	-1.34
8	2.6	94.6	0.03	-0.91
9	5.1	50.6	0.10	-0.11
10	12.8	48.4	0.26	0.91

1 inch = 25.4 mm

Figure 95 shows the frequency of occurrence histogram of λ. The probability plot for λ values using the FHWA method is depicted in figure 96. The curve follows a lognormal distribution.

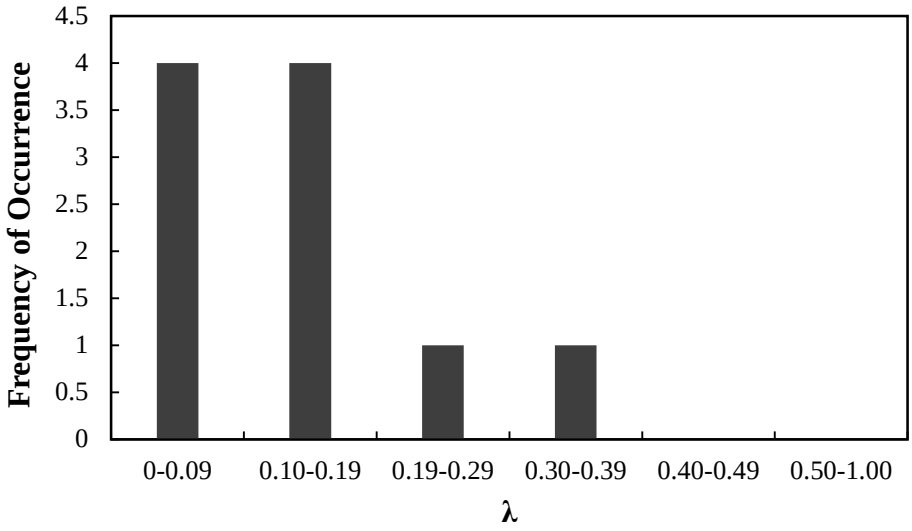

Figure 95. Graph. Frequency of occurrence histogram of / for the lateral displacement of GRS walls and abutments using the FHWA method.

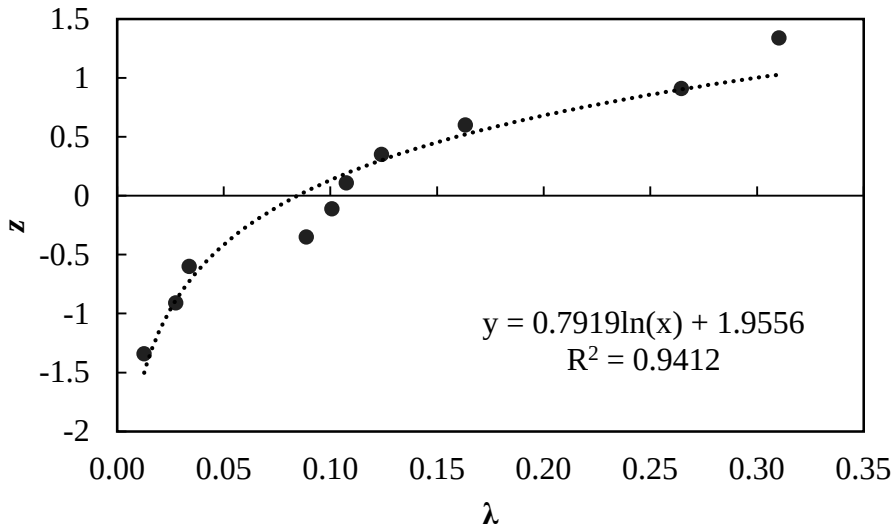

Figure 96. Graph. Probability plot for measured and predicted lateral displacement of GRS walls using the FHWA method.

Conclusion:

Any interpretations of the results in this study should consider that the number of measured data points is statistically small. With this limitation, it was observed that the lower-than-unity mean λ (0.12) of the FHWA method indicates the method is highly conservative, and the predictions significantly overestimate the lateral deformations by a factor of 8.33. The relatively low COV value (0.83) indicates a fair reliability of this method.

Geoservices Method

Table 26 lists the predicted and measured values of the lateral displacements of GRS walls and abutments and λ and *z* for each data point. Based on the results, the mean λ is 1.38, s is 1.59, and COV is 1.15.

Table 26. Predicted and measured lateral displacements of GRS walls and abutments using the Geoservices method.

Case History No.	Elevation (m)	Measured Lateral Displacement (mm)	Predicted Lateral Displacement (mm)	/ (Measured/ Predicted)	*z*	Notes
1	3.3	1.5	0.7	2.11	0.84	Results are obtained at EOC
	2.7	5.1	2.4	2.12	0.98	
	2.1	5.2	3.0	1.74	0.55	
	1.5	5.0	8.9	0.56	-0.35	
	0.9	3.7	7.4	0.51	-0.5	
	0.3	2.4	6.9	0.34	-1.06	
2	3.3	6.3	4.5	1.39	0.40	Results are obtained at EOC
	2.7	8.0	5.9	1.35	0.30	
	2.1	6.4	6.9	0.93	0.11	
	1.5	4.7	12.3	0.38	-0.98	
	0.9	3.8	9.9	0.39	-0.91	
	0.3	1.2	7.2	0.17	-1.46	
3	3.1	2.1	9.4	0.22	-1.33	Results are obtained at EOC
	2.2	6.0	8.7	0.69	-0.25	
	1.3	5.2	8.4	0.62	-0.3	
	0.5	2.1	6.6	0.32	-1.14	
4	3.6	0.8	0.0	N/A	N/A	Results are obtained at EOC
	2.8	9.8	7.2	1.36	0.35	
	2	15.7	9.6	1.64	0.45	
	1.2	8.6	0.9	9.56	2.09	
	0.4	13.1	6.0	2.18	1.14	
9	3.6	0.2	0.2	1.33	0.25	Results are obtained at EOC
	2.8	5.1	7.3	0.67	-0.21	
	2	4.2	9.6	0.44	-0.78	
	1.2	2.3	3.0	0.76	0.02	
	0.4	2.8	6.0	0.47	-0.60	
10	3.3	3.9	5.0	0.78	0.07	Results are obtained at EOC
	2.7	9.9	13.4	0.74	-0.07	
	2.1	11.4	15.9	0.72	-0.11	
	1.5	12.6	13.4	0.94	0.16	
	0.9	8.1	16.4	0.49	-0.55	
	0.3	1.9	6.3	0.30	-1.23	
11	4.5	81.5	47.5	1.72	0.5	Results are obtained under 84 kPa of applied pressure
	4	82.1	44.0	1.87	0.66	
	3.5	82.7	42.5	1.95	0.72	
	3	78.2	44.0	1.78	0.60	
	2.5	71.1	33.5	2.12	1.06	
	2	60.3	28.5	2.12	0.91	
	1.5	45.1	21.5	2.10	0.78	

	1	31.5	11.0	2.86	1.23	
	0.5	18.9	6.5	2.91	1.33	
12	6.5	8.0	2.1	3.81	1.60	Results are obtained under 131 kPa of applied pressure
	5.9	8.0	2.6	3.08	1.46	
	5.1	14.0	2.2	6.36	1.79	
13	3.8	83.3	111.3	0.75	-0.02	Results are obtained under 190 kPa of applied pressure
	2.6	57.7	46.6	1.24	0.21	
	1.5	21.6	30.2	0.71	-0.16	
	0.6	7.2	15.7	0.46	-0.66	
14	3.8	106.7	244.2	0.44	-0.72	Results are obtained under 190 kPa of applied pressure
	2.6	96.9	182.2	0.53	-0.45	
	1.5	21.8	53.6	0.41	-0.84	
	0.6	0.9	8.8	0.10	-1.79	
15	2.4	1.1	19.8	0.06	-2.09	Results are obtained under 115 kPa of applied pressure
	4	4.0	23.8	0.17	-1.60	
	4.8	4.0	7.4	0.54	-0.40	

1 ft = 0.305 m
1 inch = 25.4 mm
1 psi = 6.89 kPa
N/A = not applicable since the predicted value is zero.

Figure 97 shows the frequency of occurrence histogram of λ. The probability plot for λ value obtained based on the result of the Geoservices method is depicted in figure 98. The curve follows a lognormal distribution.

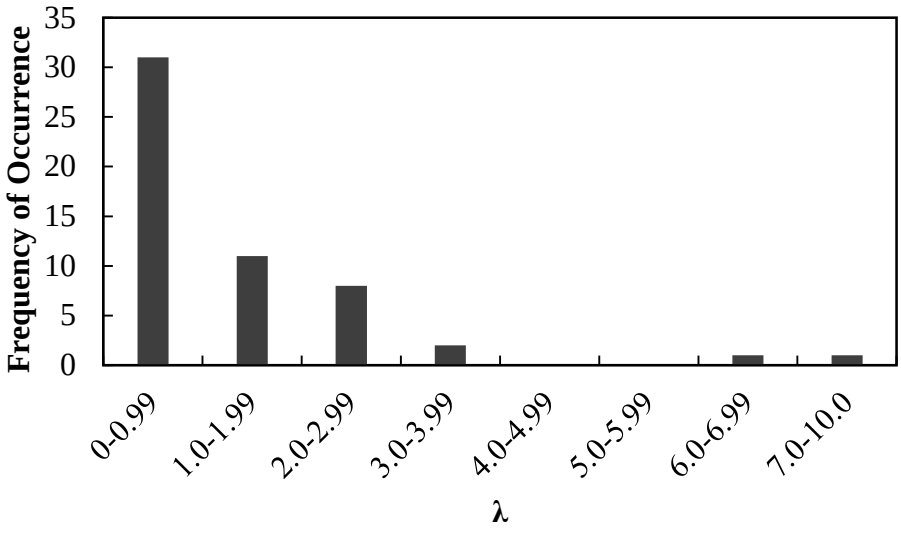

Figure 97. Graph. Frequency of occurrence histogram of / for the lateral displacement of GRS walls and abutments using the Geoservices method.

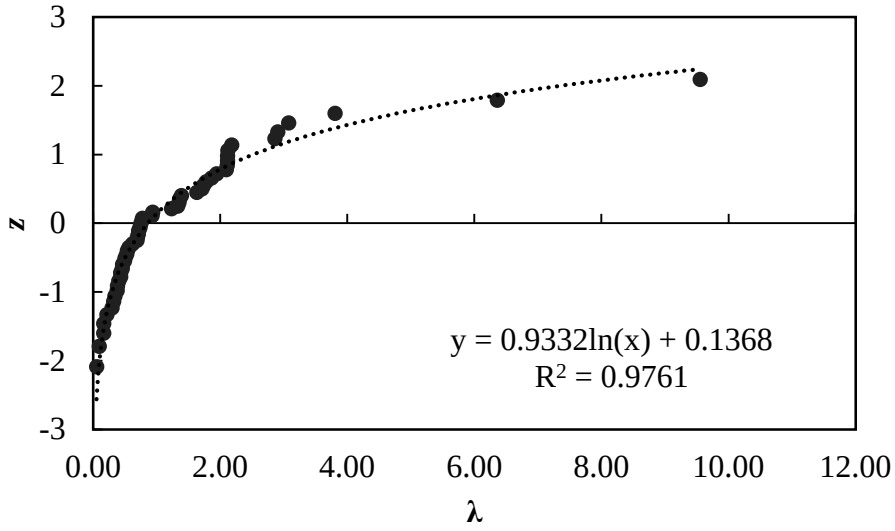

Figure 98. Graph. Probability plot for measured and predicted lateral displacement of GRS walls using the Geoservices method.

Conclusion:

Any interpretations of the results in this study should consider that the number of measured data points is statistically small. With this limitation, it was observed that the greater-than-unity value of the mean λ (1.38) indicates the Geoservices method is an unconservative prediction method, and the predicted lateral displacement is on average 72 percent of the actually measured lateral displacements. The relatively high COV value (1.15) indicates a relatively low reliability of this method.

CTI Method

Table 27 lists the predicted and measured values of the lateral displacements of GRS walls and abutments and λ and *z* for each data point. Based on the results, the mean λ is 0.59, s is 0.64, and COV is 1.08.

Table 27. Predicted and measured maximum lateral displacements of GRS walls using the CTI method.

Case History No.	Elevation (m)	Measured Maximum Lateral Displacement (mm)	Predicted Maximum Lateral Displacement (mm)	/ (Measured/ Predicted)	*z*	Notes
1	3.3	1.5	1.4	1.07	1.33	Results are obtained at EOC
	2.7	5.1	4.7	1.09	1.46	
	2.1	5.2	5.9	0.88	1.06	
	1.5	5.0	17.3	0.29	-0.4	
	0.9	3.7	14.4	0.26	-0.72	
	0.3	2.4	13.5	0.18	-1.33	
2	3.3	6.3	8.7	0.72	0.78	Results are obtained at EOC
	2.7	8.0	11.5	0.70	0.60	
	2.1	6.4	13.4	0.48	0.11	
	1.5	4.7	23.8	0.20	-1.14	
	0.9	3.8	19.3	0.20	-1.06	
	0.3	1.2	13.9	0.09	-1.79	
3	3.1	2.1	18.3	0.11	-1.6	Results are obtained at EOC
	2.2	6.0	16.8	0.36	-0.21	
	1.3	5.2	16.3	0.32	-0.35	
	0.5	2.1	12.8	0.16	-1.46	
4	3.6	0.8	0	N/A	N/A	Results are obtained at EOC
	2.8	9.8	15.4	0.64	0.4	
	2	15.7	20.5	0.77	0.91	
	1.2	8.6	1.9	4.53	2.09	
	0.4	13.1	12.8	1.02	1.23	
9	3.6	0.2	0.3	0.67	0.5	Results are obtained at EOC
	2.8	5.1	15.6	0.33	-0.3	
	2	4.2	20.5	0.20	-0.91	
	1.2	2.3	6.4	0.36	-0.16	
	0.4	2.8	12.8	0.22	-0.84	
10	3.3	3.9	5.4	0.72	0.72	Results are obtained at EOC
	2.7	9.9	14.5	0.68	0.55	
	2.1	11.4	17.2	0.66	0.45	
	1.5	12.6	14.5	0.87	0.98	
	0.9	8.1	17.7	0.46	-0.02	
	0.3	1.9	6.8	0.28	-0.50	
11	4.5	81.5	190.0	0.43	-0.11	Results are obtained under 84 kPa of applied pressure
	4	82.1	176.0	0.47	0.07	
	3.5	82.7	170.0	0.49	0.16	
	3	78.2	176.0	0.44	-0.07	
	2.5	71.1	134.0	0.53	0.30	
	2	60.3	114.0	0.53	0.25	

	1.5	45.1	86.0	0.52	0.21	
	1	31.5	44.0	0.72	0.66	
	0.5	18.9	26.0	0.73	0.84	
12	6.5	8.0	7.3	1.10	1.10	Results are obtained under 131 kPa of applied pressure
	5.9	8.0	8.8	0.91	1.14	
	5.1	14.0	7.6	1.84	1.79	
13	3.8	83.3	180.4	0.46	0.02	Results are obtained under 190 kPa of applied pressure
	2.6	57.7	104.2	0.55	0.35	
	1.5	21.6	77.7	0.28	-0.55	
	0.6	7.2	36.6	0.20	-1.06	
14	3.8	106.7	398.2	0.27	-0.6	Results are obtained under 190 kPa of applied pressure
	2.6	96.9	338.5	0.29	-0.45	
	1.5	21.8	121.0	0.18	-1.23	
	0.6	0.9	22.6	0.04	-2.09	
15	2.4	1.1	3.2	0.34	-0.25	Results are obtained under 115 kPa of applied pressure
	4	4.0	15.2	0.26	-0.66	
	4.8	4.0	16.4	0.24	-0.78	

1 ft = 0.305 m
1 inch = 25.4 mm
1 psi = 6.89 kPa
N/A = The value could not be calculated.

Figure 99 shows the frequency of occurrence histogram of λ. The probability plot for λ value obtained based on the result of the CTI method is depicted in figure 100. The curve follows a lognormal distribution.

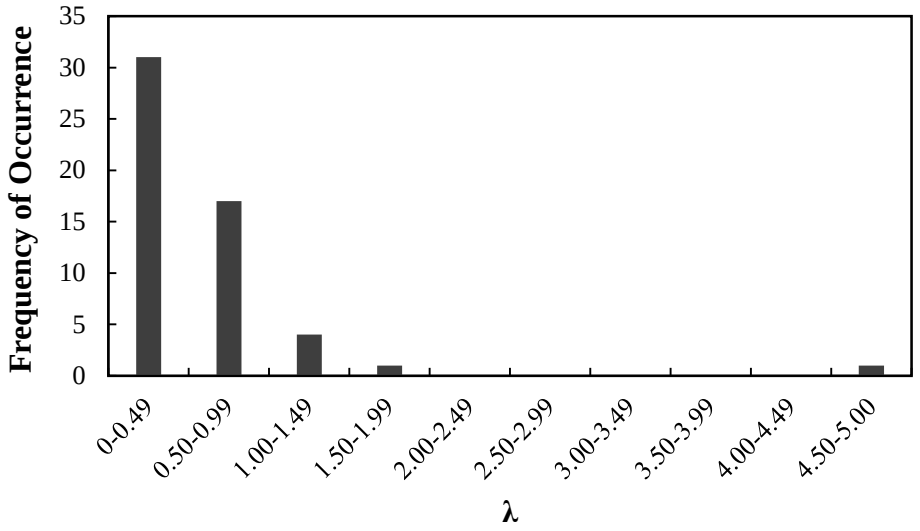

Figure 99. Graph. Frequency of occurrence histogram of / for the lateral displacement of GRS walls and abutments using the CTI method.

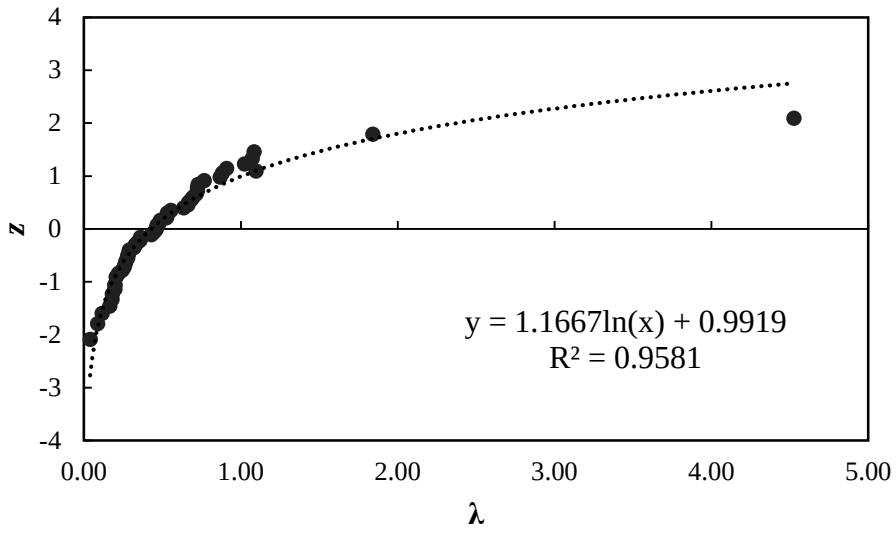

Figure 100. Graph. Probability plot for measured and predicted lateral displacement of GRS walls using the CTI method.

Conclusion:

Any interpretations of the results in this study should consider that the number of measured data points is statistically small. With this limitation, it was observed that the lower-than-unity mean λ (0.59) indicates the CTI method is a conservative prediction method, and it overestimates the lateral deformation by a factor of 1.69. The relative high COV value (1.08) indicates a relatively low reliability of this method.

Jewell-Milligan Method

Table 28 lists the predicted and measured values of the lateral displacements of GRS walls and abutments and λ and *z* for each data point. Based on the results, the mean λ is 0.74, s is 0.59, and COV is 0.80.

Table 28. Predicted and measured lateral displacements of GRS walls and abutments using the Jewell-Milligan method.

Case History No.	Elevation (m)	Measured Lateral Displacement (mm)	Predicted Lateral Displacement (mm)	/ (Measured/ Predicted)	*z*	Notes
4	3.6	0.79	6.0	0.13	-1.28	Results are obtained at EOC
	2.8	9.8	14.0	0.70	0.25	
	2.0	15.7	16.7	0.94	0.67	
	1.2	8.6	14.2	0.61	0	
	0.4	13.1	6.4	2.05	1.28	
9	3.6	0.2	5.9	0.03	-1.65	Results are obtained at EOC
	2.8	5.1	13.8	0.37	-0.67	
	2.0	4.2	16.4	0.26	-0.84	
	1.2	2.3	14.0	0.16	-1.04	
	0.4	2.8	6.3	0.44	-0.52	
11	4.5	81.5	36.1	2.26	1.65	Results are obtained under 84 kPa of applied pressure
	4	82.1	62.6	1.31	1.04	
	3.5	82.7	82.1	1.01	0.84	
	3	78.2	94.8	0.82	0.52	
	2.5	71.1	98.0	0.73	0.39	
	2	60.3	94.2	0.64	0.13	
	1.5	45.1	83.2	0.54	-0.13	
	1	31.5	62.3	0.51	-0.25	
	0.5	18.9	39.1	0.48	-0.39	

1 ft = 0.305 m
1 inch = 25.4 mm
1 psi = 6.89 kPa

Figure 101 shows the frequency of occurrence histogram of λ. The probability plot for λ value obtained based on the results of the Jewell-Milligan method is depicted in figure 102. The curve follows a lognormal distribution.

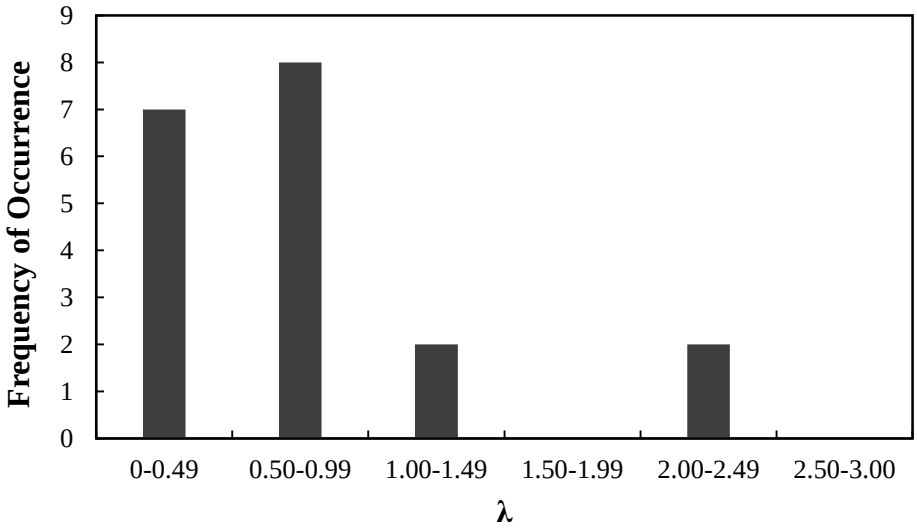

Figure 101. Graph. Frequency of occurrence histogram of / for the lateral displacement of GRS walls and abutments using the Jewell-Milligan method.

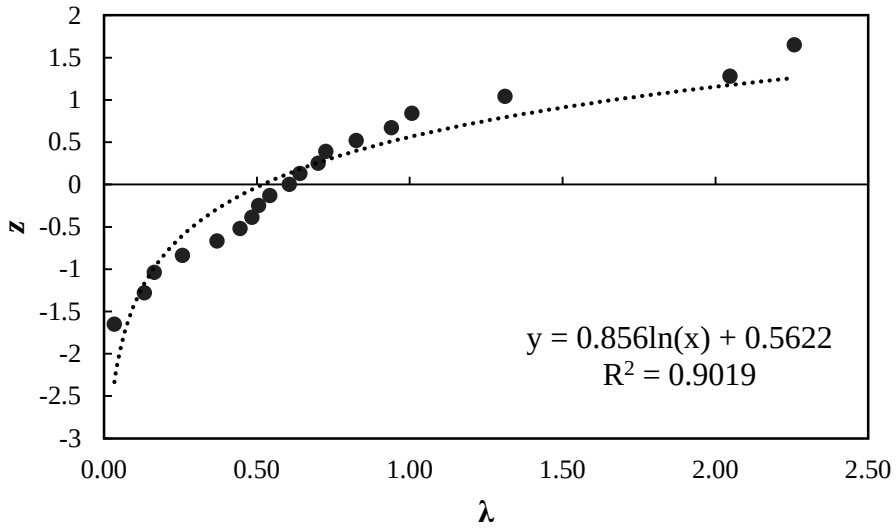

Figure 102. Graph. Probability plot for measured and predicted lateral displacement of GRS walls using the Jewell-Milligan method.

Conclusion:

Any interpretations of the results in this study should consider that the number of measured data points is statistically small. With this limitation, it was observed that the lower-than-unity mean λ (0.74) indicates the Jewell-Milligan method is a conservative prediction method, and it overestimates lateral deformation by a factor of 1.35. The relative low COV value (0.80) indicates the method has fair reliability.

Wu Method

Table 29 lists the predicted and measured values of the lateral displacements of GRS walls and abutments and λ and *z* for each data point. Based on the results, the mean λ is 0.24, s is 0.12, and COV is 0.50.

Table 29. Predicted and measured lateral displacements of GRS walls and abutments with modular block facing using the Wu method.

Case History No.	Elevation (m)	Measured Lateral Displacement (mm)	Predicted Lateral Displacement (mm)	/ (Measured/ Predicted)	*z*	Notes
1	3.3	1.5	4.7	0.3191	0.56	Results are obtained at EOC
	2.7	5.1	13.8	0.3696	1.18	
	2.1	5.2	18.4	0.2826	0.42	
	1.5	5.0	18.7	0.2674	0.32	
	0.9	3.7	14.5	0.2552	0.19	
	0.3	2.4	5.9	0.4068	1.49	
1	3.3	9.3	40.7	0.2285	0.11	Results are obtained at 30 kPa of applied pressure
	2.7	7.2	43.3	0.1663	-0.37	
	2.1	6.5	41.5	0.1566	-0.42	
	1.5	5.2	35.3	0.1473	-0.61	
	0.9	3.3	24.5	0.1347	-0.83	
	0.3	1.4	9.1	0.1538	-0.46	
1	3.3	31.6	88.9	0.3555	0.89	Results are obtained at 70 kPa of applied pressure
	2.7	31.3	82.0	0.3817	1.27	
	2.0	25.6	70.8	0.3616	1.1	
	1.5	15.5	56.1	0.2763	0.37	
	1.1	11.1	45.9	0.2418	0.15	
	0.5	4.7	23.5	0.2000	-0.11	
2	3.3	6.27	9.4	0.6670	2.12	Results are obtained at EOC
	2.7	7.98	27.5	0.2902	0.46	
	2.1	6.41	36.8	0.1742	-0.32	
	1.5	4.68	37.3	0.1255	-1.1	
	0.9	3.83	29.0	0.1321	-0.96	
	0.3	1.22	11.9	0.1025	-1.49	
2	3.3	11.4	81.8	0.1394	-0.71	Results are obtained at 30 kPa of applied pressure
	2.7	11.5	86.6	0.1328	-0.89	
	2.0	10.5	81.9	0.1282	-1.03	
	1.5	7.1	69.1	0.1027	-1.37	
	1.1	8.0	58.6	0.1365	-0.77	
	0.5	3.9	32.0	0.1219	-1.18	
2	3.3	46.5	177.3	0.2623	0.28	Results are obtained at 70 kPa of applied pressure
	2.7	57.9	164.3	0.3524	0.77	
	2.0	50.6	140.7	0.3596	1.03	

	1.4	37.0	110.9	0.3336	0.66	
	1.1	32.6	91.8	0.3551	0.83	
	0.5	15.8	46.1	0.3427	0.71	
3	3.1	2.07	9.2	0.2250	0.06	Results are obtained at EOC
	2.2	6.00	20.2	0.2970	0.51	
	1.3	5.24	20.0	0.2620	0.24	
	0.5	2.14	10.4	0.2058	-0.02	
10	3.3	3.9	8.2	0.4756	1.83	Results are obtained at EOC
	2.7	9.9	24.0	0.4125	1.64	
	2.1	11.4	32.0	0.3563	0.96	
	1.5	12.6	32.5	0.3877	1.37	
	0.9	8.1	25.2	0.3214	0.61	
	0.3	1.9	10.3	0.1845	-0.19	
10	3.3	10.4	69.5	0.1496	-0.51	Results are obtained at 30 kPa of applied pressure
	2.7	10.6	74.1	0.1430	-0.66	
	2.1	7.8	71.1	0.1097	-1.27	
	1.5	6.1	59.9	0.1018	-1.64	
	0.8	3.5	37.7	0.0928	-1.83	
	0.5	1.7	25.7	0.0661	-2.12	
10	3.3	27.5	151.0	0.1821	-0.24	Results are obtained at 70 kPa of applied pressure
	2.7	29.7	140.9	0.2108	0.02	
	2.1	25.0	122.6	0.2039	-0.06	
	1.5	18.3	96.5	0.1896	-0.15	
	0.8	10.1	57.1	0.1769	-0.28	
	0.5	5.4	36.6	0.1475	-0.56	

1 ft = 0.305 m
1 inch = 25.4 mm
1 psi = 6.89 kPa

Figure 103 shows the frequency of occurrence histogram of λ. The probability plot for the λ value obtained based on the result of the analytical model is depicted in figure 104. The curve follows a lognormal distribution.

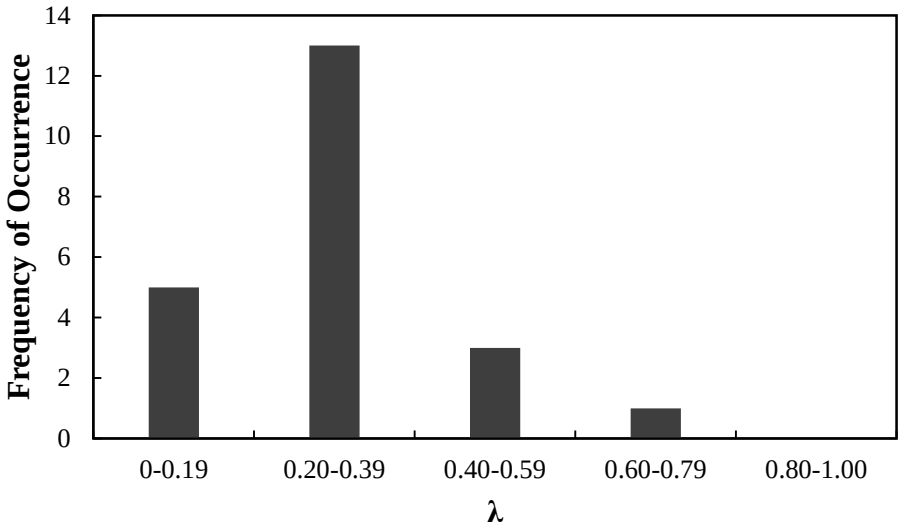

Figure 103. Graph. Frequency of occurrence histogram of / for the lateral displacement of GRS walls and abutments using the Wu method.

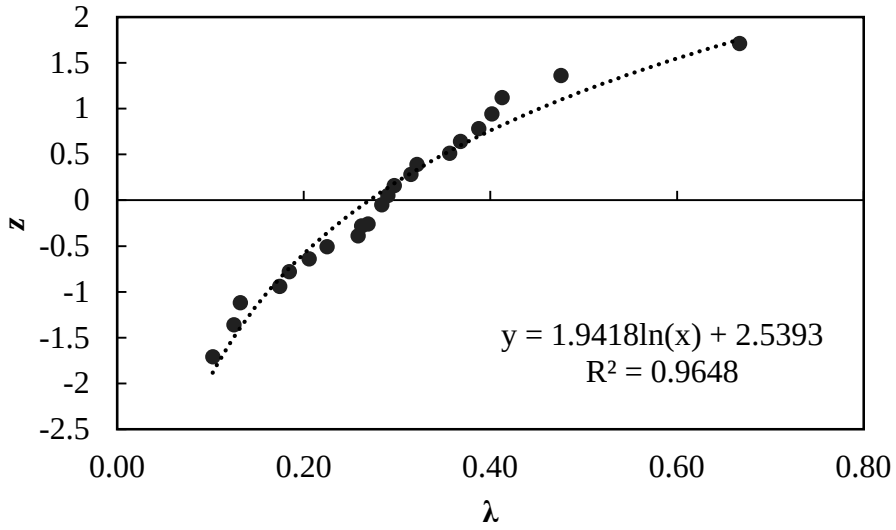

Figure 104. Graph. Probability plot for measured and predicted lateral displacement of GRS walls using the Wu method.

Conclusion:

Any interpretations of the results of this study should consider that the number of measured data points is statistically small. With this limitation, it was observed that the lower-than-unity mean λ (0.24) indicates the Wu method is a conservative prediction method, and it overestimates lateral deformation by a factor of 4.17. The low COV value (0.50) indicates the method has good reliability.

Adams Method

Table 30 lists the predicted and measured values of the lateral displacements of GRS walls and abutments and λ and *z* for each data point. Based on the results, the mean λ is 1.13, s is 0.41, and COV is 0.36.

Table 30. Predicted and measured lateral displacements of GRS walls and abutments using the Adams method.

Case History No.	Applied Pressure (kPa)	Measured Lateral Displacement (mm)	Predicted Lateral Displacement (mm)	/ (Measured/ Predicted)	*z*	Notes
11	84	82.7	73.4	1.13	-0.10	None
12	131	14.3	15.2	0.94	-0.29	None
13	0	8.6	11.4	0.75	-0.50	Results are obtained at EOC
14	0	11.1	15.3	0.73	-0.74	Results are obtained at EOC
15	115	10	5.6	1.79	1.43	None
16	115	9	12.7	0.71	-1.02	None
17	115	7	16.0	0.44	-1.43	None
18	207	23.4	16.3	1.44	0.74	None
	475	57.3	41.8	1.37	0.50	
19	214	36.4	27.5	1.32	0.29	None
	317	57.8	45.4	1.27	0.10	
	414	113.4	69.2	1.64	1.02	

1 psi = 6.89 kPa
1 inch = 25.4 mm

Figure 105 shows the frequency of occurrence histogram of λ. The normal probability plot for λ value obtained based on the results of the Adams method is depicted in figure 106. The curve follows a normal distribution.

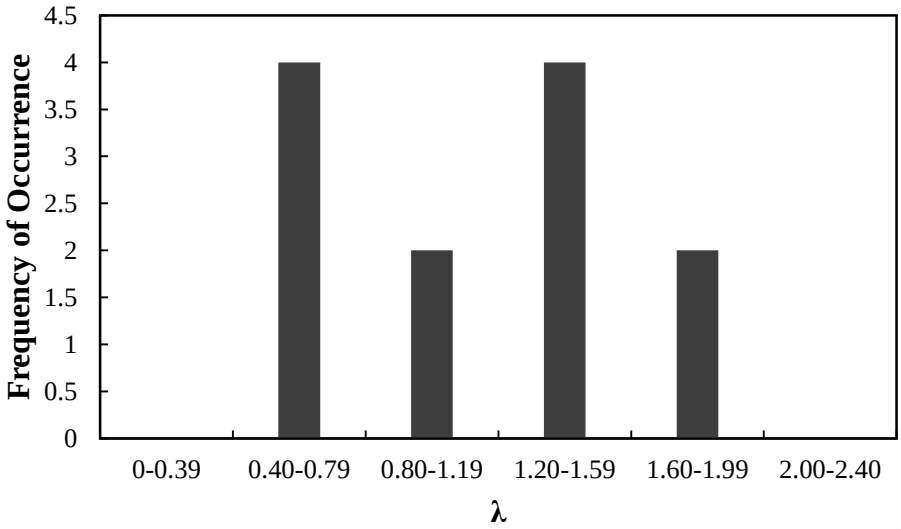

Figure 105. Graph. Frequency of occurrence histogram of / for the lateral displacement of GRS walls and abutments using the Adams method.

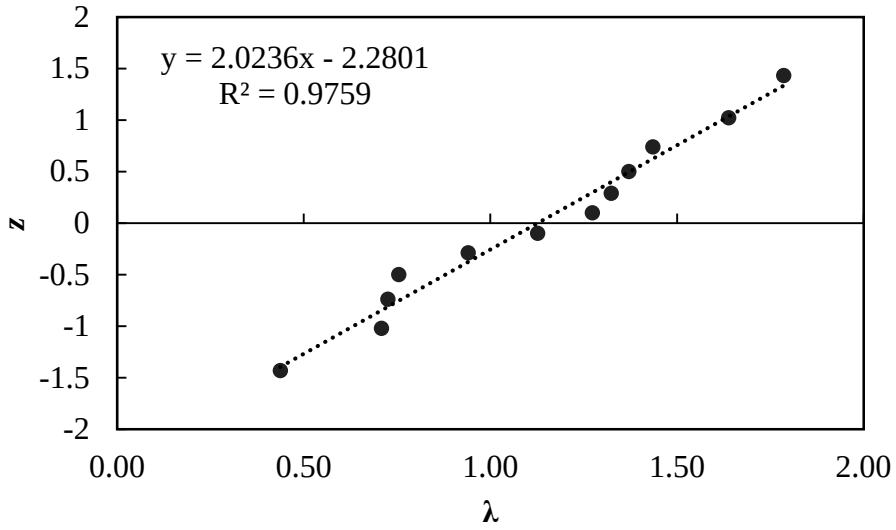

Figure 106. Graph. Probability plot for measured and predicted lateral displacement of GRS walls using the Adams method.

Conclusion:

Any interpretations of the results of this study should consider that the number of measured data points is statistically small. With this limitation, it was observed that the slightly higher-than-unity mean λ (1.13) indicates the Adams method is a slightly unconservative prediction method, and the predicted lateral displacement is on average 88 percent of the actually measured lateral deformation. The low COV value (0.36) indicates the method has good reliability.

Comparison of the Six Prediction Methods for Lateral Displacement of GRS Abutments and Walls

Table 31 summarizes the statistical analyses of the six prediction methods for lateral displacement of GRS abutments and walls. The Adams method is the most accurate method for predicting the maximum lateral displacement of GRS walls and abutments with the mean λ the closest to unity and small COV. The Jewell-Milligan method is a conservative and relatively accurate method for predicting the lateral displacement of GRS walls and abutments with negligible facing rigidity. For predicting the displacement of GRS walls and abutments with CMU facing block, the CTI method may also be used, although it may overestimate lateral deformations by a factor of 1.69 with relatively low reliability.

Table 31. Summary of the statistical analyses of the six prediction methods for lateral displacements of GRS abutments and walls.

Statistical Parameters	FHWA Method	Geoservices Method	CTI Method	Jewell-Milligan Method	Wu Method	Adams Method
Mean λ	0.12	1.38	0.59	0.74	0.24	1.13
s	0.10	1.59	0.64	0.59	0.12	0.41
COV	0.38	1.15	1.08	0.80	0.50	0.36

CHAPTER 5. NUMERICAL AND CONSTITUTIVE MODELS FOR COMPACTED FILL AND REINFORCED SOIL FOR BRIDGE SUPPORTS

5.1 MODELING OF COMPACTED SOILS

Various constitutive models have been utilized to model compacted soils, such as the linear elastic model, elastic-plastic Mohr-Coulomb model, hyperbolic stress-strain models, modified Cam Clay model, elastic-plastic viscoplastic models, extended two-invariant geologic cap model, and generalized plasticity models. (See references 121, 72, 122–128, 74, 129–135, 70, and 136.) An excellent review of the capabilities and shortcomings of different soil constitutive models can be found in Lade's publication, "Overview of Constitutive Models for Soils."[137] The soils can be any type: plastic or non-plastic, open-graded or well-graded, and coarse-grained or fine-grained, if appropriate models with appropriate input parameters are used.

Assignment of reasonable values for parameters used in soil constitutive models greatly influences the success and accuracy of any numerical analysis. For simple soil constitutive models, material parameters are often readily available from routine laboratory tests; however, that is not always the case for advanced constitutive models and precise identification of parameter values imposes a significant challenge. The effect of constitutive models on simulated responses of GRS structures has been investigated. Hatami and Bathurst compared the results of finite difference analyses (using FLAC2DÔ) for GRS SRWs with measured results from physical tests.[71] They modeled compacted fill soil using the hyperbolic stress-strain model proposed by Duncan et al. combined with a Mohr-Coulomb failure criterion and the simple linear elastic-plastic Mohr-Coulomb model.[138] The simple elastic-plastic soil model was shown to be sufficient for predicting wall deformation, footing reaction response, and peak strain values in reinforcement layers for strains of less than 1.5 percent if appropriate values for the constant elastic modulus and Poisson's ratio for the sand backfill soil are used. However, it is problematic to select a suitable single-value elastic modulus given the stress level dependency of granular soils. Different trends in the distribution of strains were observed when the nonlinear and linear elastic–plastic soil models were used, with the former giving a better fit to the measured data.

Huang et al. employed three well-known constitutive soil models in finite difference analyses (using FLAC2DÔ) of two instrumented reinforced soil segmental walls reported by Hatami and Bathurst.[139,71,118] These models (in order of increasing complexity) are the linear elastic-plastic Mohr-Coulomb model, the Duncan-Chang hyperbolic model with a modification by Boscardin et al., and Lade's single hardening constitutive model for frictional soils. (See references 138 and 140–143.) The modified Duncan-Chang model accounts for plane strain condition in addition to the triaxial condition considered in the original version of the model.[138,71] Lade's model considers a single yield surface and can capture both work-hardening and softening for frictional geomaterials.[141–143] Major advantages of such a model lies in the fact that the effects of stress-dependent stiffness, shear dilatancy, and strain softening on soil mechanical behavior are accounted for. Moreover, the effects of plane strain conditions are explicitly accounted for within this model, and no empirical adjustment, as done for the modified Duncan-Chang model, is required to increase elastic modulus values from triaxial test results. On the downside, several model parameters lack physical meaning, and thus application of this model demands significant expertise in interpreting available test results, calibration of model

parameters using element test results, and assignment of correct values for the model parameters. Predictions from analyses using the considered soil constitutive models were within measurement accuracy for the end-of-construction and surcharge load levels corresponding to working stress conditions. The elastic-plastic Mohr-Coulomb model was reported to be best suited for the analysis of reinforced soil walls that are at incipient collapse than for the working stress conditions. The modified Duncan-Chang model with plane strain boundary condition was reported to be a better candidate considering an optimal balance between prediction accuracy and availability of parameters from conventional triaxial compression tests.

Helwany et al. used a cap plasticity model to represent soil constitutive behavior in plane strain FEAs (using finite element (FE) code DYNA3D, an older version of LS-DYNA) of full-scale GRS bridge abutment testing.[70,144] Drucker and Prager yield criterion is used in association with a strain hardening elliptic cap model.[145,146] Such a model is capable of accounting for the effects of stress history, loading path, and intermediate principal stress on mechanical behavior of soil.[147] However, a two-invariant based model, such as the one used by Helwany et al. cannot capture dilatancy and anisotropy (stress-induced and fabric).[70] Recently, Wu et al. conducted two-dimensional numerical analyses using PLAXIS to simulate laboratory-scale GSGC tests that aimed to investigate the performance of GRS masses with different reinforcing conditions.[74] In the numerical analyses, the compacted soil was modeled using a hardening soil model, the reinforcement was modeled as a linear elastic material with an ultimate T_f, and sequential placement of reinforcements and compaction-induced stresses were considered. The FE results were in good agreement with laboratory test results. The FEAs demonstrated that the presence of geosynthetic reinforcement had a tendency to suppress dilation of the surrounding soil, which was potentially due to increased confinement provided by the embedded reinforcement layers and, thus, reduced the angle of dilation of the soil mass. Soil dilation is an important mechanism that controls the efficiency of load transfer from the reinforcement to the soil during shear deformations in reinforced soil structures.[148] The dilation behavior offers a new explanation of the reinforcing mechanism, and the angle of dilation provides a quantitative measure of the degree of reinforcing effect of a GRS mass.

In summary, past research studies have shown that various constitutive behaviors of compacted fill play an important role in the response of structures founded on engineered fills, which may manifest at different strain levels. For example, the strain-softening behavior may be important for pullout conditions but negligible for working conditions and SLS conditions with small allowable strains. The effect of strain hardening and dilation at SLS conditions may or may not be significant and warrants additional investigation. Although constitutive models that are capable of producing nonlinear stress-strain behaviors have shown to be more advantageous, simple linear elastic-plastic models may be sufficient for predicting the deformation of engineered fills and strains in reinforcement layers for working conditions and SLS conditions if appropriate model parameters are used.

5.2 MODELING REINFORCED SOIL AS A SINGLE COMPOSITE MATERIAL

In early numerical analyses of reinforced soils, the reinforcement and its surrounding soil are modeled as a single composite material.[149–151] In this approach, it is assumed that: (1) the friction between reinforcements and compacted soil is large enough so that there is no relative displacement between the two materials, and (2) the strain of compacted soil in the horizontal

direction is equal to that of the reinforcements. The assumptions behind this approach, however, may not be valid for SLS, where slippage between reinforcement and soil may not be negligible.[118] In recent numerical analyses, the reinforcement and surrounding compacted soil are hence modeled separately.

5.3 MODELING OF REINFORCEMENTS

Geosynthetic or metallic reinforcements are often modeled as a linear elastic material. (See references 72, 74, 121, 123, 124, 127, 128, 131, 132, and 152–155.) This treatment is considered sufficient as the stress and strain levels in working condition are generally low. In FE models, reinforcements are often modeled as slender objects (e.g., cable element) with a normal stiffness but with no bending stiffness.[124] This simplification is generally valid.[156]

The nonlinear stress-strain behavior of geosynthetic reinforcement has been considered. Ling et al. modeled the geosynthetic reinforcement as a nonlinear material, having developed a hyperbolic load-strain relationship.[157,158] Using their FEM model, Ling et al. simulated the construction response of a GRS retaining wall with a concrete-block facing.[157] Comparisons between measured and predicted behavior were presented for the wall deformation, vertical and lateral stresses, and strains in the geogrid layers. Satisfactory agreement between the measured and predicted results was observed. Under the working condition, however, the strains in the geogrid layers were small (less than 1 percent); hence, the geogrid essentially behaved as a linear elastic material. Fakharian and Attar simulated the well-instrumented Founders/Meadows segmental GRS bridge abutment near Denver, CO, where the geosynthetic reinforcement was modeled using elastic-plastic cable elements in FLAC 2D.[134] Satisfactory agreement was observed between the simulated and recorded facing displacement, vertical earth pressures, and geogrid strains. They observed that the maximum horizontal displacement of the facing due to deck load for the bridge abutment occurred at an elevation equivalent to 60 percent of the height of the front face of the abutment. They also observed that the geogrid experienced small strains (less than 1 percent) under the working condition.

For some cases, time-dependent behaviors of reinforcements could be important. For example, secondary settlement behavior has recently been observed in experimental studies on foundations supported by GRS.[21,27] Hence, it is important that time-dependent behaviors (e.g., creep) of geosynthetic reinforcements are accounted for in the modeling of GRS. For example, Sharma et al. modeled the reduction of linear elastic stiffness values with time based on the results of creep tests.[159] Lopes et al. simulated the load-strain-time response of an instrumented sloped reinforced wall by using a viscoelastic creep model.[160] Karpurapu and Bathurst modeled both the nonlinear load–strain and time-dependent responses of a polymeric geogrid using a parabolic load–strain model fitted to the results of creep tests.[129] The geosynthetic reinforcements were recently modeled using an elastic-viscoplastic bounding surface model to investigate the long-term performance of GRS structures.[135,161] Kongkitkul et al. presented an elastic-viscoplastic model that describes rate-dependent load-strain behavior of polymer geosynthetic materials.[162] The constitutive model is comprised of three components: a hypo-elastic component, a nonlinear inviscid component, and a nonlinear viscous component. Omission of one or more nonlinear components in this model yields the nonlinear elastic-plastic or hypo-elastic models, which are rather common in literature.

In summary, past research has shown that for reinforced soils, it is reasonable to model the reinforcements as linear elastic materials under working conditions because the strains developed in the reinforcements are generally small. The effect of nonlinear and time-dependent stress-strain behaviors of reinforcements, particularly geosynthetic reinforcements, on engineered fills at SLS and long term conditions is relatively unknown and warrants additional research.

5.4 MODELING OF SOIL-REINFORCEMENT INTERACTIONS

Several research studies have investigated soil-reinforcement interactions using analytical and numerical methods. (See references 153 and 163–170.) Palmeira provides a comprehensive summary of different experiments and theoretical models used to evaluate soil-geosynthetics interactions under different loading and boundary conditions.[171] Common numerical analyses (mostly using FE or finite difference scheme) of GRS structures and foundations on reinforced soil usually idealize geogrid layers as equivalent planar reinforcement layers with frictional characteristics. The geometric shape of the geogrid layer, particularly the presence or absence of transverse reinforcement, and bending stiffness are often ignored. Although these simplifications may not be valid under pullout loading conditions, they are generally valid under working conditions and, likely, SLS conditions.[172,173]

The basic differences between metal and geosynthetic reinforcement are their stiffness, structures, and the interactions occurring at the reinforcement-soil interfaces.[115] Metal reinforcement is usually in the form of straps or mats, whereas geosynthetic reinforcement is usually in the form of grids or planar sheets. The planar structure and flexibility of geosynthetics enable the shear forces inside the soil mass to be transferred to geosynthetic reinforcement more uniformly and without interruptions. Metal reinforcements usually have smooth surfaces; whereas most geosynthetics have fabric-like surfaces (geotextiles) or grid structures (geogrids), which produce better soil-reinforcement bonding. Consequently, slippage occurs at the interface between soil and metal reinforcement, but in GRSs, the slippage surfaces were observed to occur inside the soil mass next to the reinforcement.[174] Many of the modeling techniques for soil-geosynthetic interactions are also applicable to the interaction between soil and metallic reinforcements after adjustments to model parameters accounting for the aforementioned differences.

In most of the earlier FEM simulations of GRS, the soil-reinforcement interface behavior was modeled by using interface elements, such as joint elements of zero or non-zero thickness and node compatibility spring elements. (See references 129, 131, 133, and 175–186.) In this approach, the interface elements were formulated as a stiff spring in each of the shear and normal directions until slip occurred, at which point deformation could occur along the interface according to a Mohr-Coulomb failure criterion. (See references 72, 122, 128, and 135.) This approach also enables the specification of a decreased interface friction compared to the friction of the soil to model residual friction at the soil-reinforcement interface.[127,130] However, this approach involves assumption of horizontal and vertical stiffness values for the interface elements that are difficult to determine experimentally.[121] In 3D FEAs of a square footing bearing on reinforced sand, Kurian et al. employed 3D interface elements with zero thickness and with shear stiffness following a hyperbolic relation.[152,187] Penalty-type interface elements that allow sliding, friction, and separation facilitate modeling of interfaces between any two dissimilar materials have also been used in FE modeling of GRS structures and foundations

bearing on reinforced soil.[70,134] More recently, the soil-reinforcement interface behavior has been modeled using contact algorisms without assuming the contact stiffness values.[121]

5.5 NUMERICAL MODELING OF STRUCTURES SUPPORTED BY ENGINEERED SOILS

Most numerical models discussed previously were utilized to conduct parametric studies to investigate the effect of various parameters such as geometry and arrangement of reinforcement and soil properties on the response of structures supported by engineered soils. Few of these models have been validated against large-scale physical tests, and they are discussed in this section.

Karpurapu and Bathurst modeled the behavior of two carefully constructed and monitored large-scale GRS retaining walls (9.84 ft (3 m) high).[129] The walls were constructed using a dense sand fill and layers of geosynthetic reinforcement attached to two different facing treatments: an incremental panel wall versus a full height panel wall. The model walls were taken to collapse using a series of uniform surcharge loads applied at the sand fill surface. To model the GRS retaining wall, a modified form of hyperbolic stress-strain model was used to model the backfill soil. A nonlinear equation developed from isochronous load-strain-time test data was used to model the reinforcement, and the soil-reinforcement interface was modeled using joint elements of zero thickness.[138] To investigate the effect of soil dilation on GRS wall performance, two sets of numerical analyses were performed: one set with a soil dilation angle of 0 degrees and the other using a value of 15 degrees based on laboratory direct shear test results. The numerical analyses with no dilation were shown to have predicted much greater panel displacements and larger reinforcement strains. In some cases, the over-prediction was greater than measured values even at working load conditions by a factor of 2; whereas the numerical analyses with 15-degree soil dilation accurately predicted panel displacements and reinforcement strains. The results of their numerical study indicate that it is possible to accurately simulate all significant performance features of GRS walls at both working load and collapse conditions, and it is important to properly model facing treatment and consider soil dilation in the behaviors of GRS walls even at working load conditions.

Holtz and Lee developed FLAC2DÔ models to simulate six case histories, including the WSDOT geotextile wall (41.34 ft (12.6 m) high) in Seattle, WA, and five of the test walls (20.01 ft (6.1 m) high) constructed at the FHWA reinforced soil project site in Algonquin, IL.[120,188] The reinforcements for these walls included woven and nonwoven geotextiles, geogrids, steel strips, and steel bar mats. In these models, the compacted soil was modeled using a nonlinear elastic-plastic Mohr-Coulomb model with a hyperbolic stress-strain relationship, and the reinforcements were modeled as linear elastic materials with tensile and compressive strength. It was assumed that no slippage occurred between the soil and geosynthetic reinforcements, and interface elements were used to model the interaction between different materials or the discontinuities between the same materials, such as interfaces between backfill soil and structural facing and interfaces between structural facing units. Construction consequence of the walls was modeled by applying a uniform vertical stress equivalent to the overburden stress from each lift to the entire surface of each new soil layer before solving the model to equilibrium. Results of this study confirmed that the developed models were able to

provide reasonable working strain information of GRS walls.[120] However, accurate material properties were the key to a successful performance modeling of GRS walls.

Hatami and Bathurst conducted numerical modeling of four full-scale reinforced-soil SRWs (11.81 ft (3.6 m) high) using FLAC2DÔ.[118] The reinforcements for these walls included PP geogrid, PET geogrid, and WWM. In their model, the compacted soil was modeled using a nonlinear elastic-plastic model with a Mohr-Coulomb failure criterion and a dilation angle.[189] Compaction-induced stresses in the segmental walls were modeled by applying a transient uniform vertical pressure to the backfill surface at each stage during the simulation of wall construction. The effect of compaction on the reduction of fill Poisson's ratio was modeled by adjusting soil model parameters from triaxial and plane strain tests to ensure reasonably low values of Poisson's ratio. These modeling techniques were shown to have greatly improved the match between measured and predicted features. Results of this study showed that it is important to include compaction effects in the simulations in order to accurately model the construction and surcharge loading response of the reinforced soil walls. Comparison of predicted and measured results also suggested that the assumption of a perfect bond between the reinforcement and the soil may not be valid. In a follow up study, Hatami and Bathurst investigated the influence of backfill material type on the performance of soil-reinforced walls under working stress condition.[190] It was concluded that the addition of a small amount of cohesive strength can significantly reduce wall lateral displacements in case of negligible relative displacement between reinforcement and backfill soil.

Helwany et al. conducted a numerical study on the effects of backfill on the performance of GRS retaining walls.[73] In their numerical model, the backfill soil was modeled using the modified hyperbolic model, and the reinforcement was modeled as linear elastic.[138] Their numerical model was validated by comparing the results with the measurements from a well-instrumented large-scale laboratory test conducted on a GRS retaining wall (9.84 ft (3 m) high) under well-controlled test conditions.[191] The validated model was then utilized to conduct a parametric study on the effects of backfill on the performance of GRS retaining walls. It was shown that the stiffness of the geosynthetic reinforcement had a considerable effect of the behavior of the GRS retaining wall when the stiffness and shear strength of the backfill were relatively low.

Ling et al. simulated the performance of a full-scale instrumented GRS retaining wall (16.40 ft (5 m) high) using an FEM model.[158] The retaining wall was backfilled with a volcanic ash clay reinforced with a woven-nonwoven geotextile, and details of the test conditions were provided by Murata et al.[192] In the FEM model, the backfill soil was modeled as a Hookean material, the geotextile was modeled as having a hyperbolic stress-strain relationship, and no slippage was allowed at the soil-reinforcement interface. Compaction stresses induced during construction were not accounted for in the model. Results of their study indicated that the FEM model was able to capture the overall behavior of the retaining wall. The results showed that the GRS retaining wall performed as an integrated system, with the facing, geosynthetic and backfill soil interacting with each other to facilitate stress transfer and thus minimized deformation. It was also shown that stiffness values of the facing and reinforcements played equally important roles in the performance of GRS walls.

In a follow-up study, Ling et al. simulated another full-scale instrumented GRS retaining wall (19.68 ft (6 m) high) using an improved FEM model.[157] The retaining wall was backfilled

with a silty sand reinforced with a UX geogrid. Details of the test conditions were provided.[193,194] In the improved FEM model, the backfilled soil was modeled using a nonlinear hyperbolic model, the geogrid was modeled as a having a hyperbolic stress-strain relationship, and the interface behaviors were modeled using interface elements allowing slippage.[138] The results indicate that the FEM model predictions matched the measured results in terms of wall deformation, vertical and lateral stress, and strains in the geogrid layers.

Rowe and Skinner modeled the performance of a full-scale GRS retaining wall (26.25 ft (8 m) high) constructed on a layered soil foundation.[122] The foundation consisted of a 2.62-ft (0.8-m) hard crust underlain by 9.68 ft (2.95 m) of soft loam (sandy/silty) and then 4.26 ft (1.3 m) of stiff clay. Below the clay was 5.74 ft (1.75 m) of fine sand underlain by a layer of clayey/fine sand extending to a depth below 32.80 ft (10 m). The wall was constructed with 16 segmented concrete facing blocks, a sandy backfill material with 30 percent fines, and 11 layers of geogrid reinforcement 19.68 ft (6 m) long. In the FEM model, the backfill and foundation soils were modeled using an elastic-plastic model with a Mohr-Coulomb failure criterion, the geogrid was modeled as linear elastic, and the soil-reinforcement interface was modeled using interface elements. Compaction stresses induced during construction were not accounted for in the model. It was observed that the predicted behavior compared reasonably well with the observed behavior of the full-scale wall. The numerical results indicate that for the case of a GRS wall constructed on a yielding foundation, the stiffness and strength of the foundation can have a significant effect on the wall's behavior. A highly compressible and weak foundation layer can significantly increase the deformations at the wall's face and base and the strains in the reinforcement layers. It is interesting to note that trial analyses (with and without considering dilation) performed during this study did not exhibit any significant effects of dilation on analyses results except for a small difference in the vertical stress at the toe of the wall.

Helwany et al. simulated the behavior of full-scale GRS bridge abutment (15.25 ft (4.65 m) high) using LS-DYNA (formerly known as DYNA3D).[70] The backfill soil was simulated utilizing an extended two-invariant geologic cap model, and the geosynthetic reinforcement was modeled as an isotropic elastic-plastic material. The FEAs show that the performance of a GRS abutment, resulting from complex interaction among the various components, subjected to a service load or a limiting failure load can be simulated in a reasonably accurate manner. This numerical investigation also showed that the performance of GRS bridge abutments is greatly affected by the soil placement conditions (signified by the friction angle of the compacted soil), reinforcement stiffness, and reinforcement spacing.

The numerical studies presented show that numerical models can realistically model the mechanical behavior of soil-geosynthetic composite and capture the performance features of GRS walls, such as the wall deformation, vertical and lateral stress, and strains in the geogrid layers, at both working load and collapse conditions. These studies have highlighted the importance of properly modeling complex constitutive behaviors of compacted fill and foundation soil (e.g., soil dilatancy and softening at large displacement), stress-strain relationship of reinforcements, and sequential construction and compaction-induced stresses. However, no numerical studies have been conducted to investigate the SLS of structures supported by engineered soil.

5.6 NUMERICAL MODELING OF LONG-TERM BEHAVIOR OF GRS STRUCTURES

Although past studies have produced reasonable solutions, particularly when the material model parameters were calibrated to fit model-scale test results, to understand short-term (immediately after load placement) load-settlement behavior of shallow foundations bearing on GRS, few of these studies could account for time-dependent secondary deformation (settlement) behavior of foundations under service load. Such secondary settlement behavior has recently been observed in experimental studies, and it is important that such deformation is accounted for in calculation of total foundation settlement.[21,27] Moreover, it is also important to understand the stress distribution profile below the footing on reinforced ground. Such understanding will further facilitate economic design by restricting fill placement only down to the zone of influence below the foundation. Several numerical studies on long-term behavior of GRS structures are summarized in this section.

Helwany and Wu developed a numerical model for analyzing long-term performance of GRS structures.[195] In their model, compacted soil was modeled using an anisotropic extension of the Cam-clay model, which is capable of describing the effects of stress anisotropy, stress reorientation, and creep of normally consolidated and lightly overconsolidated clays. A generalized geosynthetic creep model developed by Helwany and Wu was used to simulate time-dependent behavior of the geosynthetic reinforcement.[195] It was assumed that slippage did not occur at the soil-geosynthetic interface under service loads, which was generally valid for extensible geosynthetic reinforcement. This investigation clearly demonstrates that the time-dependent deformation behavior of the confining soil played an important role in the long-term creep behavior of GRS structures. Hence, a rational design of GRS structures must account for the long-term soil-geosynthetic interaction.

Liu and Won and Liu et al. modeled the long-term behavior of GRS retaining walls with different backfill soils.[186,135] According to Liu and Won, the backfill soil was assumed to be time independent and modeled using a generalized plasticity model for sand, the reinforcement was modeled using the elastic-plastic viscoplastic bounding surface model for geosynthetics, and the soil-reinforcement interface was modeled using interface elements. (See references 186, 136, 161, and 196.) According to Liu et al., the backfill soil was modeled as time dependent using an elastic-plastic viscoplastic model obeying Drucker-Prager yield criterion and Singh-Mitchell creep model but with nonlinear elastic properties.[135] The reinforcement and soil-reinforcement interface were modeled in the same way as Liu and Won.[186] In both studies, the numerical models were validated using the experimental results of a long-term PT on sand-geosynthetic composite reported in Helwany and Wu and Helwany.[197,198]

Liu and Won and Liu et al. demonstrated that the load distribution in backfill soil and reinforcement depended on their time-dependent properties, which determine the long-term performance of GRS walls.[186,135] It was shown that large soil creep can lead to a significant increase in both wall displacement and reinforcement load. Conversely, if soil creep is smaller than reinforcement creep, reinforcement load would decrease due to load relaxation, but the soil stress could increase significantly. This indicates that backfill soil must have adequate strength to compensate the long-term reduction of load carried by reinforcement due to load relaxation. The results of these studies indicate that in the design of GRS structures, it is necessary to take into

account the relative creep rate of reinforcement and backfill soil, especially if backfill soil with high cohesive fines contents is used.

Past numerical studies have shown that the creep deformation of a GRS wall is a result of soil-geosynthetic interaction. The creep rate of the geosynthetic reinforcement may accelerate or decrease depending on the relative creep rate between the backfill and geosynthetic reinforcement.[199] For a GRS structure with a well-compacted granular backfill, the time-dependent deformation is small and the rate of deformation of the soil-geosynthetic composite typically decreases rapidly with time.[199] Hence, creep deformation of geosynthetic reinforcement in a GRS structure may or may not be a design issue, depending on the soil-geosynthetic interaction. It should be noted that no numerical studies have been conducted to investigate the long-term deformation of GRS walls supported by reinforced soil.

5.7 SIMILARITIES AND DIFFERENCES BETWEEN PIER AND ABUTMENT FOUNDATION DEFORMATION MODELS

In common transportation engineering practice, deep foundations are frequently used to support lateral and vertical loads at pier and abutment locations for bridges. However, recent research shows that spread footings, if analyzed and designed adequately, can be an economic option for bridge support.[200] Although shallow foundations may provide a viable alternative in terms of their capacity to support structural load, their use is often restricted to avoid excessive settlement at bridge foundation locations. Nonetheless, settlement calculations and the serviceability limit state criteria set to check the calculated settlement are often overly conservative in terms of actual load-settlement response of shallow spread footings bearing on compacted, reinforced or unreinforced engineered fills and the tolerable movement criteria used to design them. While similar foundation-soil load transfer mechanisms can be expected, for a given bearing stratum (i.e., engineered fills with or without embedded reinforcement layers) at both pier and abutment locations, the load-deformation behavior is expected to vary at these locations. The major difference would arise from the 3D (close or similar to a triaxial condition) stress state existing below square, rectangular, and circular spread footings when compared to a confined plane strain condition (i.e., strain in the out-of-the plane direction is zero) strain existing at the abutment locations.

Dimensions of shallow foundation affect bearing capacity and load-displacement behavior on granular soil.[201] Fakher and Jones point out that the foundation dimension effects should be studied in order to critically judge the behavior of foundations on reinforced soil and that the role of reinforcement in enhancing foundation performance might be misjudged without the consideration of such effect.[202] Based on results of FE simulations, Chen and Abu-Farsakh show that foundation dimension effects became negligible when reinforcement depth ratio (i.e., ratio of total reinforcement depth to foundation width) and reinforcement ratio ($E_R A_r / E_s A_s$; where A_r and A_s are area of reinforcement and reinforced soil per unit width, respectively) remains constant.[154] Such a conclusion is valid for design for ULS (e.g., bearing capacity of foundation) with a specified relative settlement (i.e., ratio of settlement and characteristic width of a foundation) criterion. However, for serviceability limit state design based on absolute values of foundation settlement, dimensions of shallow foundations are expected to play a major role in SLS.

Apart from the difference in bearing capacity failure mechanism under the above stated conditions, an additional difference is expected to arise from state-dependent strength behavior of compacted granular fill material and placement conditions; a reflection of this would be through different degrees of dilation for the same compacted density.[70,203] Such differences in strength-deformation behavior are likely to change the load-deformation behavior of shallow foundations at pier bents and the compacted fill at abutment locations. Another key difference might arise from the load eccentricity caused by the combined loading and the ratio of lateral to vertical loading. Load eccentricity may have a larger impact on lateral and vertical movements of spread footings below bridge piers when compared to its effect in controlling movements at abutment support locations.

CHAPTER 6. CONCLUSIONS

6.1 CONCLUSIONS

In the evaluation of five widely used methods of estimating immediate settlement of shallow foundations on granular soils, it was observed that four of the five methods (modified Schmertmann, Hough, Peck and Bazaraa, and Burland and Burbidge) overestimate immediate settlement, and the D'Appolonia method slightly underestimates immediate settlement. In comparison, the D'Appolonia method is the most accurate method with the mean λ the closest to unity and relatively small COV, followed by the Peck and Barazaa method and the Burland and Burbidge method. Both the modified Schmertmann method and the Hough method overestimate immediate settlement of shallow foundations on granular soils by a factor of approximately 2. It is noted that this conclusion is based on measured data whose population may be statistically small.

In the evaluation of six prediction methods for lateral displacements of GRS abutments and walls, it was concluded that the Adams method is the most accurate method for predicting the maximum lateral displacement of GRS walls and abutments with the mean λ the closest to unity and small COV. The Jewell-Milligan method is a conservative and relatively accurate method for predicting the lateral displacement of GRS walls and abutments with negligible facing rigidity. For predicting the displacement of GRS walls and abutments with CMU facing block, the CTI method may also be used, although it may overestimate lateral deformations by a factor of 1.69 with a relatively high COV. It is noted that this conclusion is based on measured data whose population may be statistically small.

Currently, there is only one method available in estimating elastic vertical deformation of GRS abutments and walls; it is an empirical equation proposed by Adams et al.[32] This method uses the composite Young's modulus of the GRS composite. Although the field observation data that are used to evaluate this empirical method show that this method is highly unconservative, it should be noted that the accuracy of the prediction method depends on the accurate determination of the composite Young's modulus, which lacks in the literature. It should also be noted that this conclusion is based on measured data whose population may be statistically small.

6.2 KNOWLEDGE GAPS AND DATA NEEDS FOR BRIDGE SUPPORTS USING ENGINEERED FILLS

Based on the synthesis of the literature and current guidelines and methods on bridge supports using engineered fills, the following knowledge gaps and data needs for bridge supports using engineered fills were identified:

- The current analyses primarily predict immediate settlement only. While it is a common assumption that granular or engineered fills do not exhibit secondary deformation, it has been observed in in-service bridge abutment applications and large-scale piers in laboratory tests.[27,32] Among the limited number of methods for predicting long-term (or time-dependent secondary post-construction) deformation of granular soils, long-term field observations or long-term PTs are needed to derive coefficients that are used in the

prediction methods. Furthermore, long-term deformation data of bridge supports on engineered fills are rather limited, so that the evaluation of currently available long-term deformation prediction methods cannot be performed.

- There is a particular lack of prediction methods for vertical (for both immediate and long-term) deformations of MSE and GRS bridge abutments and piers.

- There is lack of comprehensive knowledge of the effects of soil characteristics and compaction efforts on the SLS performances of bridge supports using engineered fills. Accordingly, current design guides provide specific requirements on engineered fills for bridge support, and design is limited to the conditions and parameters under which testing has occurred. In addition, the parameters used (e.g., f, c, etc.) may vary depending on the measurement technique and the design method selected, which may have an impact on the SLS analysis. Other different types of fill materials are not being used due to a lack of data on their impact.

- Stress distribution in soils can be influenced by various soil conditions (i.e., grain size distribution, strength parameters, relative density, and fine content), reinforcement characteristics (i.e., T_f, stiffness, N, and S_v), and loading conditions. Some of these parameters were investigated previously.[90] However, the current literature suggests there is a lack of documentation and understanding of the effects of various parameters on the stress distribution in reinforced engineered fills as bridge supports in SLS.

- The dynamic effect of transient load on bridge supports using engineered fills has not been investigated. There is a lack of literature on the time-dependent and live (transient) load on the stress-deformation behaviors of bridge supports using engineered fills.

REFERENCES

1. Mertz, D. (2012). *Steel Bridge Design Handbook: Limit States*, Report No. FHWA-IF-12-052-Vol.10, Office of Bridge Technology, Federal Highway Administration, Washington, DC.

2. DiMillio, A.F. (1982). *Performance of Highway Bridge Abutments on Spread Footings on Compacted Fill*, Report No. FHWA RD-81-184, Federal Highway Administration, Washington, DC.

3. Gifford, D.G., Kraemer, S.R., Wheeler, J.R., and McKown, A.F. (1987). *Spread Footings for Highway Bridges*, Report No. FHWA RD-86-185, Federal Highway Administration, Washington, DC.

4. Zevgolis, I. and Bourdeau, P.L. (2007). *Mechanically Stabilized Earth Wall Abutments for Bridge Support*, Report No. FHWA/IN/JTRP-2006/38, Joint Transportation Research Program, Indiana Department of Transportation and Purdue University, West Lafayette, IN.

5. Abu-Hejleh, N.M., Alzamora, D., Mohamed, K., Saad, T., and Anderson, S. (2014). *Implementation Guidance for Using Spread Footings on Soils to Support Highway Bridges*, Report No. FHWA-RC-14-001, Federal Highway Administration Resource Center, Matteson, IL.

6. Samtani, N.C. and Nowatzki, E.A. (2006a). *Soils and Foundations Reference Manual: Volumes I*, Report No. FHWA-NHI-06-088, Federal Highway Administration, Washington, DC.

7. Samtani, N.C., Nowatzki, E.A., and Mertz, D.R. (2010). *Selection of Spreading Footings on Soils to Support Highway Bridge Structures*, Report No. FHWA-RC/TD-10-001, Federal Highway Administration, Washington, DC.

8. AASHTO. (2014). *AASHTO LRFD Bridge Design Specifications*, 7th Edition, American Association of State Highway and Transportation Officials, Washington, DC.

9. AASHTO. (2008). *Manual for Bridge Evaluation*, American Association of State Highway and Transportation Officials, Washington, DC.

10. Modjeski and Masters, Inc., University of Nebraska, Lincoln, University of Delaware, and NCS Consultants, LLC. (2015). *Bridges for Service Life Beyond 100 Years: Service Limit State Design*, SHRP2 Report S2-R19B-RW-1, Transportation Research Board of National of Academies, Washington, DC.

11. Paikowsky, S.G., Lesny, K., Amatya, S., Kisse, A., Muganga, R., and Canniff, M.Â. (2010). *LRFD Design and Construction of Shallow Foundations for Highway Bridge Structures*, NCHRP Report No. 651 for Project NCHRP 24-31, National Cooperative Highway Research Program, Washington, DC.

12. Kimmerling, R.E. (2002). *Geotechnical Engineering Circular No. 6: Shallow Foundations*, Report No. FHWA-SA-02-054, Federal Highway Administration, Washington, DC.

13. American Association of State and Highway Transportation Officials. (2015). "AASHTO T27-14: Sieve Analysis of Fine and Coarse Aggregates," *Standard Specifications for Transportation Materials and Methods of Sampling and Testing*, 35th Edition and AASHTO Provisional Standards, 2015 Edition. Washington, DC.

14. American Association of State and Highway Transportation Officials. (2015). "AASHTO T90-15: Determining the Plastic Limit and Plasticity Index of Soils," *Standard Specifications for Transportation Materials and Methods of Sampling and Testing*, 35th Edition and AASHTO Provisional Standards, Washington, DC.

15. American Association of State and Highway Transportation Officials. (2015). "AASHTO T104-99 (2011): Soundness of Aggregate by Use of Sodium Sulfate or Magnesium Sulfate," *Standard Specifications for Transportation Materials and Methods of Sampling and Testing*, 35th Edition and AASHTO Provisional Standards, Washington, DC.

16. American Association of State and Highway Transportation Officials. (2015). "AASHTO T99-15: Moisture-Density Relations of Soils Using a 2.5-kg (5.5-lb) Rammer and a 305-mm (12-in.) Drop," *Standard Specifications for Transportation Materials and Methods of Sampling and Testing*, 35th Edition and AASHTO Provisional Standards, Washington, DC.

17. American Association of State and Highway Transportation Officials. (2015). "AASHTO T180-15: Moisture-Density Relations of Soils Using a 4.54-kg (10-lb) Rammer and a 457-mm (18-in.) Drop," *Standard Specifications for Transportation Materials and Methods of Sampling and Testing*, 35th Edition and AASHTO Provisional Standards, Washington, DC.

18. Samtani, N.C. and Nowatzki, E.A. (2006b). *Soils and Foundations Reference Manual: Volume II*, Report No. FHWA-NHI-06-089, Federal Highway Administration, Washington, DC.

19. Vidal, H. (1969). "The Principle of Reinforced Earth," *Highway Research Record 282*, 1–16, Transportation Research Board, Washington, DC.

20. Hanna, B.E. (1977). "The Use of Reinforced Earth Walls as Bridge Abutments," *Proceedings of the 28th Annual Highway Geology Symposium*, 57–60, South Dakota School of Mines & Technology, Rapid City, SD.

21. Adams, M., Nicks, J., Stabile, T., Wu, J., Schlatter, W., and Hartmann, J. (2011a). *Geosynthetic Reinforced Soil Integrated Bridge System Synthesis Report*, Report No. FHWA-HRT-11-027, Federal Highway Administration, Washington, DC.

22. Adams, M. (1997). "Performance of a Pre-Strained Geosynthetic Reinforced Soil Bridge Pier," *International Symposium on Mechanically Stabilized Backfill*, 35–53.

23. Wu, J.T.H., Ketchart, K., and Adams, M. (2001). *GRS Bridge Piers and Abutments*, Report No. FHWA-RD-00-038, Federal Highway Administration, Washington, DC.

24. Sun, C. and Graves, C. (2013). *Evaluation of Mechanically Stabilized Earth (MSE) Walls for Bridge Ends in Kentucky: What Next?*, KTC-13-11/SPR443-12-1F, Kentucky Transportation Center, University of Kentucky, Lexington, KY.

25. Abernathy, C. (2013). *Geosynthetic Reinforced Soil—Integrated Bridge System (GRS-IBS)*, Experimental Projects Construction Report, Montana Department of Transportation, Helena, MT.

26. Talebi, M., Meehan, C., Cacciola, D., and Becker, M. (2014). "Design and Construction of a Geosynthetic Reinforced Soil Integrated Bridge System," *Proceedings of GeoCongress 2014*, GSP No. 234, American Society of Civil Engineers, Atlanta, GA.

27. Adams, M. and Nicks, J. (2014). "Secondary Settlement of Geosynthetic Reinforced Soil Piers: Preliminary Results," *Proceedings of GeoCongress 2014*, GSP No. 234, 4,228–4,237, American Society of Civil Engineers, Atlanta, GA.

28. Warren, K., Whelan, M., Hite, J., and Adams, M. (2014). "Three Year Evaluation of Thermally Induced Strain and Corresponding Lateral End Pressures for a GRS IBS in Ohio," *Proceedings of GeoCongress 2014*, GSP No. 234, American Society of Civil Engineers, Atlanta, GA.

29. Budge, A., Dasenbrock, D., Mattison, D., Bryant, G., Grosser, A., Adams, M., and Nicks, J. (2014). "Instrumentation and Early Performance of a Large Grade GRS-IBS Wall," *Proceedings of GeoCongress 2014*, GSP No. 234, American Society of Civil Engineers, Atlanta, GA.

30. Tatsuoka, F. (2008) "Recent Practice and Research of Geosynthetic-Reinforced Earth Structures in Japan," *Journal of GeoEngineering*, *3*(3), 77–100.

31. Kempton, G., Özçelik, H., Naughton, P., Mum, N., and Dundar, F. (2008). *The Long Term Performance of Polymeric Reinforced Walls Under Static and Seismic Conditions*, Fourth European Geosynthetics Conference, Paper No. 181, Edinburgh, UK.

32. Adams, M., Nicks, J., Stabile, T., Wu, J., Schlatter, W., and Hartmann, J. (2011b). *Geosynthetic Reinforced Soil Integrated Bridge System Interim Implementation Guide*, Report No. FHWA-HRT-11-026, Federal Highway Administration, Washington, DC.

33. Cheney, R.S. and Chassie, R.G. (2000). *Soils and Foundation Workshop Reference Manual*, Publication No. FHWA NHI-00-045, Federal Highway Administration, Washington, DC.

34. Anderson, P.L. and Brabant, K. (2010). *Increased Use of MSE Abutments*, Association for Metallically Stabilized Earth, Reston, VA. Obtained from: http://amsewalls.org/technical_papers.html. Site last accessed November 11, 2015.

35. Elias, V. and Christopher, B.R. (1998). *Mechanically Stabilized Earth Walls and Reinforced Soil Slopes Design and Construction Guidelines*, FHWA Report No. FHWA-SA-96-071, Federal Highway Administration, Washington, DC.

36. Elias, V., Christopher, B.R., and Berg, R.R. (2001). *Mechanically Stabilized Earth Walls and Reinforced Soil Slopes Design and Construction Guidelines*, FHWA Report No. FHWA-NHI-00-043, Federal Highway Administration, Washington, DC.

37. Berg, R.R., Christopher, B.R., and Samtani, N.C. (2009). *Design of Mechanically Stabilized Earth Walls and Reinforced Soil Slopes—Volume I*, Publication No. FHWA-NHI-10-024, National Highway Institute, Federal Highway Administration, Washington, DC.

38. Koerner, R.M. and Soong, T-Y. (2001), "Geosynthetic Reinforced Segmental Retaining Walls," *Geotextiles and Geomembranes*, *19*(6), 359–386.

39. National Concrete Masonry Association. (1997). *Design Manual for Segmental Retaining Walls*, Collin, J.G. (Ed.), 289, Herndon, VA.

40. Munfakh, G., Arman, A., Collin, J.G., Hung, J.C., and Brouillette, R.P. (2001). *Shallow Foundations Reference Manual*, Report No. FHWA-NHI-01-023, Federal Highway Administration, Washington, DC.

41. Adams, M. and Collin, J. (1997). "Large Model Spread Footing Load Tests on Geosynthetic Reinforced Soil Foundations," *Journal of Geotechnical and Geoenvironmental Engineering*, *123*(1), 66–72.

42. Nicks, J.E., Adams, M.T., Ooi, P.S.K., and Stabile, T. (2013). *Geosynthetic Reinforced Soil Performance Testing—Axial Load Deformation Relationships*, Report No. FHWA-HRT-13-066, Federal Highway Administration, Washington, DC.

43. Moulton, L.K., Ganga Rao, H.V.S., and Halvorsen, G.T. (1982). *Tolerable Movement Criteria for Highway Bridges*, Report No. FHWA/RD-81/162, Federal Highway Administration, Washington, DC.

44. Moulton, L.K., Ganga Rao, H.V.S., and Halvorsen, G.T. (1985). *Tolerable Movement Criteria for Highway Bridges*, Report No. FHWA/RD-85/107, Federal Highway Administration, Washington, DC.

45. Barker, R.M., Duncan, J.M., Rojiani, K.B., Ooi, P.S.K., Tan, C.K., and Kim, S.G. (1991). *Manuals for the Design of Bridge Foundations*, NCHRP Report 343, National Cooperative Highway Research Program, Washington, DC.

46. Washington State Department of Transportation. (2014). *Geotechnical Design Manual*, WSDOT, Tumwater, WA.

47. Arizona Department of Transportation. (2009). *Bridge Design Guidelines*, AZDOT, Phoenix, AZ.

48. Wahls, H. (1983). *NCHRP Synthesis of Highway Practice Report 107: Shallow Foundations for Highway Structures*, National Cooperative Highway Research Program, Washington, DC.

49. Bozozuk, M. (1978). "Bridge Foundations Move," *Transportation Research Record 678*, 17–21, Transportation Research Board, Washington, DC.

50. Walkinshaw, J.L. (1978). "Survey of Bridge Movements in the Western United States," *Transportation Research Record 678*, 6–11, Transportation Research Board, Washington, DC.

51. Wahls, H.E. (1990). *Design and Construction of Bridge Approaches*, NCHRP Synthesis of Highway Practice 159, 45, Transportation Research Board, Washington, DC.

52. AASHTO. (2002). *Standard Specifications for Highway Bridges*, 17th Ed., American Association of State Highway and Transportation Officials, Washington, DC.

53. Fragaszy, R.J. and Lawton, E. (1984). "Bearing Capacity of Reinforced Sand Subgrades," *Journal of Geotechnical Engineering*, *110*(10), 1,500–1,507.

54. Basudhar, P.K., Saha, S., and Deb, K. (2007). "Circular Footings Resting on Geotextile-Reinforced Sand Bed," *Geotextiles and Geomembranes*, *25*, 377–384.

55. Omar, M.T., Das, B.M., Puri, V.K., and Yen, S.C. (1993). "Ultimate Bearing Capacity of Shallow Foundations on Sand with Geogrid-Reinforcement," *Canadian Geotechnical Journal, 30*, 545–549.

56. Chen, Q., Abu-Farsakh, M.Y., Sharma, R., and Zhang, X. (2007). "Laboratory Investigation of Behavior of Foundations on Geosynthetic-Reinforced Clayey Soil," *Transportation Research Record 2004*, 28–38, Transportation Research Board, Washington, DC.

57. ASTM D 1196-93. (2004). "Standard Test Method for Nonrepetitive Static Plate Load Tests of Soils and Flexible Pavement Components, for Use in Evaluation and Design of Airport and Highway Pavements," *Book of Standards Volume 04.08*, ASTM International, West Conshohocken, PA.

58. Das, B.M., Shin, E.C., and Omar, M.T. (1994). "The Bearing Capacity of Surface Strip Foundations on Ggeogrid-Reinforced Sand and Clay—Comparative Study," *Geotechnical and Geological Engineering, 12*(1), 1–14.

59. Phanikumar, B.R., Prasad, R., and Singh, A. (2009). "Compressive Load Response of Geogrid-Reinforced Fine, Medium and Coarse Sands," *Geotexiles and Geomembranes*, *27*, 183–186.

60. Huang, C.C. and Tatsuoka, F. (1990). "Bearing Capacity of Reinforced Horizontal Sandy Ground," *Geotextiles and Geomembranes*, *9*(1), 51–82.

61. Latha, G.M. and Somwanshi, A. (2009). “Bearing Capacity of Square Footings on Geosynthetic Reinforced Sand,” *Geotexiles and Geomembranes, 27*, 281–294.

62. Elton, D.J. and Patawaran, M.A. (2004). “Mechanically Stabilized Earth Reinforcement Tensile Strength from Tests of Geotextile-Reinforced Soil,” *Transportation Research Record 1868*, 81–88, Transportation Research Board, Washington, DC.

63. Abu-Hejleh, N., Wang, T., and Zornberg, J.G. (2000). “Performance of Geosynthetic-Reinforced Walls Supporting Bridge and Approaching Roadway Structures,” *Advances in Transportation and Geoenvironmental Systems Using Geosynthetics*, ASCE/Geotechnical Special Publication No. 103, 218–243.

64. Abu-Hejleh, N., Zornberg, J.G., Wang, T., and Watcharamonthein, J. (2002). “Monitored Displacements of Unique Geosynthetic-Reinforced Soil Bridge Abutments,” *Geosynthetics International*, *9*(1), 71–95.

65. ASTM D 2487. (2011). “Standard Practice for Classification of Soils for Engineering Purposes (Unified Soil Classification System,” *Book of Standards Volume 04.08*, ASTM International, West Conshohocken, PA.

66. American Association of State and Highway Transportation Officials. (2015). “AASHTO M145-91 (2012): Classification of Soils and Soil-Aggregate Mixtures for Highway Construction Purposes,” *Standard Specifications for Transportation Materials and Methods of Sampling and Testing*, 35th Edition and AASHTO Provisional Standards, Washington, DC.

67. Das, B.M. and Omar, M.T. (1994). “The Effects of Foundation Width on Model Tests for the Bearing Capacity of Sand with Geogrid Reinforcement,” *Geotechnical and Geological Engineering*, *12*(2), 133–141.

68. Mandal, J.N. and Sah, H.S. (1992). “Bearing Capacity Tests on Geogrid-Reinforced Clay,” *Geotexiles and Geomembranes*, *11*, 327–333.

69. Binquet, J. and Lee, K.L. (1975). “Bearing Capacity Tests on Reinforced Earth Slabs,” *Journal of the Geotechnical Engineering Division*, *101*(12), 1,241–1,255.

70. Helwany, S.M.B, Wu, J.T.H., and Kitsabunnarat, A. (2007). “Simulating the Behavior of GRS Bridge Abutments,” *Journal of Geotechnical and Geoenvironmental Engineering*, *133*(10), 1,229–1,240.

71. Hatami, K. and Bathurst, R.J. (2005). “Development and Verification of a Numerical Model for the Analysis of Geosynthetic-Reinforced Soil Segmental Walls Under Working Stress Conditions,” *Canadian Geotechnical Journal*, *42*(4), 1,066–1,085.

72. Skinner, G.D. and Rowe, R.K. (2003). “Design and Behavior of Geosynthetic Reinforced Soil Walls Constructed on Yielding Foundations,” *Geosynthetics International*, *10*(6), 200–214.

73. Helwany, S.M.B., Reardon, G., and Wu, J.T.H. (1999). “Effects of Backfill on the Performance of GRS Retaining Walls,” *Geotextiles and Geomembranes*, *17*(1), 1–16.

74. Wu, J.T.H., Pham, T.Q., and Adams, M.T. (2013). *Composite Behavior of Geosynthetic Reinforced Soil Mass*, Report No. FHWA-HRT-10-077, Washington, DC.

75. Gotteland, P., Gourc, J.P., and Villard, P. (1997) “Geosynthetic Reinforced Structures as Bridge Abutment: Full Scale Experimentation and Comparison with Modelisations,” *International Symposium on Mechanically Stabilized Backfill*, 25–34.

76. Bathurst, R.J., Nernheim, A., Walters, D.L., Allen, T.M., Burgess, P., and Saunders, D.D. (2009). “Influence of Reinforcement Stiffness and Compaction on the Performance of Four Geosynthetic Reinforced Soil Walls,” *Geosynthetics International*, *16*(1), 43–59.

77. Tatsuoka, F., Tateyama, M., and Murata, O. (1989). “Earth Retaining Wall with a Short Geotextile and a Rigid Facing,” *Proceedings of the 12th International Conference on Soil Mechanics and Foundation Engineering 2*, 1,311–1,314, Rio de Janeiro, Brazil.

78. Tateyama, M. (1996). *Reinforced-Soil Retaining Wall Soil with Full-Height Rigid Facing and its Appliance*, Doctoral Thesis, University of Tokyo, Japan.

79. Cao, Y.B. and Peng, F.L. (2011). “Numerical Study on Effects of the Number of Reinforcement Layers for Reinforced-Sand Retaining Wall,” *Geo-Frontiers 2011 Advances in Geotechnical Engineering*, 3,505–3,515, American Society of Civil Engineers, Atlanta, GA.

80. Olson, S.M., Holloway, K.P., Buenker, J.M., Long, J.H., and LaFave, J.M. (2013). *Thermal Behavior of IDOT Integral Abutment Bridges and Proposed Design Modifications*, Illinois Center for Transportation Research Report, ICT-12-022, University of Illinois at Urbana-Champaign, Champaign, IL.

81. Kim, J.S. and Barker, R.M. (2002). “Effect of Live Load Surcharge on Retaining Walls and Abutments,” *Journal of Geotechnical and Geoenvironmental Engineering*, *128*(10), 803–813.

82. Esmaeili, M. and Fatollahzadeh, A. (2013). “Effect of Train Live Load on Railway Bridge Abutments,” *Journal of Bridge Engineering*, *18*(6), 576–583.

83. Boussinesq, J.V. (1885). “Sur la résistance qu’oppose un fluide indéfini au repos, sans pesanteur, au mouvement varié d’une sphère solide qu’il mouille sur toute sa surface, quand les vitesses restent bien continues et assez faibles pour que leurs carrés et produits soient négligeables.” *Comptes Rendu de l'Academie des Sciences*, *100*, 935–937.

84. Westergaard, H.M. (1938). “A Problem of Elasticity Suggested by a Problem in Soil Mechanics; Soft Material Reinforced by Numerous Strong Horizontal Sheets,” *Mechanics of Solids*, Stephen Timoshenko 60th Anniversary Volume, 268-277, MacMillan Co., New York, NY.

85. Allen, T.M., Christopher, B.R., and Holtz, R.D. (1991). “Performance of a 12.6-m-High Geotextile Wall in Seattle, Washington,” *Proceedings of the International Symposium on Geosynthetic-Reinforced Soil Retaining Walls*, 81–100, Netherlands.

86. Bathrust, R.J., Karpurapu, R., and Jarrett, P.M. (1992). “Finite Element Analysis of a Geogrid Reinforced Soil Wall,” *Grouting, Soil Improvement and Geosynthetics*, 1,213–1,224, American Society of Civil Engineers, Atlanta, GA.

87. Fishman, K.L., Desai, C.S., and Sogge, R.L. (1993). “Field Behavior of Instrumented Geogrid Soil Reinforced Wall,” *Journal of Geotechnical Engineering*, *119*(8), 1,293–1,307.

88. Zornberg, J.G. and Mitchell, J.K. (1994). “Finite Element Prediction of the Performance of an Instrumented Geotextile-Reinforced Wall,” *Proceedings of the 8th International Conference of the International Association for Computer Methods and Advances in Geomechanics*, 1,433–1,438, Morgantown, WV.

89. Christopher, B.R., Gill, S.A., Giroud, J-P., Juran, I., Mitchell, J.K., Schlosser, F., and Dunnicliff, J. (1990). *Reinforced Soil Structures Volume 1: Design and Construction Guidelines*, Report No. FHWA-RD- 89-043, Federal Highway Administration, Washington, DC.

90. Rowe, R.K. and Ho, S.K. (1993). “Continuous Panel Reinforced Soil Walls on Rigid Foundations,” *Journal of Geotechnical and Geoenvironmental Engineering*, *123*(10), 912–920.

91. Das, B. (2013) E*lastic Settlement of Shallow Foundations on Granular Soil: A Critical Review*, California State University, Sacramento, CA. Obtained from: http://gle.wisc.edu/wp-content/uploads/2013/07/Elastic-Settlement-Shallow-Foundations_A-Critical-Review-2.pdf. Site last accessed November 11, 2015.

92. Schmertmann, J.H. (1970). “Static Cone to Compute Static Settlement Over Sand,” *Journal of Soil Mechanics & Foundations Division*, *96*(3), 1,011–1,043.

93. Schmertmann, J.H., Hartman, J.P., and Brown, P.R. (1978). “Improved Strain Influence Factor Diagrams,” *Journal of the Geotechnical Engineering Division*, *104*(GT8), 1,131–1,135.

94. Hough, B.K. (1959). “Compressibility as Basis for Soil Bearing Value,” *Journal of the Soil Mechanics and Foundations Division*, *85*(SM4, Part 1), 11–39.

95. Peck, R.B. and Bazaraa, A.R.S.S. (1969). “Discussion of Paper by D’Appolonia et al.,” *Journal of the Soil Mechanics and Foundations Division*, *95*(3), 305–309.

96. Burland, J.B. and Burbidge, M.C. (1985). “Settlement of Foundations on Sand and Gravel,” *Proceedings of the Institution of Civil Engineers*, *78*(1), 1,325–1,381.

97. D'Appolonia, D.J., D'Appolonia, E.E., and Brissette, R.F. (1968). "Settlement of Spread Footings on Sand," *Journal of the Soil Mechanics and Foundations Division*, *94*(SM3), 735–760.

98. D'Appolonia, D.J., D'Appolonia, E.E., and Brissette, R.F. (1970). "Closure to Discussions on 'Settlement of Spread Footings on Sand,'" *Journal of the Soil Mechanics and Foundations Division*, *96*(SM2), 754–761.

99. Terzaghi, K. and Peck, R.B. (1948). *Theoretical Soil Mechanics*, 2nd Ed., John Wiley & Sons, New York, NY.

100. Christian, J.T. and Carrier, W.D. (1978). "Janbu, Bjerrum and Kjaernsli's Chart Reinterpreted," *Canadian Geotechnical Journal*, *15*, 123–128.

101. Crouse, P.E. and Wu, J.T.H. (1996). *Long-Term Performance of GRS Retaining Walls*, Research Report, Department of Civil Engineering, University of Colorado at Denver, Denver, CO.

102. Wu, J.T.H. (2001). *Revising the AASHTO Guidelines for Design and Construction of GRS Walls*, Report CDOT-DTD-R-2001-16, University of Colorado at Denver, Denver, CO.

103. Terzaghi, K., Peck, R.B., and Mesri, G. (1996). *Soil Mechanics in Engineering Practice*, Third Ed., John Wiley & Sons, New York, NY.

104. Briaud, J-L. and Garland, E. (1985). "Loading Rate Method for Pile Response in Clay," *Journal of Geotechnical Engineering*, *111*(3), 319–335.

105. Briaud, J-L. (2007). "Spread Footings in Sand: Load Settlement, Curve Approach," *Journal of Geotechnical and Geoenvironmental Engineering*, *133*(8), 905–920.

106. Briaud, J-L. and Gibbens, R.M. (1999). "Behavior of Five Large Spread Footings in Sand," *Journal of Geotechnical Engineering*, *125*(9), 787–796.

107. Gibson, R.E. (1967). "Some Results Concerning Displacements and Stresses in a Non-Homogeneous Elastic Half Space," *Geotechnique*, *17*, 58–67.

108. Giroud, J.P. (1989). *Geotextile Engineering Workshop-Design Examples*, Report No. FHWA HI-89-002, Federal Highway Administration, Washington, DC.

109. Wu, J.T.H. (1994). *Design and Construction of Low Cost Retaining Walls: The Next Generation in Technology*, Report No. CTI-UCD-1-94, Colorado Transportation Institute, Denver, CO.

110. Jewell, R.A. (1988). "Reinforced Soil Wall Analysis and Behavior," *The Application of Polymeric Reinforcement in Soil Retaining Structures*, NATO Advanced Research Workshop, Kluwer, Netherlands.

111. Jewell, R.A. and Milligan, G.W. (1989). “Deformation Calculation for Reinforced Soil Walls,” *Proceedings of the 12th International Conference on Soil Mechanics and Foundation Engineering*, 1,259–1,262, Rio de Janeiro, Brazil.

112. DeBeer, E. (1948). “Settlement Records of Bridges Founded on Sand,” *Proceedings of the Second International Conference on Soil Mechanics and Foundation Engineering*, *2*, 111.

113. Bergdahl, V. and Ottosson, E. (1982). “Calculation of Settlements on Sands from Field Test Results,” *Proceedings of the Second European Symposium on Penetration Testing*, *1*, 229–234.

114. DeBeer, E.E. and Martens, A. (1956). “Discussion of ‘Penetration Tests and Bearing Capacity of Cohesionless Soils by GG Meyerhof,’” *Journal of the Soil Mechanics and Foundations Division*, 1,095–1,097.

115. Holtz, R.D. and Lee, W.F. (2002). *Internal Stability Analysis of Geosynthetic Reinforced Retaining Walls*, Report No. WA-RD 532.1, Washington State Transportation Center, Seattle, WA.

116. Ketchart, K. and Wu, J.T.H. (1997). “Performance of Geosynthetic-Reinforced Soil Bridge Pier and Abutment, Denver, Colorado, USA,” *International Symposium on Mechanically Stabilized Backfill*, 101–116.

117. Bueno, B.S., Benjamim, C.V.S., and Zornberg, J.G. (2005). “Field Performance of a Full-Scale Retaining Wall Reinforced with Nonwoven Geotextiles,” *Proceedings of Geo-Frontier 2005*, Austin, TX.

118. Hatami, K. and Bathurst, R.J. (2006a). “A Numerical Model for Reinforced Soil Segmental Walls Under Surcharge Loading,” *Journal of Geotechnical and Geoenvironmental Engineering*, *132*(6), 673–684.

119. Benjamim, C.V.S., Bueno, B.S., and Zornberg, J.G. (2007). “Field Monitoring Evaluation of Geotextile-Reinforced Soil-Retaining Walls,” *Geosynthetics International*, *14*(2), 100–118.

120. Benigni, C., Bosco, G., Cazzuffi, D., and Col, R.D. (1996). “Construction and Performance of an Experimental Large Scale Wall Reinforced with Geosynthetics,” *Earth Reinforcement*, *1*, 315–320.

121. Basudhar, P.K., Dixit, P.M., Gharpure, A., and Deb, K. (2008). “Finite Element Analysis of Geotextile-Reinforced Sand-Bed Subjected to Strip Loading,” *Geotextiles and Geomembranes*, *26*, 91–99.

122. Rowe, R.K. and Skinner, G.D. (2001). “Numerical Analysis of Geosynthetic Reinforced Retaining Wall Constructed on a Layered Soil Foundation,” *Geotextiles and Geomembranes*, *19*, 387–412.

123. Leshchinsky, D. and Vulova, C. (2001). “Numerical Investigation of the Effects of Geosynthetic Spacing on Failure Mechanisms in MSE Block Walls,” *Geosynthetics International*, *8*(4), 343–365.

124. Boushehrian, J.H. and Hataf, N. (2003). “Experimental and Numerical Investigation of the Bearing Capacity of Model Circular and Ring Footings on Reinforced Sand,” *Geotextiles and Geomembranes*, *21*, 241–256.

125. Skinner, G.D. and Rowe, R.K. (2005). “Design and Behavior of a Geosynthetic Reinforced Retaining Wall and Bridge Abutment on a Yielding Foundation,” *Geotextiles and Geomembranes*, *23*, 234–260.

126. Ghazavi, M. and Lavasan, A.A. (2008). “Interface Effect of Shallow Foundations Constructed on Sand Reinforced with Geosynthetics,” *Geotextiles and Geomembranes*, *26*, 404–415.

127. Alamshahi, S. and Hataf, N. (2009). “Bearing Capacity of Strip Footings on Sand Slopes Reinforced with Geogrid and Grid-Anchor,” *Geotextiles and Geomembranes*, *27*, 217–226.

128. Chen, B., Luo, R., and Sun, J. (2011). “Time-Dependent Behaviors of Working Performance of Biaxial Reinforced Composite Foundation,” *Institute of Electrical and Electronics Engineers Conference 2011*, 915–920.

129. Karpurapu, R. and Bathurst, R.J. (1995). “Behavior of Geosynthetic Reinforced Soil Retaining Walls Using the Finite Element Method,” *Computers and Geotechnics*, *17*(3), 279–299.

130. El Sawaaf, M. (2007). “Behavior of Strip Footing on Geogrid-Reinforced Sand Over a Soft Clay Slope,” *Geotextiles and Geomembranes*, *25*(1), 50–60.

131. Ahmed, A., El-Tohami, A.M.K., and Marei, N.A. (2008). “Two-Dimensional Finite Element Analysis of Laboratory Embankment Model,” *Geotechnical Engineering for Disaster Mitigation and Rehabilitation*, 1,003–1,018.

132. Zidan, A.F. (2012). “Numerical Study of Behavior of Circular Footing on Geogrid-Reinforced Sand Under Static and Dynamic Loading,” *Geotechnical and Geological Engineering*, *30*, 499–510.

133. Bhattacharjee, A. and Krishna, A.M. (2013). “Strain Behavior of Backfill Soil of Wrap Faced Reinforced Soil Walls: A Numerical Study,” *Proceedings of the 18th Southeast Asian Geotechnical Conference, Advances in Geotechnical Infrastructure*, Singapore.

134. Fakharian, K. and Attar, I.H. (2007). “Static and Seismic Numerical Modeling of Geosynthetic-Reinforced Soil Segmental Bridge Abutments,” *Geosynthetics International*, *14*(4), 228–243.

135. Liu, H., Wang, X., and Song, E. (2009). “Long-Term Behavior of GRS Retaining Walls with Marginal Backfill Soils,” *Geotextiles and Geomembranes*, *27*, 295–307.

136. Ling, H.I. and Liu, H. (2003). “Pressure Dependency and Densification Behavior of Sand Through a Generalized Plasticity Model,” *Journal of Engineering Mechanics*, *129*(8), 851–860.

137. Lade, P.V. (2005). “Overview of Constitutive Models for Soils,” *Soil Constitutive Models: Evaluation, Selection and Calibration,* ASCE Geotechnical Special Publication No. 128, 1–34.

138. Duncan, J.M., Byrne, P.M., Wong, K.S., and Mabry, P. (1980). *Strength, Stress-Strain and Bulk Modulus Parameters for Finite Element Analyses of Stresses and Movements in Soil Masses*, Report No. UCB/GT/80-01, University of California, Berkeley, Berkeley, CA.

139. Huang, B., Bathurst, R.J., and Hatami, K. (2009) “Numerical Study of Reinforced Soil Segmental Walls Using Three Different Constitutive Soil Models,” *Journal of Geotechnical and Geoenvironmental Engineering*, *135*(10), 1,486–1,498.

140. Boscardin, M.D., Selig, E.T., Lin, R.S., and Yang, G.R. (1990). “Hyperbolic Parameters for Compacted Soils,” *Journal of Geotechnical Engineering*, *116*(1), 88–104.

141. Kim, M.K. and Lade, P.V. (1988). “Single Hardening Constitutive Model for Frictional Materials I: Plastic Potential Function,” *Computers and Geotechnics, 5*(4), 307–324.

142. Lade, P.V. and Kim, M.K. (1988a). “Single Hardening Constitutive Model for Frictional Materials II: Yield Criterion and Plastic Work Contours,” *Computers and Geotechnics*, *6*(1), 13–29.

143. Lade, P.V. and Kim, M.K. (1988b). “Single Hardening Constitutive Model for Frictional Materials III: Comparisons with Experimental Data,” *Computers and Geotechnics*, *6*(1), 31–47.

144. Hallquist, J.O. and Whirley, R.G. (1989). *Dyna3D User’s Manual: Nonlinear Dynamic Analysis of Structures in Three Dimensions,* Rev. 5, Report UCID-19592, Lawrence Livermore National Laboratory University of California, Livermore, CA.

145. Drucker, D.C. and Prager, W. (1952). “Soil Mechanics and Plasticity Analysis or Limit Design,” *Quarterly of Applied Mathemat*ics, *10*(2), 157–165.

146. DiMaggio, F.L. and Sandler, I.S. (1971). “Material Model for Granular Soils,” *Journal of the Engineering Mechanics Division, 97*(3), 935–950.

147. Huang, T.K. and Chen, W.F. (1990). “Simple Procedure for Determining Cap-Plasticity-Model Parameters,” *Journal of Geotechnical Engineering*, *116*(3), 492–513.

148. Johnston, R.S. and Romstad, K.M. (1989). “Dilation and Boundary Effects in Large Scale Pull-Out Tests,” *Proceedings of the 12th International Conference on Soil Mechanics and Foundation Engineering,* 1,263–1,266, Rio de Janeiro, Brazil.

149. Otani, J., Ochiai, H., and Miyata, Y. (1994). “Bearing Capacity of Geogrid Reinforced Ground,” *Fifth International Conference on Geotextiles, Geomembranes and Related Products,* Singapore.

150. Otani, J., Ochiai, H., and Yamamoto, K. (1998). “Bearing Capacity Analysis of Reinforced Foundations on Cohesive Soil,” *Geotextiles and Geomembrane*, *16*, 195–206.

151. Yamamoto, K. and Otani, J. (2002). “Bearing Capacity and Failure Mechanism of Reinforced Foundations Based on Rigid-Plastic Finite Element Formulation,” *Geotextiles and Geomembranes*, *20*, 367–393.

152. Kurian, N.P., Beena, K.S., and Kumar, R.K. (1997). “Settlement of Reinforced Sand in Foundations,” *Journal of Geotechnical and Geoenvironmental Engineering*, *123*(9), 818–827.

153. Dias, A.C. (2003). *Numerical Analyses of Soil–Geosynthetic Interaction in Pull-out Tests*, M.Sc. Thesis, University of Brasilia, Brasilia, Brazil.

154. Chen, Q. and Abu-Farsakh, M. (2011). “Numerical Analysis to Study the Scale Effect of Shallow Foundation on Reinforced Soils,” *Proceedings of GeoFrontiers 2011*, 595–604.

155. Raftari, M., Kassim, K.A., Rashid, A.S., and Moayedi, H. (2013). “Settlement of Shallow Foundations near Reinforced Slopes,” *Electronic Journal of Geotechnical Engineering*, *18*, 797–808.

156. Chakraborty, D. and Kumar, J. (2014). “Bearing Capacity of Strip Foundations in Reinforced Soils,” *International Journal of Geomechanics*, *14*(1), 45–58.

157. Ling, H.I., Cardany, C.P., Sun, L-X., and Hashimoto, H. (2000). “Finite Element Study of a Geosynthetic-Reinforced Soil Retaining Wall with Concrete-Block Facing,” *Geosynthetics International*, *7*(3), 163–188.

158. Ling, H.I., Tatsuoka, F., and Tateyama, M. (1995). “Simulating Performance of GRS-RW by Finite-Element Procedure,” *Journal of Geotechnical Engineering*, *121*(4), 330–340.

159. Sharma, K.G., Rao, G.V., and Raju, G.V.S.S. (1994). “Elasto-Plastic Analysis of a Reinforced Soil Wall by FEM,” *Proceedings of the 8th International Conference on Computer Methods and Advances in Geomechanics*, Morgantown, WV.

160. Lopes, M.L., Cardoso, A.S., and Yeo, K.C. (1994). “Modelling Performance of a Sloped Reinforced Soil Wall Using Creep Function,” *Geotextiles and Geomembranes*, *13*, 181–197.

161. Liu, H. and Ling, H.I. (2007). “A Unified Elastoplastic-Viscoplastic Bounding Surface Model of Geosynthetics and its Applications to GRS-RW Analysis,” *Journal of Engineering Mechanics*, *133*(7), 801–815.

162. Kongkitkul, W., Chantachot, T., and Tatsuoka, F. (2014). “Simulation of Geosynthetic Load-Strain-Time Behaviour by the Non-Linear Three-Component Model,” *Geosynthetics International*, *21*(4), 244–255.

163. Abramento, M. (1993). *Analysis and Measurement of Stresses in Planar Soil Reinforcements*, Ph.D. Thesis, Massachusetts Institute of Technology, Boston, MA.

164. Bergado, D.T. and Chai, J.C. (1994). “Pullout Force/Displacement Relationship of Extensible Grid Reinforcement,” *Geotextiles and Geomembranes*, *13*(5), 295–316.

165. Sobhi, S. and Wu, J.T.H. (1996). “An Interface Pullout Formula for Extensible Sheet Reinforcement,” *Geosynthetics International*, *3*(5), 565–582.

166. Madhav, M.R., Gurung, N., and Iwao, Y. (1998). “A Theoretical Model for the Pull-Out Response of Geosynthetic Reinforcement,” *Geosynthetics International*, *5*(4), 399–424.

167. Gurung, N. (2001). “1-D Analytical Solution for Extensible and Inextensible Soil/Rock Reinforcement in Pull-Out Tests,” *Geotextiles and Geomembranes*, *19*(4), 195–212.

168. Gurung, N. and Iwao, Y. (1999). “Comparative Model Study of Geosynthetic Pull-Out Response,” *Geosynthetics International*, *6*(1), 53–68.

169. Perkins, S.W. (2001). *Numerical Modelling of Geosynthetic Reinforced Flexible Pavements*, Report No. FHWA/MT-01-003/99160-2, Federal Highway Administration, Washington, DC.

170. Khedkar, M.S. and Mandal, J.N. (2009). “Pullout Behaviour of Cellular Reinforcements,” *Geotextiles and Geomembranes*, *27*(4), 262–271.

171. Palmeira, E.M. (2009). “Soil-Geosynthetic Interaction: Modelling and Analysis,” *Geotextiles and Geomembranes*, *27*, 368–390.

172. Santos, E.C.G. (2007). *The Use of Construction Residues and Recycled Rubble in Reinforced Soil Structures*. M.Sc. Thesis, University of Sao Paulo, Sao Carlos, Brazil.

173. Brown, S.F., Kwan, J., and Thom, N.H. (2007). “Identifying the Key Parameters that Influence Geogrid Reinforcement of Railway Ballast,” *Geotextiles and Geomembranes*, *25*(6), 326–335.

174. Boyle, S.R. (1995). *Deformation Prediction of Geosynthetic Reinforced Soil Retaining Walls*, Ph.D. Dissertation, University of Washington, Seattle, WA.

175. Brown, B.S. and Poulos, H.G. (1981). “Analysis of Foundations on Reinforced Soil,” *Proceedings of the 10th International Conference on Reinforced Soil*, *3*, 595–598, Stockholm, Sweden.

176. Andrawes, K.Z., Mcgown, A., Wilson-Fahmy, R.F., and Mashhour, M.M. (1982). "The Finite Element Method of Analysis Applied to Soil–Geotextile Systems," *Second International Conference of Geotextiles,* 695–700, Las Vegas, NV.

177. Love, J.P., Burd, H.J., Milligan, G.W.E., and Houlsby, G.T. (1987). "Analytical and Model Studies of Reinforcement of a Layer of Granular Fill on a Soft Clay Subgrade," *Canadian Geotechnical Journal*, *24*, 611–622.

178. Rowe, R.K. and Soderman, K.L. (1987). "Stabilization of Very Soft Soils Using High Strength Geosynthetics: The Role of Finite Element Analyses," *Geotextiles and Geomembranes*, *6*, 53–80.

179. Matsui, T. and San, K.C. (1988). "Finite Element Stability Analysis Method for Reinforced Slopecutting," *International Geotechnical Symposium on Theory and Practice of Earth Reinforcement*, 317–322, Fukoka, Japan.

180. Gens, A., Carol, I., and Alonso, E.E. (1988). "An Interface Element Formulation for the Analysis of Soil-Reinforcement Interaction," *Computer and Geotechnics*, *7*(1–2), 133–151.

181. Poran, C.J., Herrmann, L.R., and Romstad, K.M. (1989). "Finite Element Analysis of Footings on Geogrid-Reinforced Soil," *Proceedings of Geosynthetics*, 231–242, San Diego, CA.

182. Hird, C.C., Pyrah, I.C., and Russell, D. (1990). "Finite Element Analysis of the Collapse of Reinforced Embankments on Soft Ground," *Geotechnique*, *40*(4), 633–640.

183. Burd, H.J. and Brocklehurst, C.J. (1990). "Finite Element Studies of the Mechanics of Reinforced Unpaved Roads," *Proceedings of the Fourth International Conference on Geotextiles, Geomembranes and Related Products*, 217–221, The Hauge, Netherlands.

184. Wilson-Fahmy, R.F. and Koerner, R.M. (1993). "Finite Element Modeling of Soil Geogrid Interface with Application to the Behavior of Geogrids in Pullout Loading Conditions," *Geotextiles and Geomembranes*, *12*, 479–501.

185. Abdel-Baki, M.S. and Raymond, G.P. (1994). "Numerical Analysis of Geotextile Reinforced Soil Slabs," *Fifth International Conference on Geotextiles, Geomembranes and Related Products*, Singapore.

186. Liu, H. and Won, M-S. (2009). "Long-Term Reinforcement Load of Geosynthetic-Reinforced Soil Retaining Walls," *Journal of Geotechnical and Geoenvironmental Engineering*, *135*(7), 875–889.

187. Duncan J.M. and Chang, C.Y. (1970). "Nonlinear Analysis of Stress and Strain in Soils," *Journal of Soil Mechanics and Foundations Divisions*, *96*(SM5), 1,629–1,654.

188. Christopher, B.R. (1993). *Deformation Response and Wall Stiffness in Relation to Reinforced Soil Wall Design*, Ph.D. Dissertation, Purdue University, West Lafayette, IN.

189. Itasca Consulting Group, Inc. (2001). *Fast Lagrangian Analysis of Continua (FLAC)*, Itasca Consulting Group, Inc., Minneapolis, MN.

190. Hatami, K. and Bathurst, R.J. (2006b). "Parametric Analysis of Reinforced Soil Walls with Different Backfill Material Properties," *North American Geosynthetics Society 2006 Conference*, 1–15, Las Vegas, NV.

191. Wu, J.T.H. (1992). "Geosynthetic-Reinforced Soil Retaining Walls," *International Symposium on Geosynthetic-Reinforced Soil Retaining Walls*, Wu (Ed.), Denver, CO.

192. Murata, O., Tateyama, M., and Tatsuoka, F. (1991). "A Reinforcing Method for Earth Retaining Walls Using Short Reinforcing Members and a Continuous Rigid Facing," *Proceedings of the ASCE Geotechnical Engineering Congress*, 935–946, New York, NY.

193. Miyatake, H., Ochiai, Y., Maruo, S., Nakane, A., Yamamoto, M., Terayama, T., Maejima, T., and Tsukada, Y. (1995). "Full-Scale Failure Experiments on Reinforced Earth Wall with Geotextiles (Part 2)—Facing with Concrete Blocks," *Proceedings of 30th Annual Conference of Geotechnical Engineering*, 2,427–2,430, Kanazawa, Japan.

194. Tajiri, N., Sasaki, H., Nishimura, J., Ochiai, Y., and Dobashi, K. (1996). "Full-Scale Failure Experiments of Geotextile-Reinforced Soil Walls with Different Facings, *Proceedings of the International Symposium on Earth Reinforcement*, *1*, 525–530, Fukuoka, Kyushu, Japan.

195. Helwany, S.M.B. and Wu, J.T.H. (1992). "A Generalized Creep Model for Geosynthetics," *Proceedings of the International Symposium on Earth Reinforcement Practice*, 79–84, Fukuoka, Kyushu, Japan.

196. Liu, H. and Ling, H.I. (2005). "Constitutive Modeling of the Time Dependent Monotonic and Cyclic Behavior of Geosynthetics," *Geosynthetics and Geosynthetic-Engineered Soil Structures*, 281–302, Columbia University Press, New York, NY.

197. Helwany, S.M.B. (1993). "Long-Term Interaction Between Soil and Geosynthetic in Geosynthetic-Reinforced Soil Structures," Ph.D. Thesis, University of Colorado at Denver, Denver, CO.

198. Wu, J.H.T. and Helwany, S.M.B. (1996). "A Performance Test for Assessment of Long-Term Creep Behavior of Soil-Geosynthetic Composites," *Geosynthetics International*, *3*(1), 107–124.

199. Wu, J.T.H. and Adams, M.T. (2007). "Myth and Fact on Long-Term Creep of GRS Structures," Geotechnical Special Publication No. 165, *Geosynthetics in Reinforcement and Hydraulic Applications, Proceedings for Geo-Denver*, Denver, CO.

200. Abu-Hejleh, N., Mohammed, K., and Alzamora, D.E. (2013). "Recommendations for the Use of Spread Footings on Soils to Support Highway Bridges," *Transportation Research Board 2013 Annual Meeting Compendium of Papers*, Transportation Research Board, Washington, DC.

201. Cerato, A.B. and Luteneger, A.J. (2007). “Scale Effects of Shallow Bearing Capacity on Granular Material,” *Journal of Geotechnical and Geoenvironmental Engineering*, *133*(10), 1,192–1,202.

202. Fakher, A. and Jones, C.J.F.P. (1996). “Discussion: Bearing Capacity of Rectangular Footings on Geogrid-Reinforced Sand,” *Journal of Geotechnical Engineering*, *122*(4), 326–327.

203. Bolton, M.D. (1986). “The Strength and Dilatancy of Sands,” *Géotechnique*, *36*(1), 65–78.

HRDI-40/02-16(WEB)E